UNCLASSIFIED

AD NUMBER

AD-881 879

CLASSIFICATION CHANGES

TO   **UNCLASSIFIED**

FROM   **NEVER CLASSIFIED**

AUTHORITY

U.S. Air Force Flight Dynamics Lab.,
Wright-Patterson AFB, OH; November 1970.

19990301075

THIS PAGE IS UNCLASSIFIED

UNCLASSIFIED

AD NUMBER

AD-881 879

NEW LIMITATION CHANGE

TO

DISTRIBUTION STATEMENT - A

Approved for Public Release; Distribution Unlimited.

LIMITATION CODE - 1

FROM

DISTRIBUTION STATEMENT - NONE

No Prior DoD Distribution Security Control Statement.

AUTHORITY

U.S. Air Force Flight Dynamics Lab.,
Wright-Patterson AFB, OH via ltr. dtd June 25, 1971.

THIS PAGE IS UNCLASSIFIED

628 18879

AIRCRAFT GUNFIRE VIBRATION

The Development of Prediction Methods and
The Synthesis of Equipment Vibration Techniques

ROBERT W. SEVY

JAMES CLARK

AD No.
FILE COPY

TECHNICAL REPORT AFFDL-TR-70-131

D D C

MAR 29 1971

B

NOVEMBER 1970

AIR FORCE FLIGHT DYNAMICS LABORATORY
AIR FORCE SYSTEMS COMMAND
WRIGHT-PATTERSON AIR FORCE BASE, OHIO

97

NOTICE

When Government drawings, specifications, or other data are used for any purpose other than in connection with a definitely related Government procurement operation, the United States Government thereby incurs no responsibility nor any obligation whatsoever; and the fact that the government may have formulated, furnished, or in any way supplied the said drawings, specifications, or other data, is not to be regarded by implication or otherwise as in any manner licensing the holder or any other person or corporation, or conveying any rights or permission to manufacture, use, or sell any patented invention that may in any way be related thereto.

AIRCRAFT GUNFIRE VIBRATION

The Development of Prediction Methods and
The Synthesis of Equipment Vibration Techniques

ROBERT W. SEVY

JAMES CLARK

FOREWORD

This technical report has been reviewed and is approved.

WILLIAM C. SAVAGE
Chief, Environmental Control Branch
Vehicle Equipment Division

ABSTRACT

This study describes in-house efforts that comprise two primary objectives. (1) the development of a prediction rationale for estimating the magnitude and character of gunfire induced, structurally-borne vibration which, in turn, represents a definition of equipment vibration inputs, and (2) the synthesis of a laboratory vibration test procedure which may be used to qualify future equipment.

Power analogies, relating gunfire blast to structural response, are meshed with a spatial parameter to describe vibration levels that are functionally related to the gunfire blast pulse in terms of gun configuration, muzzle energy, gunfire rate, and the vector distance separating the equipment from the gun muzzles.

A basic, normalized, test level function has been synthesized and integrated into a laboratory vibration test procedure. The test technique developed from this work has been published as Method T519 of MIL-STD-810B.

TABLE OF CONTENTS

ILLUSTRATIONS

SYMBOLS

C_r	correlation coefficient or goodness of fit
D	vector distance from gun muzzle to point under consideration (in)
E	energy in pulse
E'	muzzle energy (ft-lbs)
F	distribution of variance, joint statistic
$F(f)$	input Fourier spectrum
G_{max}	$G_o(f)$ when applied to specification levels (G^2/Hz)
$G_o(f), G(\omega)$	structural response (G^2/Hz)
$H(f)$	generalized frequency response
$|H(\omega)|$	transfer function
N	number of pulses
p	gun blast pressure at any time, t (lbs/in^2); gun cycling period (sec)
p_{max}, p_m	maximum gun blast pressure (lbs/in^2)
$P(\omega), P(f)$	Fourier transform of p(t)
$R(f)$	structural response function
S_r'	standard error of the sample
T	period of one pressure pulse or pulse train (sec)
a	intercept of regression line with Y axis
$2|a_k|$	magnitude of line spectrum (lbs/in^2)
b	slope of regression line
e	base of Naperian or natural logarithms (2.7182818)
Δf	harmonic separation (Hz)
$|g(\omega)|$	Fourier transform of p(t) (variable firing rate model) (lbs/in^2-sec)
h	perpendicular distance from gun muzzle to aircraft surface (in)
j	$\sqrt{-1}$
k	integers, 1, 2, 3, 4, —— ——
m	mass of projectile (lbs-sec^2/ft)
n	number of guns
n_o	reference number of guns
r	firing rate (Hz)
r_1	firing rate of unknown gun (Hz)
r_o	reference firing rate (Hz)
t	time; period of one pulse (sec)
t_a	elapsed time of firing rate increase; variable firing rate model (sec)

t_b	elapsed time of constant firing rate (variable firing rate model) (sec)
t_c	elapsed time of firing rate decrease (variable firing rate model) (sec)
t_u	elapsed time of the positive pressure portion of a pressure pulse (sec)
$t_{1, 2, 3} \text{---}$	time of pulse occurrences (sec)
v	muzzle velocity of projectile (ft/sec)
$\bar{x}$	arithmetic average of the log (D) data values
y_{cb}	confidence band
$\bar{y}$	arithmetic average of the log $(G_o f)$ data values

Greek Symbols

α	proportionality constant
α_o	reference proportionality constant
β	proportionality constant
$\delta(t)$	unit impulse function
$\delta(\omega)$	Fourier transform of unit impulse function, $\delta(t)$
$\theta(\omega)$	power conversion efficiency
Π	average power
π	3.1416 ———
$\Psi(\omega)$	power density spectrum (G^2/Hz)
ω	circular frequency (rads/sec)

SECTION I

INTRODUCTION

Gunfire vibration data programs and studies have yielded few, if any, correlatives with which the character and magnitude of the resultant structural vibration can be associated. From the equipment viewpoint, apart from protective design considerations, one desires a rationale for estimating vibration levels, spectral shape, and so on, in order that one may synthesize a simulation environment to which equipment may be exposed and from which the successful emergence will provide good confidence that the item will survive and properly operate during real gunfire exposure.

Prediction technology, always important, is especially so for the case of gunfire vibration. Normally, one may provide estimates of the vibration of an aircraft structure and indulge the latitude of assigning a general and averaged description over a zone of the structure, say six feet or so—adjusting the levels from zone to zone. In contrast the large magnitudes and sharp gradients of gunfire vibration do not permit a comparable luxury for the case of gunfire because within a distance of six feet the vibration levels may change one order of magnitude. Moreover, gunfire levels, though relatively brief in time duration, are sufficiently high (as much as one or two orders above the normal, ambient vibration levels) to inhibit the customary practice of test level "scaling-up." Here, we allude to the test level magnification technique employed to introduce an equivalent laboratory time-to-failure — a technique which serves as compensation for the necessarily limited exposure times provided by laboratory tests.

The stress, therefore, is on a prediction rationale, as reliable and accurate as the technology will allow, in order that gunfire vibration levels may be derived and real time simulation techniques applied.

This work embraces two elements essential to the development and conclusions of the program. One, that there exists a power relationship between the gun pulses and the structural response. Two, that the gunfire blast energy is coupled, in concentrated form near the gun muzzle and decays in some inverse form of the distance from the muzzle. All of the procedures employed, analytics used, and data processing techniques introduced reflect either one or both of these assertions.

It is not the intent of this introduction to historicize; to catalog a lengthy list of equipment failures and resultant field retrofit programs—these are largely a matter of record and of references, a number of which are contained in this report. Rather, it is hoped that the description of the somewhat unique character of gunfire vibration and the identification of the major modelling principles is sufficiently adumbrated in this discussion to identify the basic elements of the problem area and in so doing, furnish the guidance necessary for the detailed approach to the problem. A brief outline and description of pertinent details of this report are given below.

Section II is concerned with the energy content and character of gun blast pulses transformed into the frequency domain by means of Fourier Series. Various gun configurations are examined; differences and commonalities noted. The equations of the Fourier Series used in the analysis of the gun blast loading are contained in Appendix I.

Section III involves the apprehension, derivation, and selection of a broad-band, random power model. The relationship between structural response and pulse spectral power is shown. Structural response is expressed in terms of gun muzzle energy, firing rate, and number of guns.

1

Section IV discusses pertinent details of gunfire data used in this study and considers the relationship of aircraft structural response to gunfire models.

Section V contains a regression analysis applied to four gunfire configurations. Data analysis is used to provide a test for the power model. A description of the regression process is contained in Appendix II.

Section VI is a refinement and final variation of Section V from which a basic normalized prediction curve is derived. An example is included to demonstrate the application of the method. A resulting gunfire vibration test method is included in Appendix IV.

Section VII elaborates upon work elements previously covered, proposes a tentative method by which the gunfire vibration field may be adjusted as a function of the gun stand off distance, discusses a laboratory simulation technique for the generation and control of gunfire low frequency content, and, finally, explores some concepts concerning future extension of the gunfire model.

Section VIII contains the conclusions.

SECTION II

PULSE SPECTRAL ANALYSIS

In aircraft vibration problems, one is apt to begin with M. Fourier—anticipates ending with him—and usually finishes up between the illustrious Frenchman.

To begin then, a typical pressure-time history of a gunblast is shown in Figure 1. The pulse duration, t_o, is set at approximately 10^{-3} secs—an average value determined from microphone data taken from the F-4E and F-5A aircraft [1] [2]. The flush mounted microphones were located approximately 2-3 feet in front of the gun muzzles and in a zone frequently referred to as the near field loading area of the aircraft structure (Figure 8).

Superimposed over the pulse is its smoothed substitute, the Friedlander blast pulse—the shape is described mathematically by the included expression. The energy of the pressure-time excitation, that is coupled to the aircraft structure results in what amounts to the chief object of our study; structural vibration. The Friedlander pulse is the pressure-time function that we propose to subject to Fourier analysis. From this endeavor, it is hoped that certain details of the spectral character will prove sufficiently informative and useful to assist in the construction of structural response models and in the synthesis of gunfire simulation methods.

Analysis of the pulse is applied to three main cases of gunfire:

Case I. The Constant Firing Rate Model—in which a single gun is assumed to generate the Friedlander pulse at a fixed period and may be characterized, spectrally, by the use of the Fourier series.

Case II. Variable Firing Rate Model—Here, the gun requires time to come up to constant speed, stays here briefly, and then reverses cycles to the cease fire state. A modification of the Fourier series is used as an approximation of this model.

Case III. Unsynchronized, Multiple Gun Arrays—This model is approximated by multiple pulse trains, randomly phased with each other, and is characterized by a special application of the Fourier transform.

Each case is discussed in the following paragraphs. Mathematical details of the first two cases are contained in Appendix I. Details of Case III are either discussed in this Section or are referenced.

1. CASE I—CONSTANT FIRING RATE MODEL

The line spectral display of three typical firing rates (25, 50, and 100 Hz) is shown in Figure 2. The spectra for each firing rate are shown with their respective harmonics separated by a frequency interval, Δf, equal to the reciprocal of their respective gunfire periods. The maximum value of the amplitude occurs at the fundamental. The harmonic amplitudes decrease smoothly with frequency, are about 3 db down at approximately 600 Hz, and from thereon describe a slowly oscillating decay rate at roughly 3 db/octave. There are no zero values of the coefficient in this spectrum. One noteworthy property of the line spectrum, already mentioned, deserves emphasis. As the gun-fire rate increases, so in proportion, does the magnitude of the harmonics, (Reference 1). Similarly, the average power of each line spectrum varies directly as the frequency (Reference 4). Indeed, this is true of Fourier series and transforms in general. The power, frequency, amplitude proportionality characteristics is of some consequence as will be seen later on in this section and early in Section II.

Taken as a model for a single gun, the series form suffers from some deficiencies that are worth discussion. What if the firing rate fluctuates somewhat?—and it does. A three sigma
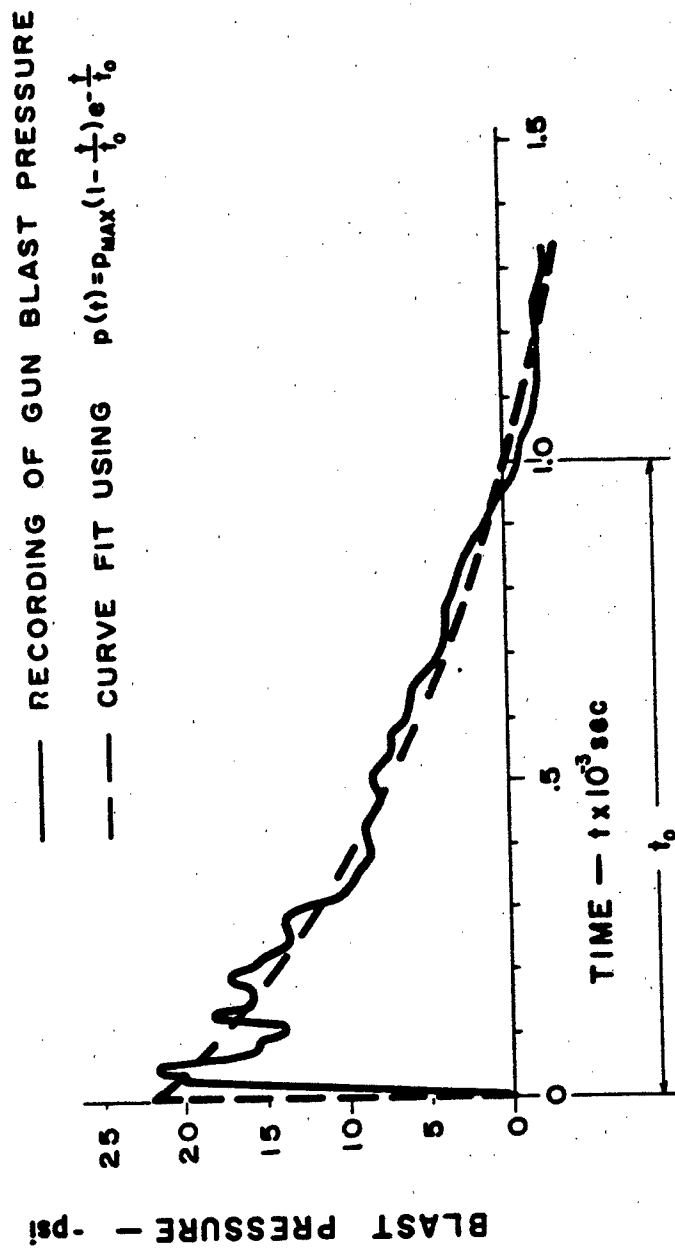
3

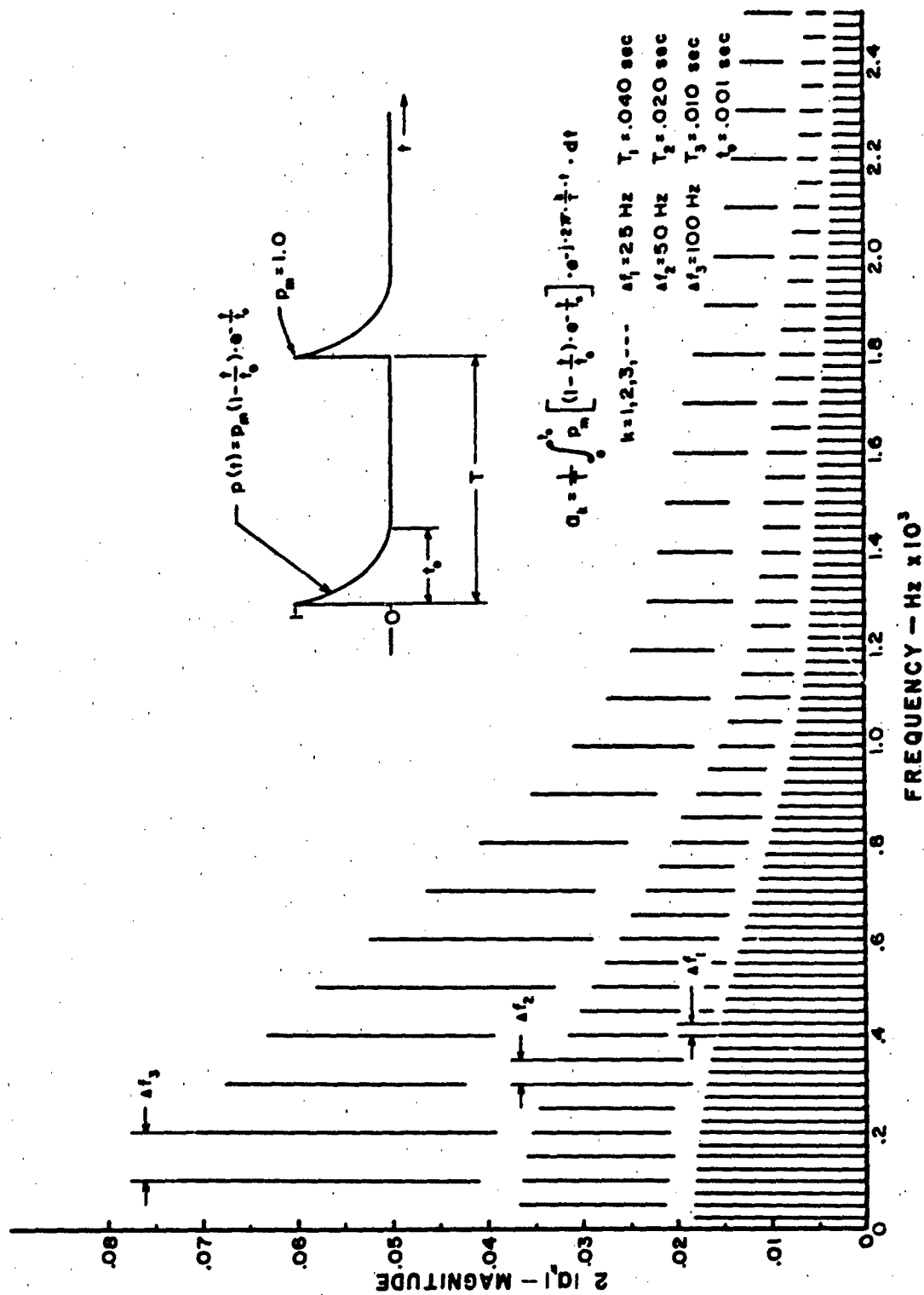Figure 1. Comparison of Curve Fit to Record Gun Blast Pressure

4

Figure 2. Harmonic Model for Constant Firing Rate

5

deviation of, say, $\pm 10\%$ produces a small shift in the spectral lines at the fundamental (Δf = 20 Hz, at 100 Hz) but the deviation at the higher frequencies can be substantial—at 500 Hz the translation is 100 Hz; at 1000 Hz, it is 200 Hz and so on. The matter is further complicated if the firing rate deviation is assumed to be continuous and randomly distributed (as it is, in fact, usually characterized) because the Fourier series, in its application, requires that the period be constant.

It occurs to the authors that the firing rate deviation helps to explain why accelerometers time histories of the aircraft structure (especially noticeable above approximately 400 Hz) exhibit amplitude distributions that are predominantly random in character rather than sinusoidal. Too, it is suspected that this is reinforced by the tuning-detuning effect on aircraft structures arising from fluctuating flight loads.

In any case, the model has decided limitations—for the low frequency portion of the spectrum it seems the more germane and useful. For the high frequency region, the application appears restricted. Not mentioned thus far is the formidable simulation difficulty associated with the generation and control of some 20 to 80 spectral magnitudes.

2. CASE II—VARIABLE FIRING RATE MODEL

The variable firing rate model is synthesized to reflect the response time characteristics of guns that require a finite time interval to come up to normal firing rate. Guns of the rotating barrel class (Vulcan) and guns that have been exposed to low temperature (Reference 5) are typical examples of the variable firing rate model. Oscillogram data (during gunfire initiation) from a gun of the Vulcan class indicated a sharp rise in the rate to approximately 50 Hz, followed by a more gradual increase. This rise continued for approximately 7/10 second at the end of which the normal firing rate of 100 Hz was reached. From the firing history, a simplified rate-time function was constructed. For constructional simplicity and computational convenience, the 7/10-second time interval was rounded off to 1 second. A total cycling history consists of a cycling up (Part 1), a constant rate (Part 2), and a cycling down (Part 3), each of 1-second duration. The history is shown in Figure 3. Segments of the corresponding pulse-time history are shown in Figure 4.

A full sequence of bursts is treated as the new function, p(t). Periodicity is introduced by allowing the burst of pulses to be repeated every 3 seconds. This amounts to 3 second gunfire bursts, repeated every three seconds.

Coefficients of the Fourier series for the pulse train were obtained from a special arrangement of the inverse Fourier transform, the details of which are contained in Appendix I.

The line spectrum results are shown in Figure 5 except that frequency amplitudes are inserted every 100 Hz; all others are omitted for shape comparison with Case I. The frequency content in between is necessarily omitted for clarity of presentation. Recall, that in order to present the assembly of pulses in terms of the Fourier series the entire pulse assembly becomes p(t) and this is made periodic by constructing a sequence of bursts, periodically spaced. The choice of three seconds between pulse bursts is arbitrary—any reasonable interval could have been chosen. Since 3 seconds was selected, the spectral lines are separated by approximately 1/3 Hz—a very dense line spectrum; hence the reason for the spectral omission in Figure 5. Probably, the most interesting feature of Figure 5 arises from the observation that the cycling process has not appreciably changed the main outline of the line spectrum. Differences occur for the most part in the region below 800 Hz and these variations do not seem noteworthy.

Characteristic distributions of side band frequencies about the main spectral magnitudes are shown in Figure 6. Again, for purposes of clarity, spectral lines are placed at spaced intervals to allow the insertion of a sample of the side bands that are, in turn, spaced ap-
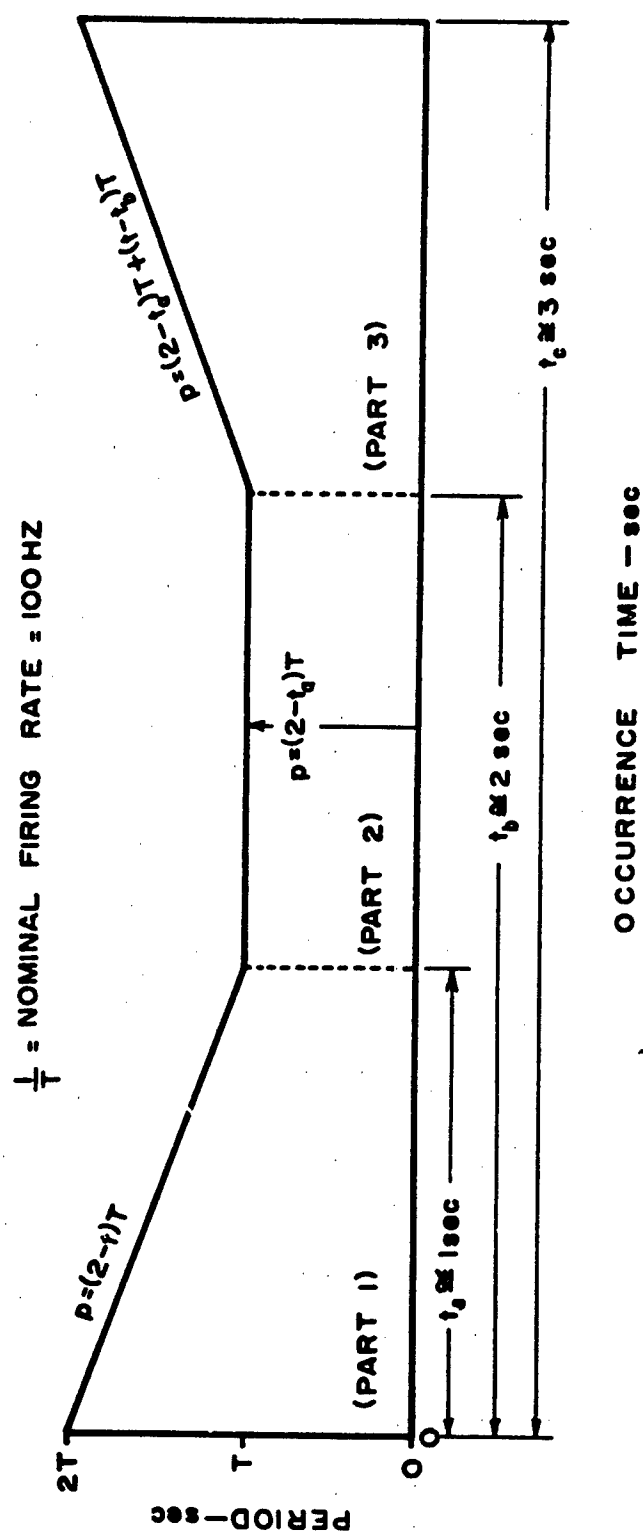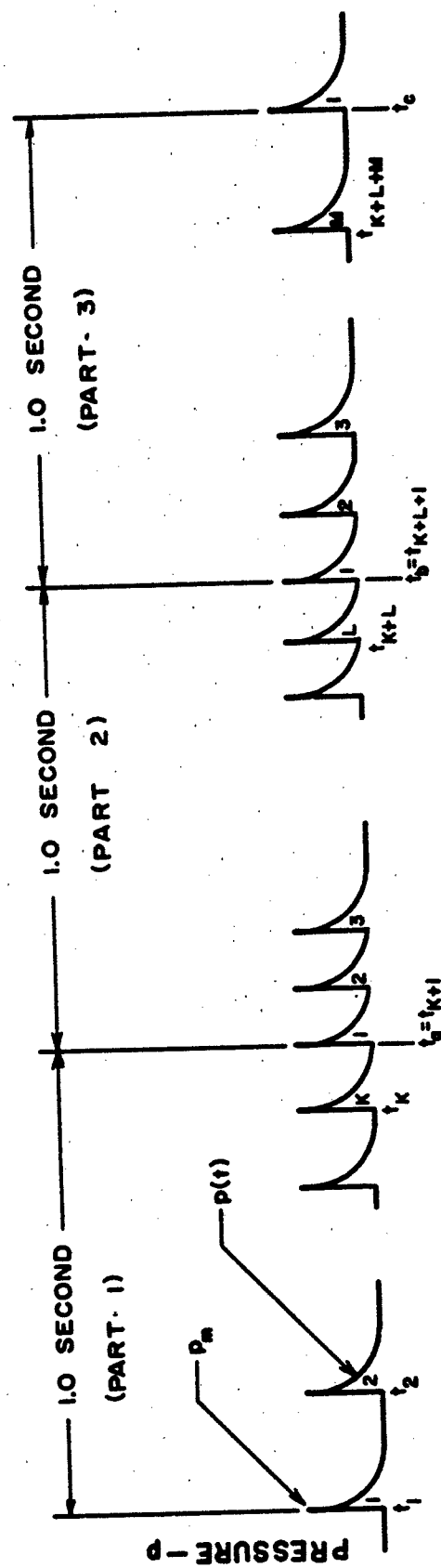
Figure 3. Variable Cycling Rate

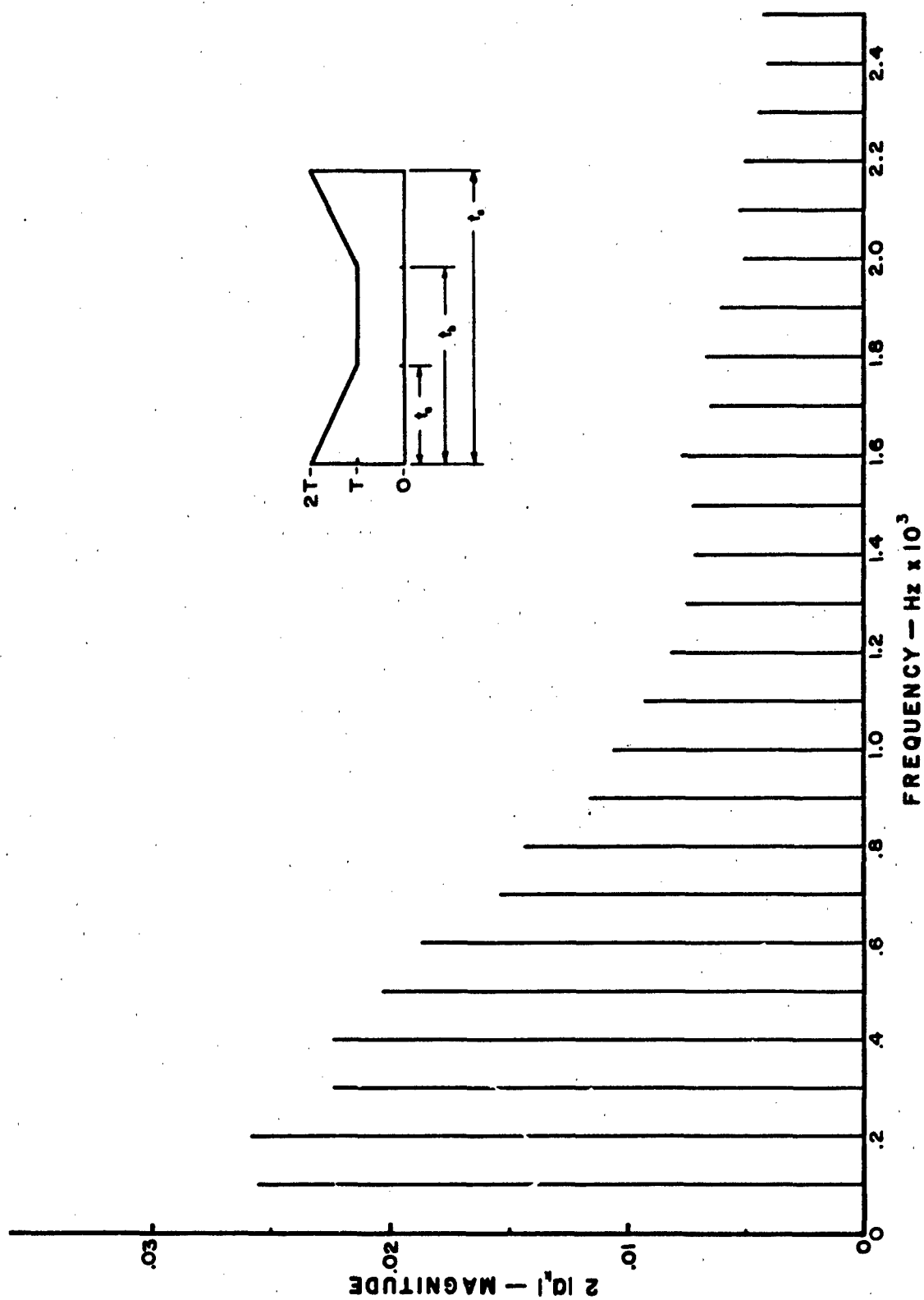Figure 4. Pulse Bursts for Variable Firing Rate

8

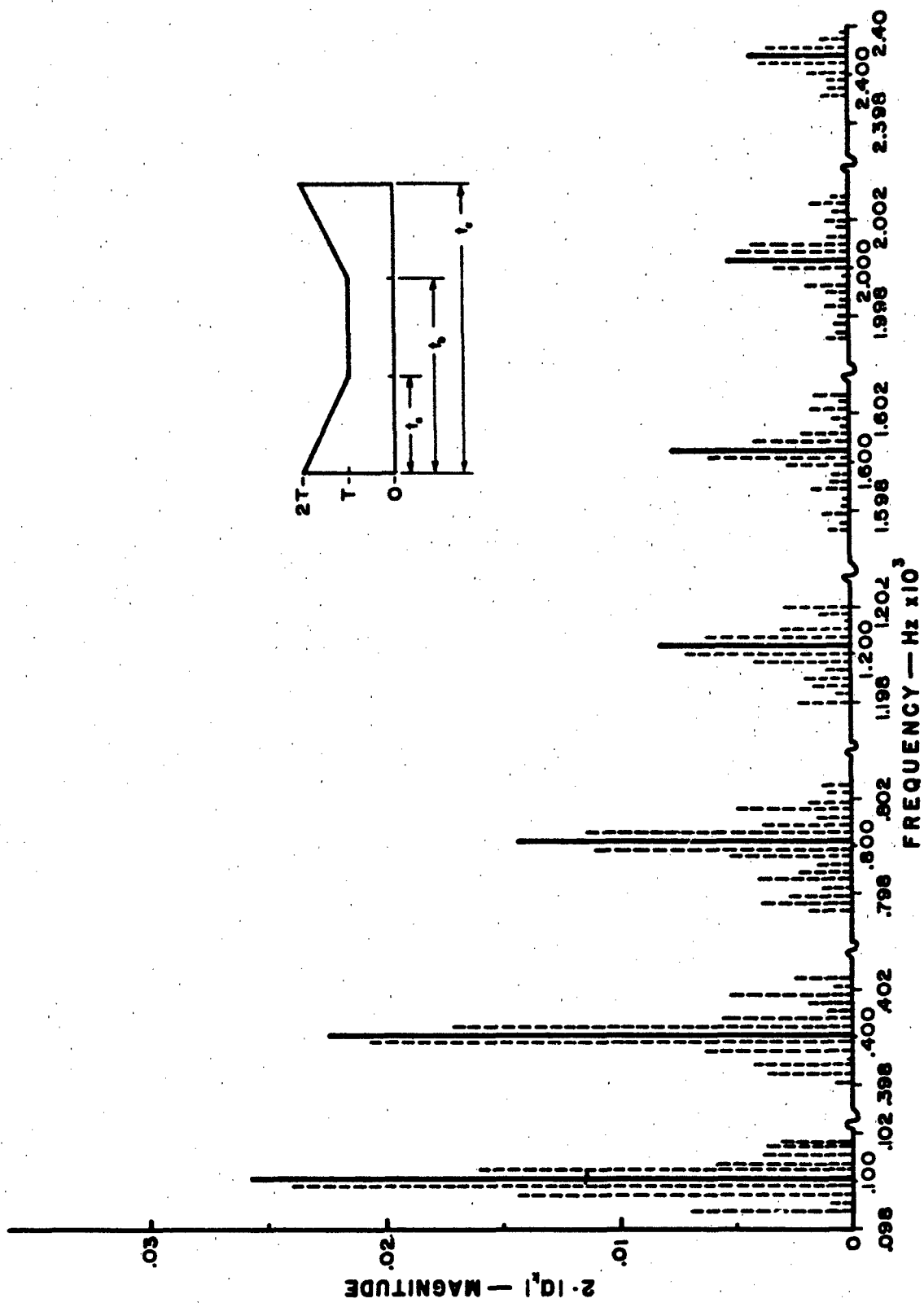Figure 5. Harmonic Model for Variable Firing Rate

Figure 6. Side Bands Generated by Variable Firing Rate Model

proximately 1/3 Hz apart. Of course, similar side band distributions occur about the omitted harmonics (200, 300, 500, 600, 700 Hz and so on).

Other gunfire oscillograms of the same type gun show roll-up times shorter than that of the gun selected for this study. Apparently, our gun (gas operated) is of a sluggish species. This note, apart from being a commentary on the variability of guns (their firing and cycling rates) provokes the thought that if a shorter roll-up time is introduced into the cycling model then one would anticipate that the weighting, provided by a proportionately longer time spent at constant rate, would result in a spectrum that tends to converge to the 100 Hz model of Case I.

In summary, the cycling model shows no significant change in the envelope of the line spectra, which is the Fourier transform P(f) for a continuous spectrum, and results in a generation of spectral side bands distributed about the fundamental firing frequency and about the harmonics.

A study of accelerometer time histories for this type of gun shows the same upper and low frequency anomalies noted in Case I. That is, amplitude distributions above approximately 400 Hz show a predominant random character. Whereas, further down the spectrum, harmonic content appears increasingly dominant.

3. CASE III—UNSYNCHRONIZED, MULTIPLE GUN ARRAYS

Multiple, randomly phased, pulse trains introduce the transform aspect of M. Fourier. But, before proceeding to this alternative, we include an additional assumption comprising this model that is extracted from Case I. We require that the pulse train of each gun be approximately periodic but allowed to deviate about its respective mean firing rate with a distribution that is approximately Gaussian. From Case II, if applicable, the roll-up and roll-down effect on the pulse sequence may also be included in the train history. Finally, the pulse train duration, T, is assumed to be much larger than the time duration of the pulse, t_o.

The available model found most realistic in simulation and tractable in application comes from electrical theory.

The following discussion outlines the main elements of a random pulse train model. For more detailed information, see Reference 4.

Consider a train of gunfire pulses occurring randomly at times $t_1, t_2, t_3 \ldots, t_n$ (Figure 7a). The pulses may overlap or may be widely spaced.

The random pulse train may be characterized in the frequency domain by application of the real translation theorm to the Fourier transform $P_t(\omega)$, of the pulse train, as follows:

$$P_t(\omega) = P(\omega)[e^{-j\omega t_1} + e^{-j\omega t_2} + \ldots + e^{-j\omega t_N}] \qquad (1)$$

where $P(\omega)$ is the transform of the pulse, $p(t)$. And the energy density spectrum $E(\omega)$ is

$$E(\omega) = \frac{1}{2\pi} \cdot |P(\omega)|^2 [e^{-j\omega t_1} + e^{-j\omega t_2} + \ldots + e^{-j\omega t_N}]^2 \qquad (2)$$

where t_1, t_2, t_3, t_4 are pulse occurrence times and are distributed randomly over an ensemble of N pulses.

The exponential series of the right side of Eqation 2 is treated as a two-dimensional random walk problem in which Equation 2 emerges in terms of the power density spectrum, $\psi(\omega)$.

$$\psi(\omega) = r^2 \overline{P}^2(o) \delta(\omega) + r|P(\omega)|^2 \cdot 1/2\pi \qquad (3)$$

where $\delta(\omega)$ is the transform of the unit impulse function, $\delta(t)$

and $\delta(\omega) = 1$ when $\omega = 0$
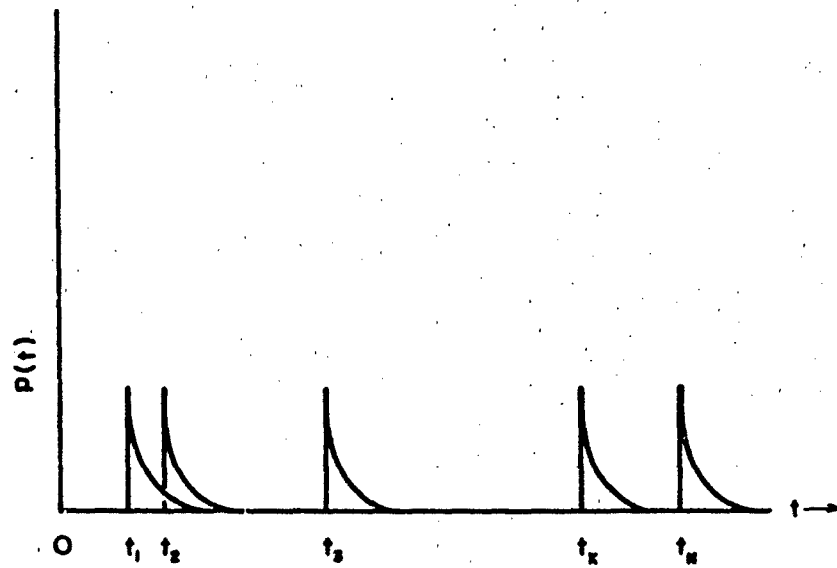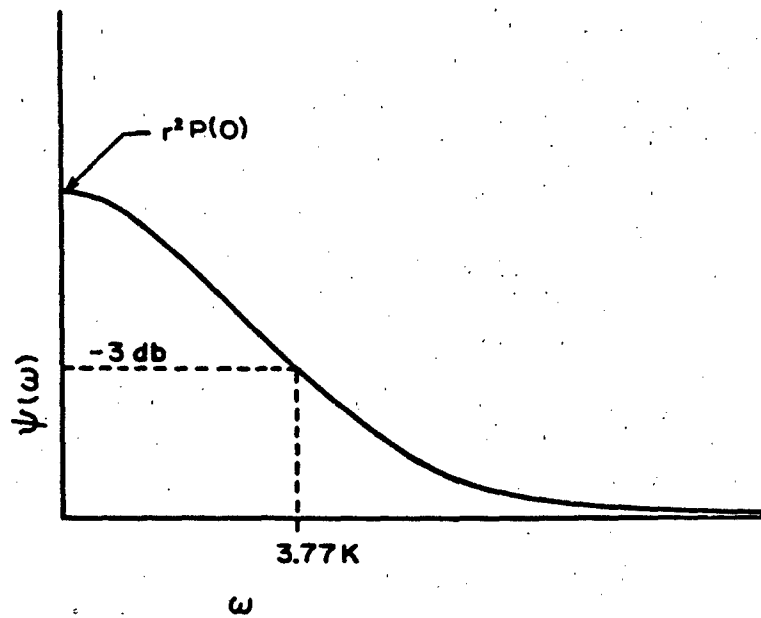
Figure 7. Random Pulse Trains (a) and Power Density Spectrum (b)

$$\delta(\omega) = 0 \text{ when } \omega \neq 0$$

The term, $r^2\overline{P}^2(0)$, represents the DC power spectrum at $\omega = 0$ and is zero elsewhere. Figure 76 depicts $\psi(\omega)$ for the pulse trains.

When the DC term is dropped, Equation 3 simplifies to

$$\psi(\omega) = r|P(\omega)|^2 \cdot \frac{1}{2\pi} \tag{4}$$

If the energy density function, $|P(\omega)|^2$, of the Friedlander pulse is replaced with the corresponding $|P(\omega)|^2$ for a sawtooth pulse, then Equation 4 provides the model for the voltage power density output (volts²/Hz) of a random noise generator—a device that utilizes a noisy diode (shot noise) for the spectrum source.

Strictly speaking, the model described by Equation 4 is not a precise match to the model requirement of Case III. The chief difference resides in the concept of random pulse trains. The gunfire pulse trains are randomly phased with each other, but though variable, each train does exhibit its own periodicity. The model described by Equation 4 admits of no periodicity whatever—only a statistical, average rate. Differences in the spectral details of these two models have not been explored analytically but are expected to be the subject of future inquiry. Experimental evidence does exist (Reference 6), however, and the results (for two guns firing) show accelerometer responses, noticeably random in character beginning at the high frequencies and extending down to below 200 Hz. Even the response amplitudes at the fundamental firing frequency (a beat modulation) can be more accurately characterized as random-like rather than sinusoidal.

The random noise model then seems an acceptable choice for Case III. In retrospect, we note that all three cases possess a significant and highly useful commonality. Above approximately 400 Hz, all exhibit structural response behavior that may be classified as predominately random-like.

It is this feature that we exploit throughout the greater part of the study, beginning with Section III.

SECTION III

THE RESPONSE MODEL

To construct a model relating the muzzle blast pressure to the resultant structural response, we introduce a gun configuration with the muzzle situated a perpendicular distance h from the aircraft surface (Figure 8). The maximum induced structural response, due to coupling with the blast pulses, is conceived to be concentrated at the near field loading area; and as we sight down the distance vector D, we visualize the response magnitudes to propagate radially-decaying as some function of D. Here, a restriction is imposed on the allowable magnitude of h, thus, constraining the parameter as a variable. From a look at Figure 9, we conclude that the pressure isobars decrease appreciably with respect to the muzzle near field values, when h is allowed to be greater than 25 calibers. For our impending model then, it is required that h be less than approximately 25 calibers. Additional restrictions come to mind while we are on the subject of model assumptions, and it is here appropriate to list others thought to be pertinent to the synthesis of the conceptual model.

1. The response contribution of the shock wave traversing the structural surface is presumed to be imperceptible, beyond the near field.

2. The influence on the response due to details of the reflected wave fronts and their interaction with the incident wave are considered to have been obscured by the averaging processes of the response model.

3. The gun muzzles are essentially clean; that is, feature no diffusion, deflectors, or special blast attenuation shrouds.

4. For the multiple gun case, the spacing between muzzles is restricted to approximately 30 calibers.

First, one must get from the gun muzzle to the structure surface. To do this, we consider the relationship between the power spectrum of the blast pulse and the power spectrum of the response.

We make use of energy models by invoking Parsevals theorem which states that the energy, E, contained in a nonperiodic pulse, is equal to $1/2 \pi$ times the area described by the square of the absolute value of the pulse energy density spectrum $|P(\omega)|^2$, or

$$E = \tfrac{1}{2}\pi \int_{-\infty}^{+\infty} |P(\omega)|^2 d\omega \tag{5}$$

The pulse energy per unit frequency is designated $E(\omega)$, so

$$E(\omega) = \tfrac{1}{2}\pi |P(\omega)|^2 \tag{6}$$

The average power per gun, Π, generated by a succession of pulses is equal to the number of pulses, N, divided by the time, T, consumed by the pulse bursts, or

$$\Pi = \frac{N}{T} \cdot E$$

but

$$\frac{N}{T} = r, \text{ the average gunfire rate (pulses/sec)}$$
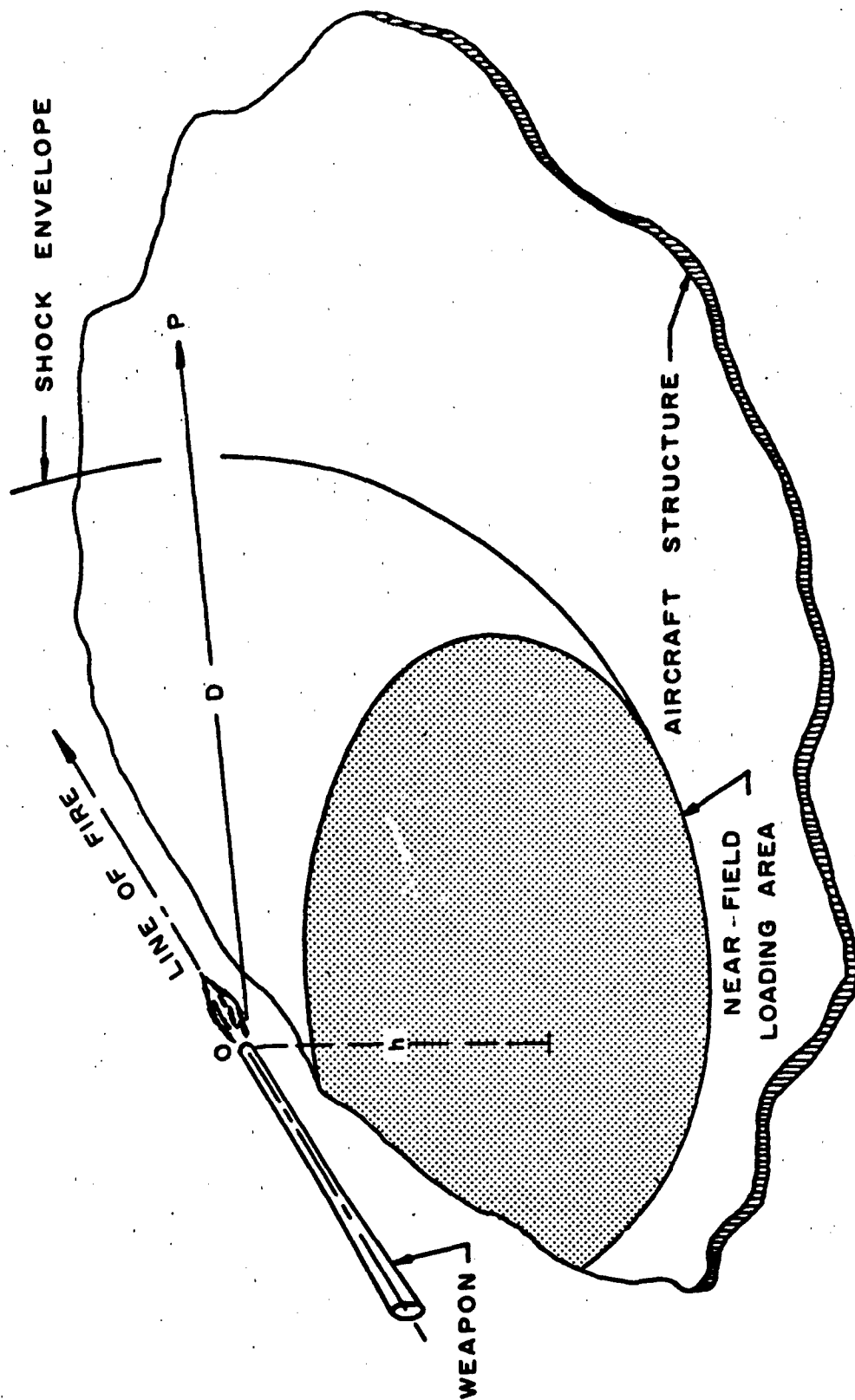
so

$$\Pi = r_1 \cdot E \tag{7}$$

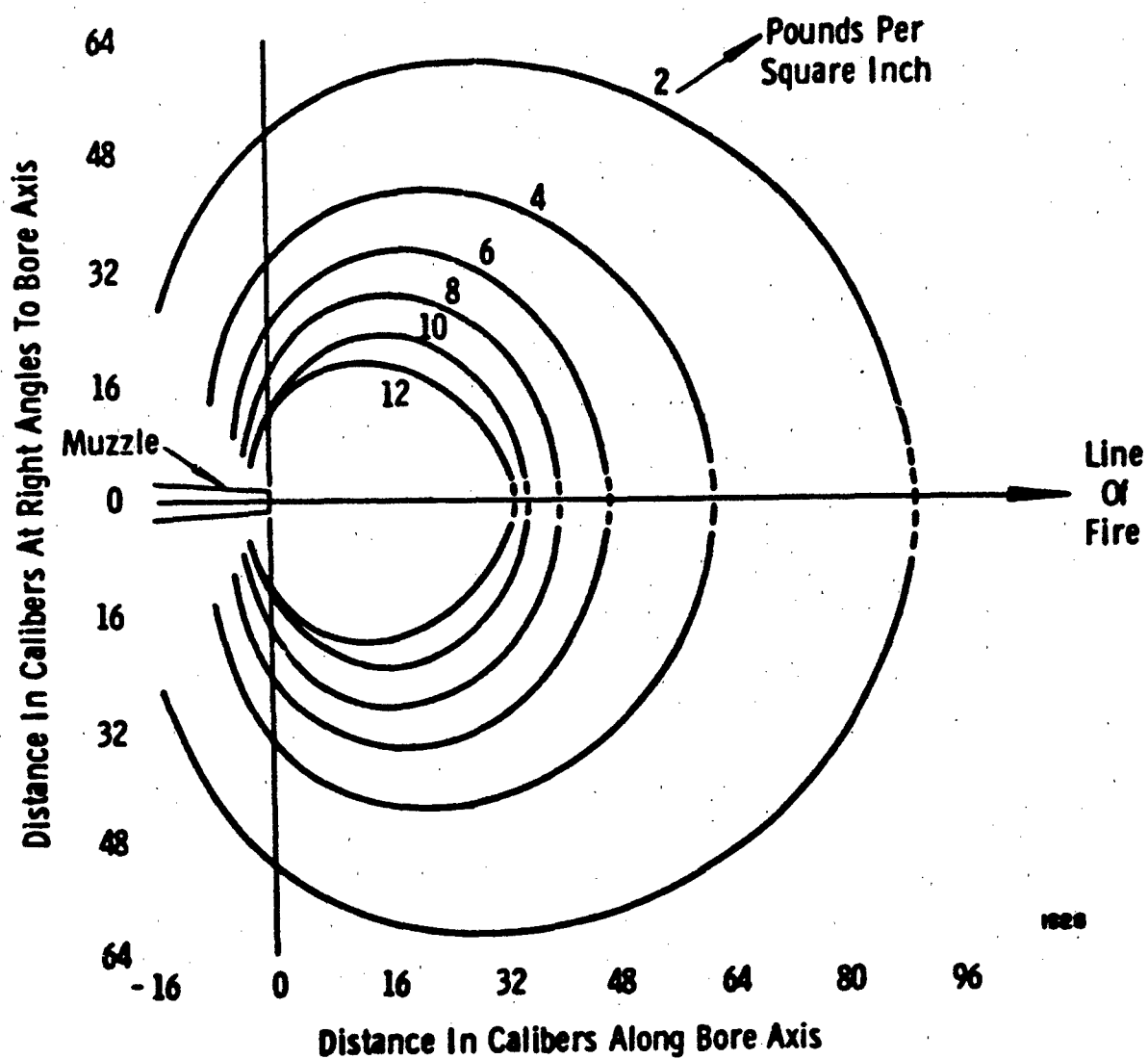Figure 8. Gun Blast Pressure Field

Figure 9. Pressure Contours vs Distance for Free Field

16

And, in spectral power terms

$$\Pi(\omega) = r_1 \cdot E(\omega) \tag{8}$$

Multiplying the energy density function $\frac{1}{2\pi}|P(\omega)|^2$ by r_1, we obtain the spectral power, $\Pi(\omega)$, in terms of $|P(\omega)|^2$. Thus

$$\Pi(\omega) = r_1 \cdot |P(\omega)|^2 \cdot \frac{1}{2\pi} \tag{9}$$

We note that in Equation 9, if we set $r = \frac{1}{t}$ where t is the time period average (of one pulse) of the energy density spectrum, the right-hand term then is the power density spectrum, $\psi(\omega)$.

Substitute in Equation 9

$$\psi(\omega) = r_1 \cdot |P(\omega)|^2 \cdot \frac{1}{2\pi} \tag{10}$$

and using Equations 6, 9 and 10, we have

$$E(\omega) \cdot r_1 = \psi(\omega) \tag{11}$$

and the total power/gun of the pulse is

$$\Pi = E \cdot r_1 = \int_{-\infty}^{+\infty} \psi(\omega) \, d\omega \tag{12}$$

For n guns,

$$\Pi = E \cdot r_1 \cdot n = n \int_{-\infty}^{+\infty} \psi(\omega) \, d\omega \tag{13}$$

To briefly recapitulate, we have expressed the pulse blast of the gunfire in terms of its Fourier transform in the power mode. The primary reason for introducing the power form is that we now propose to linearily relate the acceleration power spectral density of the air-craft structural response to the pressure power spectral density generated by the gunfire pulse trains.

If we knew how much of $\psi(\omega)$ is coupled to the structure and if one could describe the transfer function $|H(\omega)|^2$ relating power input to structural response, $G(\omega)$, then we could designate the power conversion efficiency as $\theta(\omega)$ and describe the structural response thus:

$$\int_{-\infty}^{+\infty} \theta(\omega) \, \psi(\omega) \, |H(\omega)|^2 d\omega \propto \int_{-\infty}^{+\infty} G(\omega) d\omega$$

Unfortunately, we cannot readily assign functional values to $\theta(\omega)$, although, as will be seen in Section IV, we do have a somewhat better (though still generalized) notion of the character of $|H(\omega)|^2$.

Our approach to this difficulty is to make use of similitudes, equate coupled power of the pulses to structural response, and eliminate intractable properties as shown in the following steps. Let $\theta(\omega) \, |H(\omega)|^2 \, \psi(\omega)$ equal the spectral power flow into the structure and let the resultant power spectral density of the structural response be designated $G(\omega)$. Equating spectral power input to structural response,

$$\theta(\omega) \, |H(\omega)|^2 \, \psi(\omega) = \beta G(\omega) \tag{14}$$

Substitute Equation 11 in 14,

$$\theta(\omega) \, |H(\omega)|^2 \, E(\omega) \, r_1 = \beta G(\omega) \tag{15}$$

Assume a reference gun (with zero subscripts),

17

$$\theta_n(\omega) \, |H_n(\omega)|^2 \, E_n(\omega) \cdot r_o = \beta G_o(\omega) \tag{16}$$

Dividing Equation 15 by 16 and rearranging gives

$$G(\omega) = E(\omega)/E_n(\omega) \cdot r_1/r_o \cdot \theta(\omega)/\theta_o(\omega) \cdot G_o(\omega) \cdot |H(\omega)|^2/H_o(\omega)|^2 \tag{17}$$

The power transfer efficiency, $\theta(\omega)$, and the power transfer function, $|H(\omega)|^2$, are assumed to be the same for both guns. Thus, $\theta(\omega) = \theta_n(\omega)$ and $|H(\omega) = |H_o(\omega)|$. Expression 17 then becomes

$$G(\omega) = E(\omega)/E_n(\omega) \cdot r_1/r_o \cdot G_o(\omega) \tag{18}$$

In terms of overall mean squared response, Equation 18, is shown as

$$\int_{-\infty}^{+\infty} G(\omega) \, d\omega = E/E_o \cdot r_1/r_o \cdot \int_{-\infty}^{+\infty} G_n(\omega) \, d\omega \tag{19}$$

We introduce the muzzle energy E' by proportioning it to E

$$E' = \alpha E \text{ and } E_n' = \alpha_n E_o \tag{20}$$

The proportionality constant, α, is assumed to be the same for both guns

$$(\alpha = \alpha_o).$$

Substituting Equation 20 into 19 gives

$$\int_{-\infty}^{+\infty} G(\omega) \, d\omega = E'/E'_o \cdot r_1/r_o \int_{-\infty}^{+\infty} G_n(\omega) \, d\omega \tag{21}$$

Finally, since the responses are normalized to one gun, we insert n and n_o to account for multiple gun configurations, see Equation 13. Thus Equation 21 becomes

$$\int_o^\infty G(\omega) \, d\omega = E'/E'_o \cdot n/n_o \cdot r_1/r_o \int_o^\infty G_o(\omega) \, d\omega \tag{22}$$

The appearance of the gun muzzle energy is welcome. Normally this property is readily available and so provides us with a much needed parameter to facilitate the prediction process. The muzzle energy is equal to $mv^2/2$; where m is the projectile mass and v is the muzzle velocity.

We have expressed the predicted overall mean squared response of an unknown gun configuration in terms of its muzzle energy, the number of guns, and the firing rate—all normalized to some known gun system having like variables.

To establish the necessary relationship of the parameters of Equation 22 to their proper place in the regression analysis beginning with Section V, we now turn to Section IV. In this section we discuss general characteristics of aircraft structural response, details of data processing and presentation, gunfire configurations, ballistic parameters, selection of accelerometers, and review other pertinent details that, in their varied ways, are associated with the development, evaluation, and application of the gunfire power model.

18

SECTION IV

DATA PROCESSING; DISPLAY

1. RESPONSE SPECTRUM

As suggested earlier, the spectral form of the response has influenced the manner in which we have selected, organized, and presented the data for regression analysis—an examination of the response characteristics is necessary to explain how the data has been processed and why it appears in the form that it does, and in what way the response envelope enters into the prediction model.

If, for example, we select as an input Fourier spectrum $F(f)$, obtained from the blast pulse (Figure 76) and supply a generalized frequency response function $H(f)$, typical of aircraft structures then for the response function, $R(f)$:

$$R(f) = F(f) H(f)$$

Phase information is assumed to be random; a continuous random spectrum is also assumed; further $F(f)$ and $R(f)$ is expressed in 1/3 octave, mean squared density ideom:

$$[R(f)]^2 = [F(f)]^2[H(f)]^2 \qquad \text{(Figure 10)}$$

The resultant spectral response is shown in Fig 10c. $[R(f)]^2$ exhibits the familiar roll-up, peak, roll-down form so frequently encountered during 1/3 octave data analysis of accelerometer outputs in response to gunfire excitation.

To continue, the spectral shape of the response is generalized by flattopping the peak region and (using log-log axes) representing the roll-up and roll-off portions of the curve with straight lines. The curve will then appear as shown in Figure 11.

19
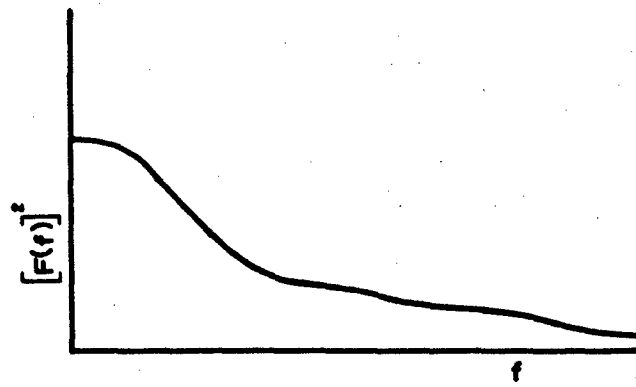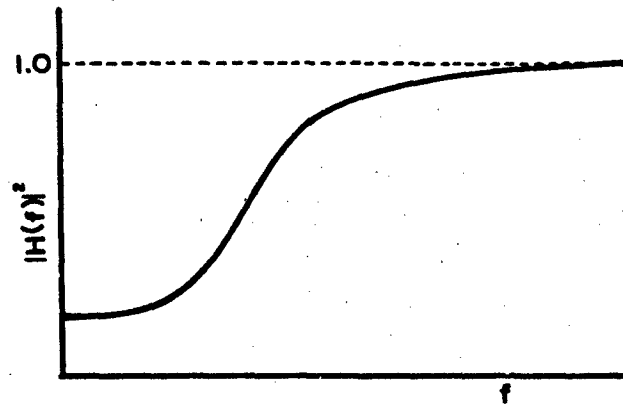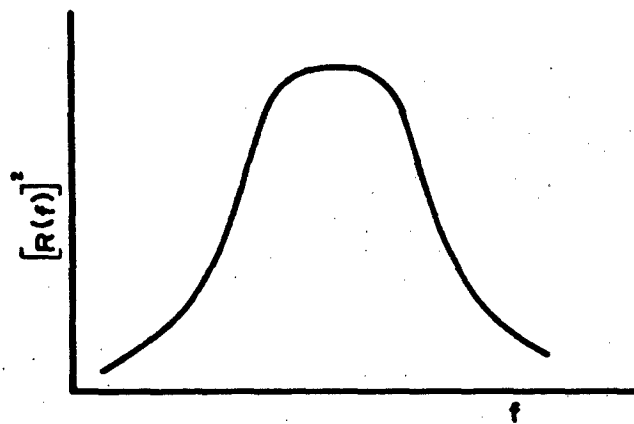
Figure 10. Generalized Vibration Field of Aircraft Structure

20
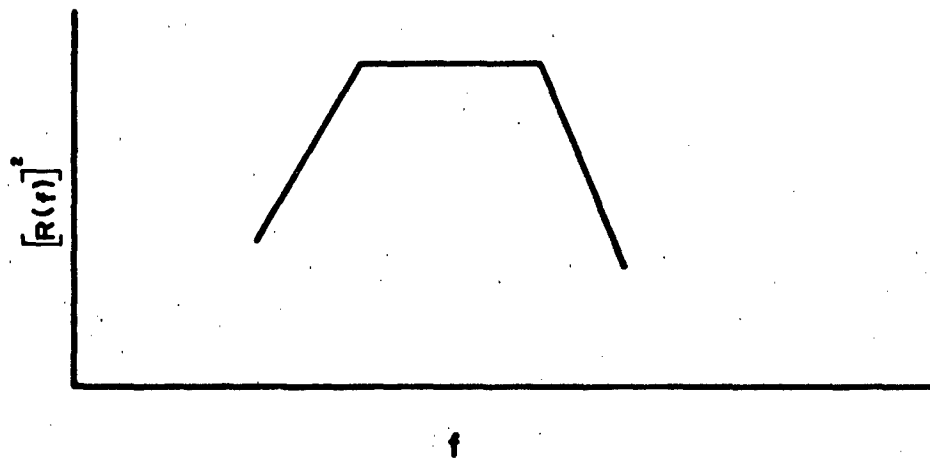
Figure 11. Generalized Response of Aircraft Structure

An examination of the gunfire data in this study (see Figures 41, 42, 43, and 44, Appendix III) results in the estimation of corner frequencies and slopes as indicated in Figure 12.
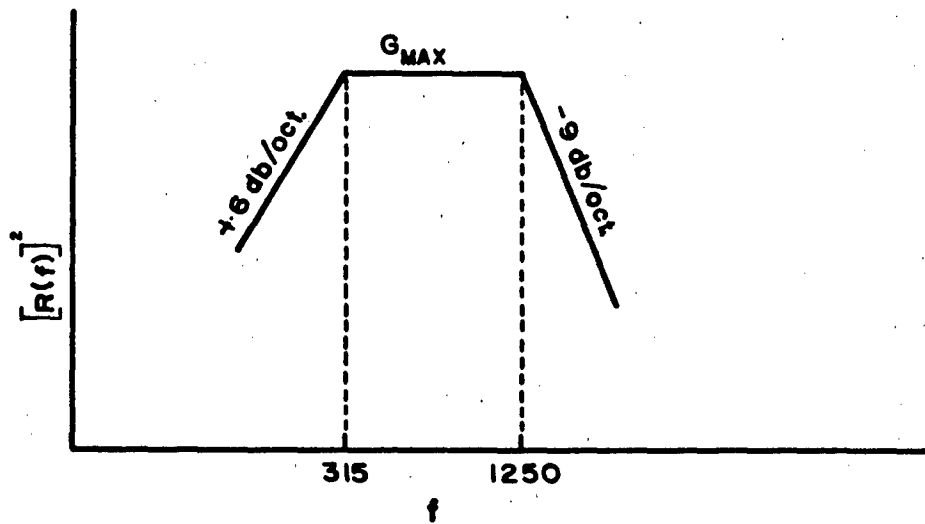
Figure 12. Corner Frequencies and Roll-Off Slopes of Structural Response

21

Now, if we concern ourselves primarily with the 1/3 octave response between 315 to 1250 Hz, then for a given accelerometer located a distance D_1 from the gun muzzle, the response data might appear as shown in Figure 13.
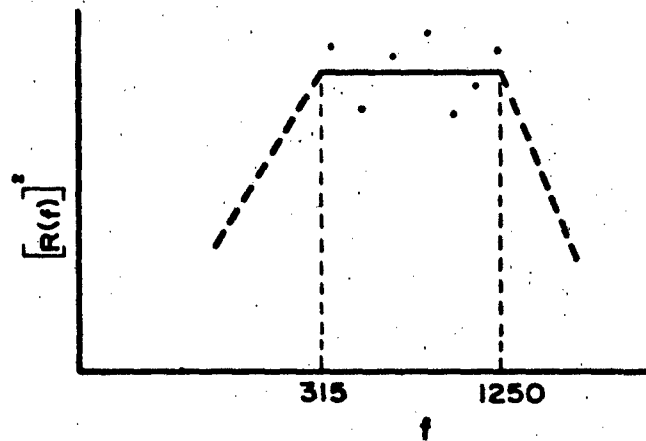
Figure 13. 1/3 Octaves of Response

Finally, if we rotate the plot 90° such that the frequency axis now runs into the page and further, if we include the responses from other accelerometer samples located at their respective distances from the gun, then we might have the following display of the data points, Figure 14.
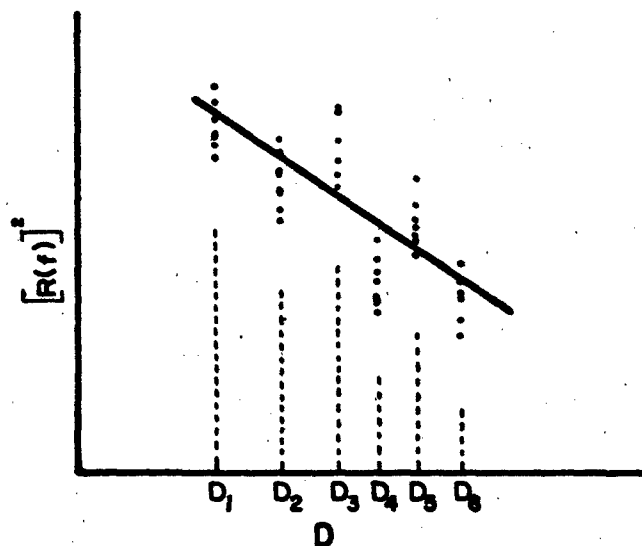
Figure 14. Presentation of Response vs Distance

The response, $[R(f)]^2$, is displayed as a function of the distance parameter, and the solid line represents the regression line generated from a least squares fit for the data. Now substitute $G_o(f)$ in place of $[R(f)]^2$. This display of the data will be encountered exclusively in the following sections. Note that, for the regression technique employed here, the structural response, $G_o(f)$, is confined to the plateaued segment of the spectral response and that the response data is presented in 1/3-octave acceleration power spectral density form.

We return to Equation 22, which is restated

$$\int_o^{+\infty} G(f)\,df = E'/E'_o \cdot n/n_o \cdot r_i/r_o \int_o^{+\infty} G_o(f)\,df \qquad (22)$$

We assume the generalized response function (Figure 10) to be invariant in shape but having a maximum ordinate value, $G_o(f)$, that is a linear function of power, thus:

$$\int_o^{+\infty} G_o(f)\,df = \beta G_o(f) \quad \text{and} \quad \int_o^{+\infty} G(f)\,df = \beta G(f)$$

Substituting the above equations into Equation 22 and rearranging into normalized form, we have

$$G(f) = E'/E'_o \cdot n/n_o \cdot r_i/r_o \cdot G_o(f) \qquad (23)$$

We sort out the reference part of the power model:

$$E'_o \cdot r_o \cdot n_o = \beta G_o(f) \qquad (24)$$

From hereon our efforts will involve a two-pronged course: to evaluate and define the parameters of Equation 24 and to attempt the description of the decay function relating $G_o(f)$ and the distance parameter, D. Both efforts involve regression analysis applied to gunfire data obtained from four different gun configurations of approximately equal muzzle energies.

2. GUN CONFIGURATIONS

The response data from accelerometers located in two different aircraft was processed. The data was obtained from three configurations of the F-4 and one of the F-5A.

The nose configuration of the F-4E is shown in Figure 15, and is referred to in the data and charts as simply F-4. This arrangement features the M-61 type cannon arranged as six barrels firing consecutively during revolution and is sometimes identified as the Vulcan or the gattling gun.

The remaining two gun configurations consist of 20-mm cannons located in pod packages that are mounted beneath the aircraft surface and on centerline. They are designated the SUU-16 and the MK-IV pods and are shown in Figure 16. The MK-IV pod consists of two barrels side by side firing simultaneously, while the SUU-16 pod features one barrel only. Both of these configurations hereafter will be referred to as the MK-IV and SUU-16.

Two M-39A2 cannons are fuselage mounted in the top side of the F-5A aircraft and forward of the cockpit as shown in Figure 17. The guns are spaced approximately 24 inches apart. This configuration will be referred to as the F-5. One important feature of the F-5A must be stressed: there are two retractable deflectors located at the gun muzzles. These devices are employed during gunfire, therefore during the data acquisition phase, and serve to deflect the gaseous charge up and away from the inlets of the engine intakes in order to prevent engine stall. This special feature and its influence on the decisions concerning the final stages of regression analysis will reappear in Section VI.

In summary, all configurations represent variations of the 20-mm cannon and all feature the
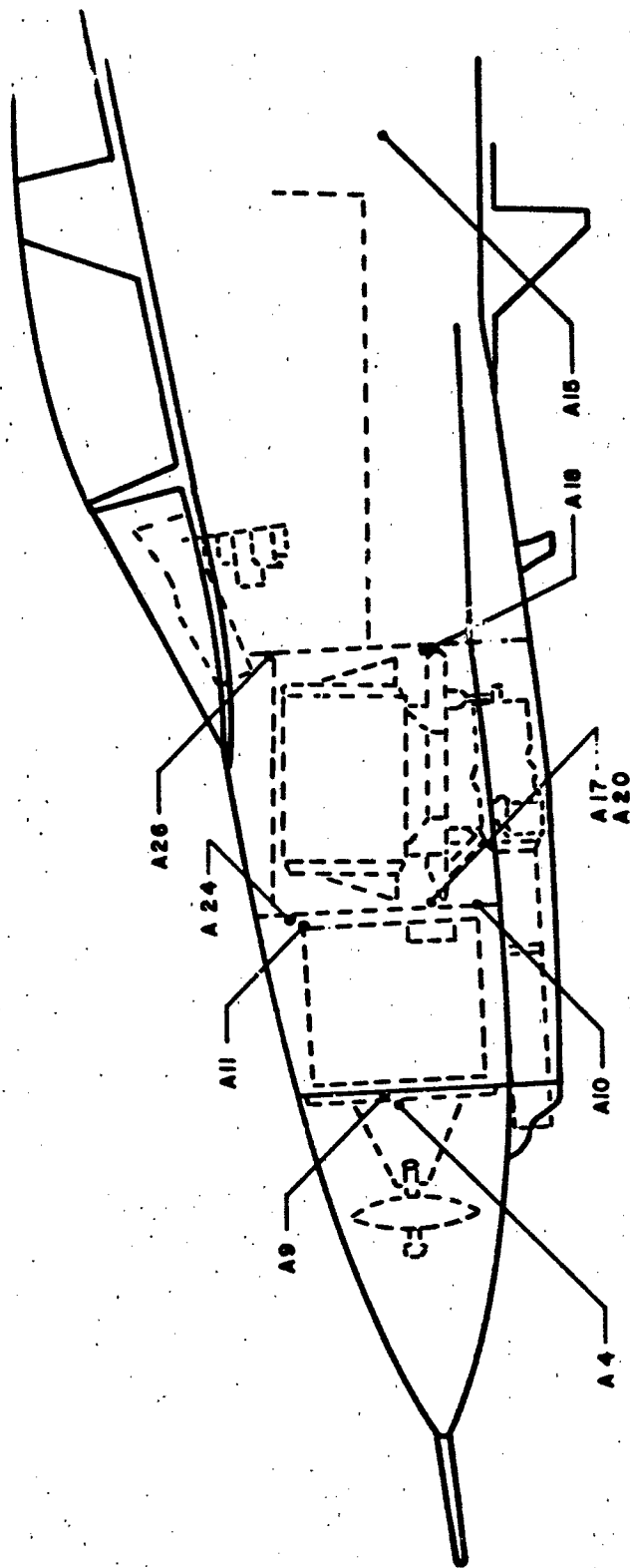
Figur 15. F-4E Gunfire Configuration and Accelerometer Locations

SCALE: 1"= 31.4"

24

Figure 16. SUU-16 and MK-IV Gunfire Configuration

SCALE: 1" = 36.5"

Figure 17. F-5A Gunfire Configuration and Accelerometer Locations

26

same muzzle energies. They differ chiefly in the number of guns and firing rates. The two parameters (number of guns and firing rate) figure importantly in the gunfire model, will be referred to frequently, and are listed in table I for reference.
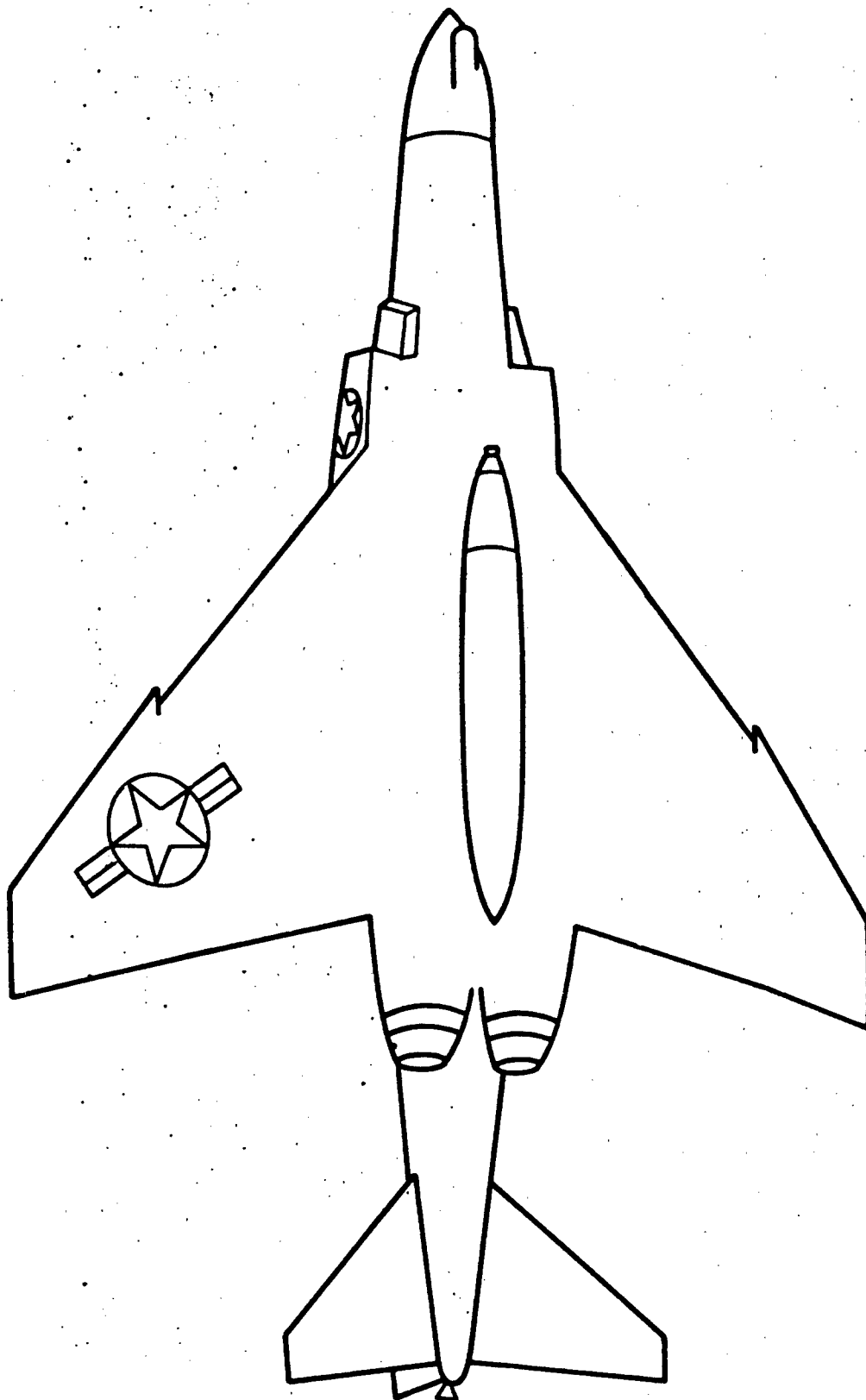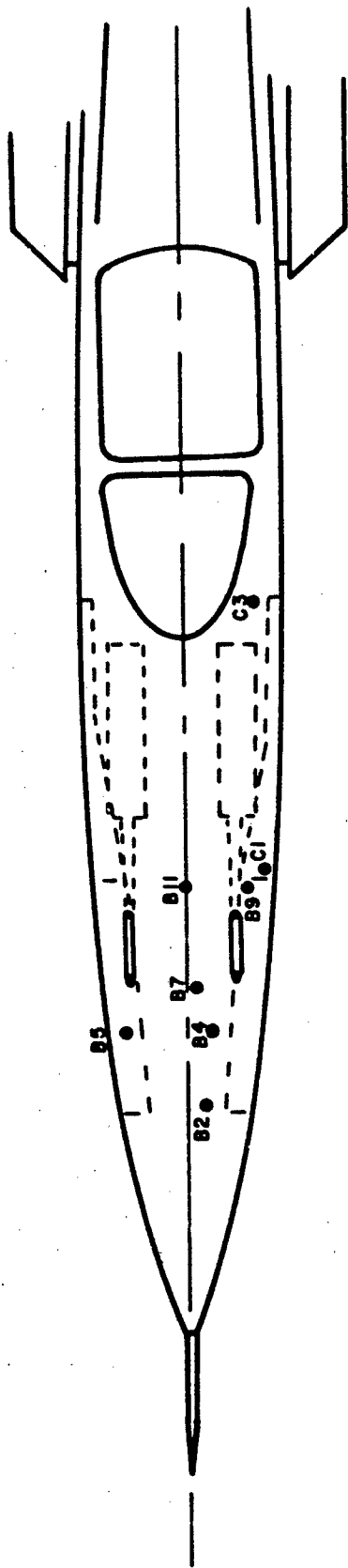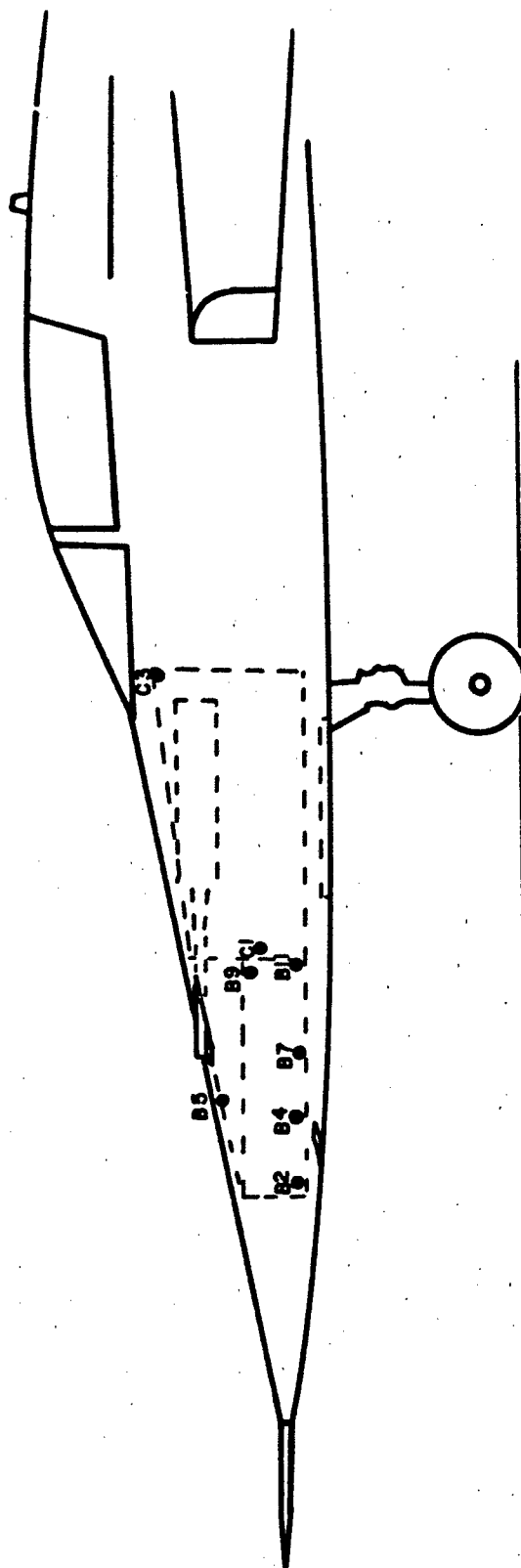
TABLE I

GUNFIRE MODEL PARAMETERS

Configuration	Firing Rate $r(Hz)$	Number of Guns, n	$n \cdot r$	$(ft - lbs)$
F-4	90	1	90	39,600
SUU-16	100	1	100	39,600
MK-IV	35	2	70	39,600
F-5	27	2	54	39,600

3. ACCELEROMETER LOCATION

Wherever possible, accelerometer data were selected from transducer locations most representative of the primary structure and positioned as close to the skin surface as possible. In general, the volume enclosed by the skin surface to a depth of 10 to 12 inches included most of the accelerometer locations.

4. DETERMINING D

The D parameter represents the vector distance from the gun muzzle point to the selected accelerometer location and was calculated from the three orthogonal distances referenced from the butt line, fuselage, and the water line coordinates. Figure 18 represents a typical spatial arrangement from which D is determined.

5. VIBRATION DATA CONVERSION

All of the gunfire data used in this study was obtained from References 1, 2, 7, and 8 and appeared in $\frac{1}{3}$ octave form. Data not processed originally in RMS g terminology was so converted. The g values were squared and divided by their appropriate $\frac{1}{3}$ octave bandwidths and presented as $G_o(f)$ in units of acceleration power spectral density.

6. GUNFIRE FLIGHT CONDITIONS

Both F-4 and F-5 gunfire data were recorded during similar flight condition at approximately 5000 feet altitude and at Mach 0.85.

7. REGRESSION ANALYSIS

Regression analysis involved the method of the least squares, the details of which are contained in Appendix I. The regression lines of the figures are bounded by 95% confidence limits for the line as a whole. Stated another way: if each of the gunfire runs were repeated, there exists a 95% probability that a regression line, obtained from the new sample, will fall within the limits indicated by the confidence band.

27
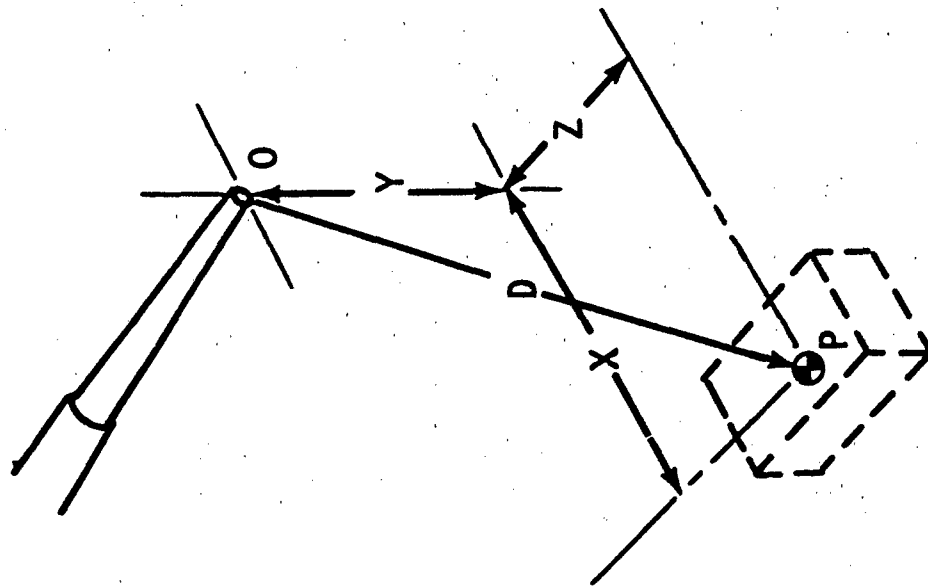
$$D = \overline{OP} = (X^2 + Y^2 + Z^2)^{1/2}$$

Figure 18. Determination of the D Vector

SECTION V

POWER MODEL EVALUATION

Figures 19 and 20 show an example of the response amplitude plotted against D and represents a gunfire vibration sample presented in both the linear and logarithmic plane, respectively. Both data plots illustrate the nature of the decay that suggests an exponential model and so the basic expression for the decay model is assumed to be a regression line of the form:

$$G_o(f) = \beta_o D^{-z} \tag{25}$$

For a given muzzle energy, the response, $G_o(f)$ is also proportional to the firing rate, r, and the number of guns, n — if we recall the power model derived earlier and represented by Equation 24. Thus, from a power model viewpoint, Equation 25 can also be expressed in the normalized mode as follows:

$$G_o(f)/r_o n_o = \beta_o D^{-z}/r_o n_o \tag{26}$$

Ideally, if the power model reigns, we could normalize the data of each configuration (F-4, F-5, SUU-16, MK-IV) to their respective n's and r's and since they have the same muzzle energies then the prediction model represented by Equation 29 requires that the corresponding $G_o(f)$'s of each configuration be equal. In fact (assuming that each configuration curve has the same decay, or slope value, the curves would converge to one line. But in the real world, (as the lamentation goes) where at best, models represent good approximations and where data scatters remains perhaps the only certainty, we are prudent to expect less dramatic results.

Suppose we compare the data in the following way: pool the data of the four separate configurations, Figure 21, and then conduct a regression analysis of the total assembly of data. The regression line obtained from the least squares fits Figure 22 is, for this case, presumed to be independent of the power parameters n and r and is of the form of Equation 25. Next, the data of each configuration is normalized to its respective n's and r's (obtained from Table I) then the data is pooled, and following this, subjected to a regression analysis (Figure 23). In comparison to the unnormalized case, we would expect (if the power model represents a viable premise) that, on the average, the data of each normalized configuration would tend to converge. If so, then the goodness of fit or multiple correlation coefficient, C_r, would increase somewhat, the dispersion and the standard error S_y' should likewise decrease. Comparative values of C_c and S_y' resulting from this procedure are listed in Table II.

TABLE II

REGRESSION ANALYSIS

	C_c	S_y'	Slope (z)
Pooled	.6162	.7062	-2.64
Pooled and Normalized	.6572	.6881	-2.87

As noted in Table II, C_c and S_y' increase and decrease respectively, in agreement with the prior hypothesis. Note that when stated in the converse, the hypothesis is not necessarily true. To rephrase: the stipulation that C_c increase and S_y' decrease is necessary but not sufficient to validate the power model. Conceivably, one could obtain similar results using some other assumed model. Nevertheless, the improvements in C_c and S_y', though small, are in the right direction. For additional checks of the power model, we must look elsewhere.

SUU–16

$G_c(f) - G^2/Hz$
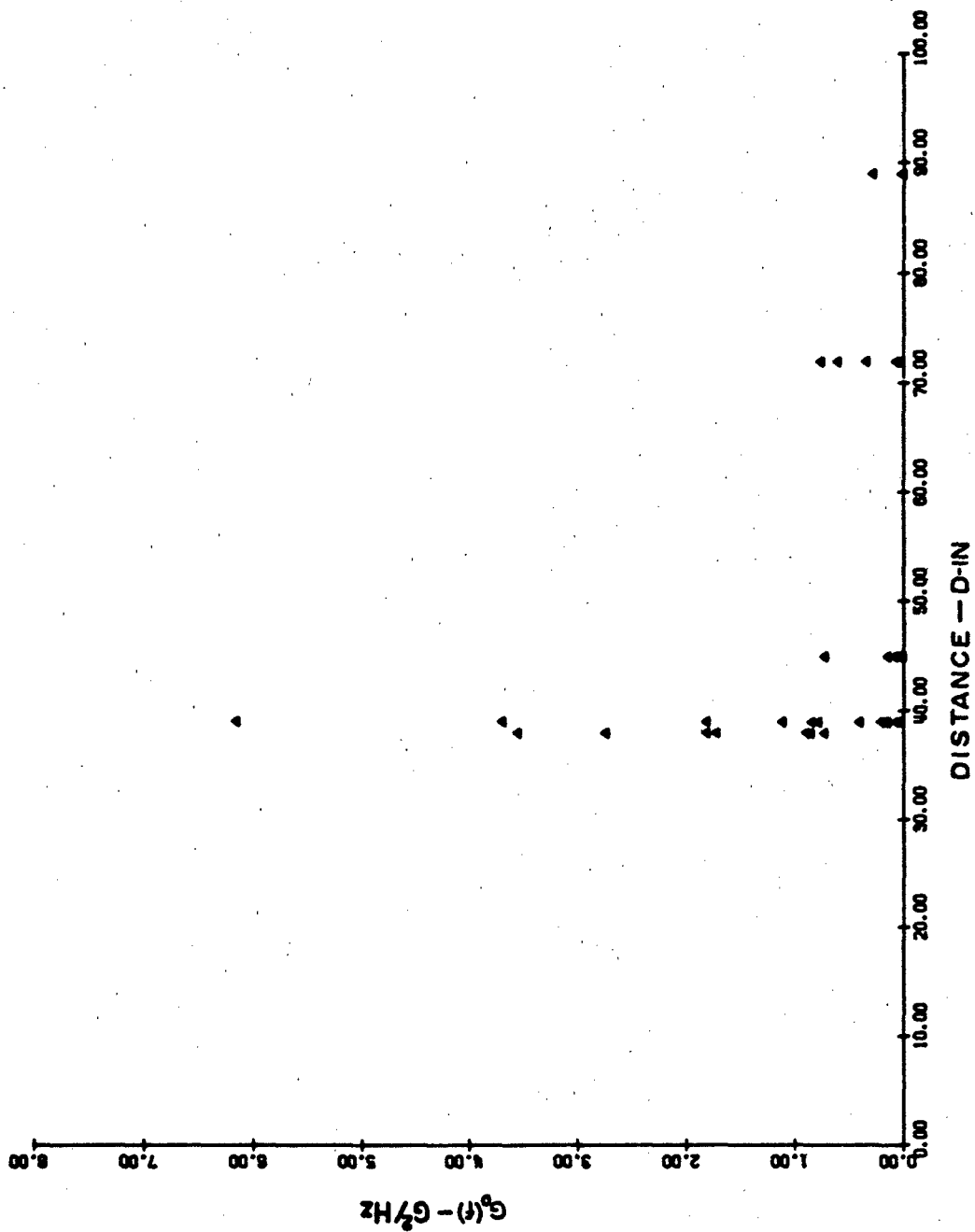
DISTANCE — D-IN

Figure 19. Structural Response vs Distance Plotted in Cartesian Plane

30

SUU-16

DISTANCE — D-IN

$\phi_g(f) - G^2/Hz$
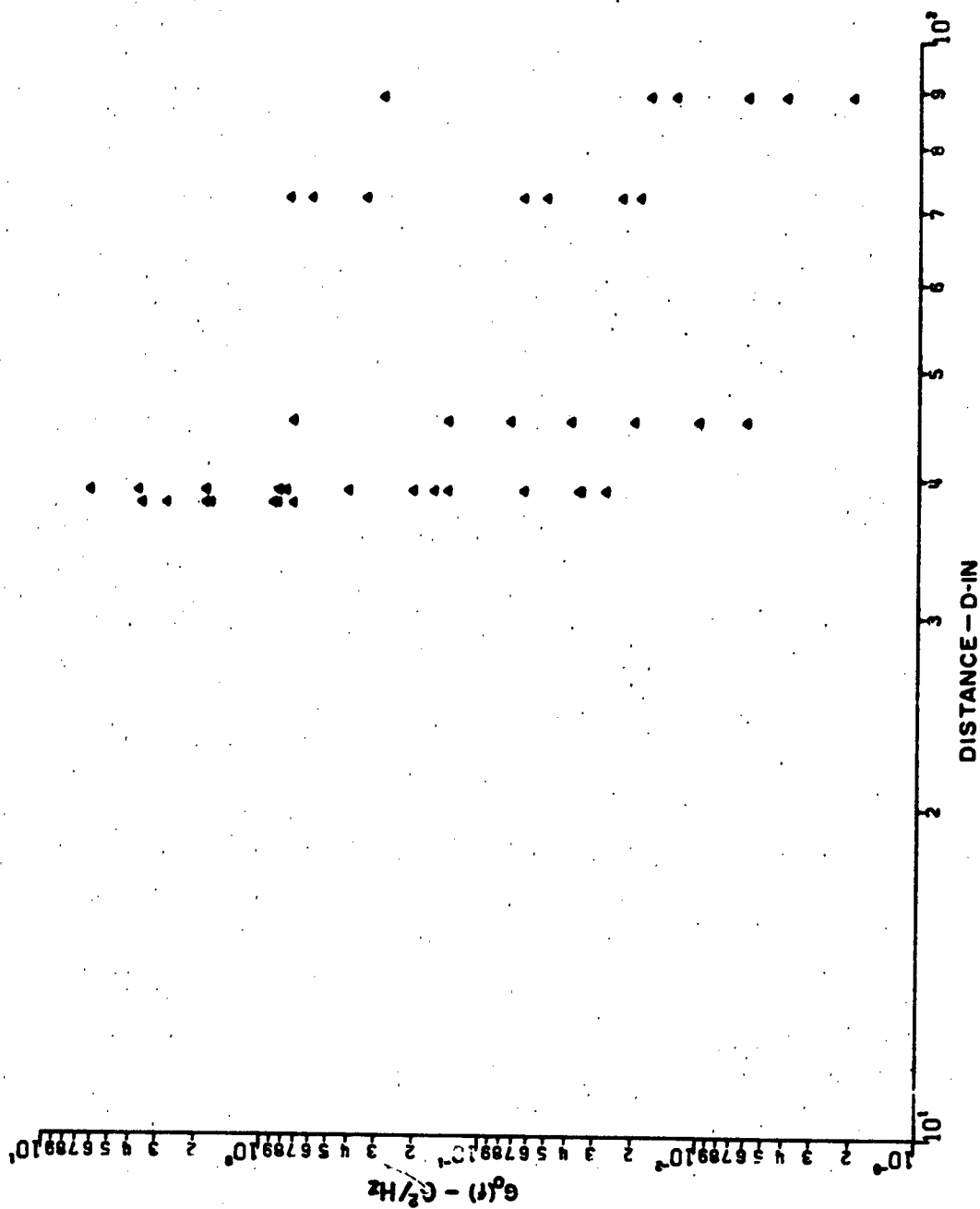
Figure 20. Structural Response vs Distance Plotted in Log-Log Plane

81
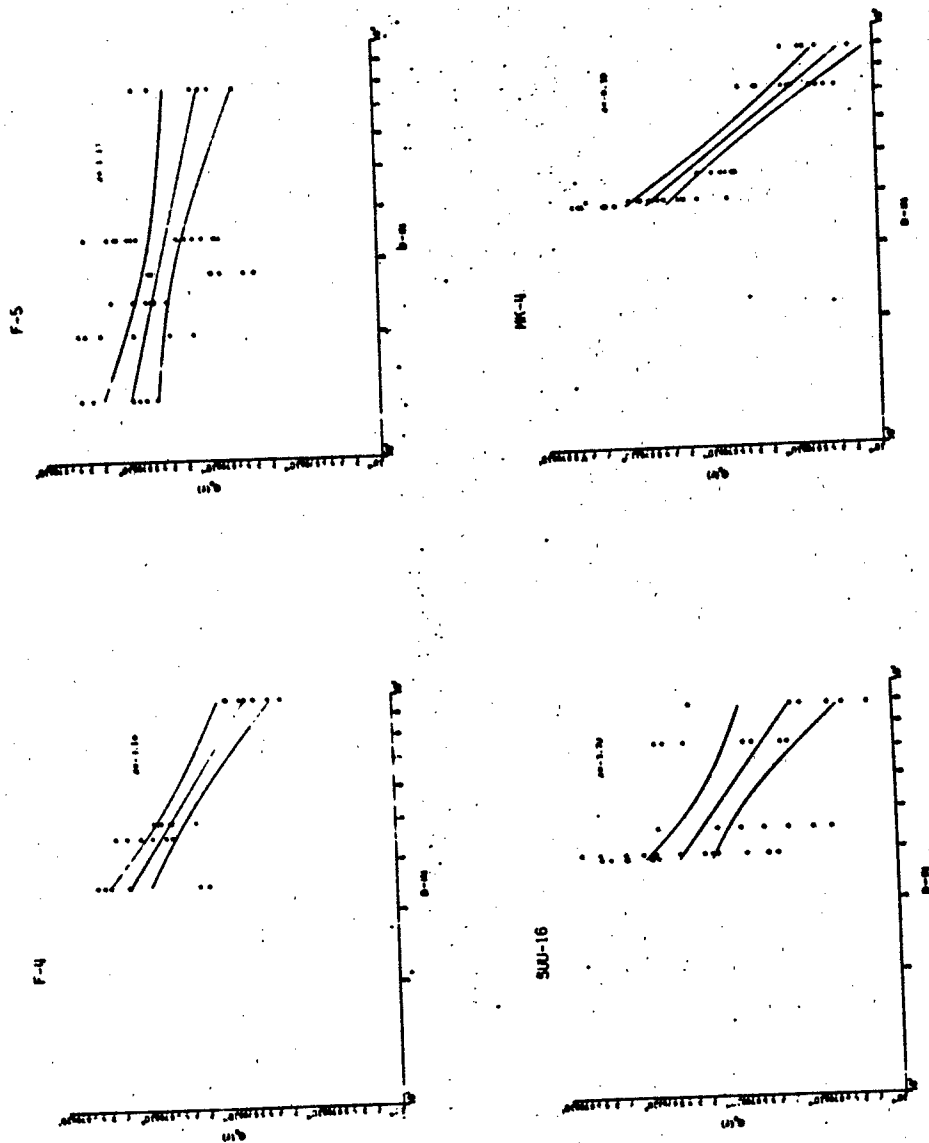
Figure 21. Regression Analysis of Gunfire Vibration for Four Gun Configurations

32
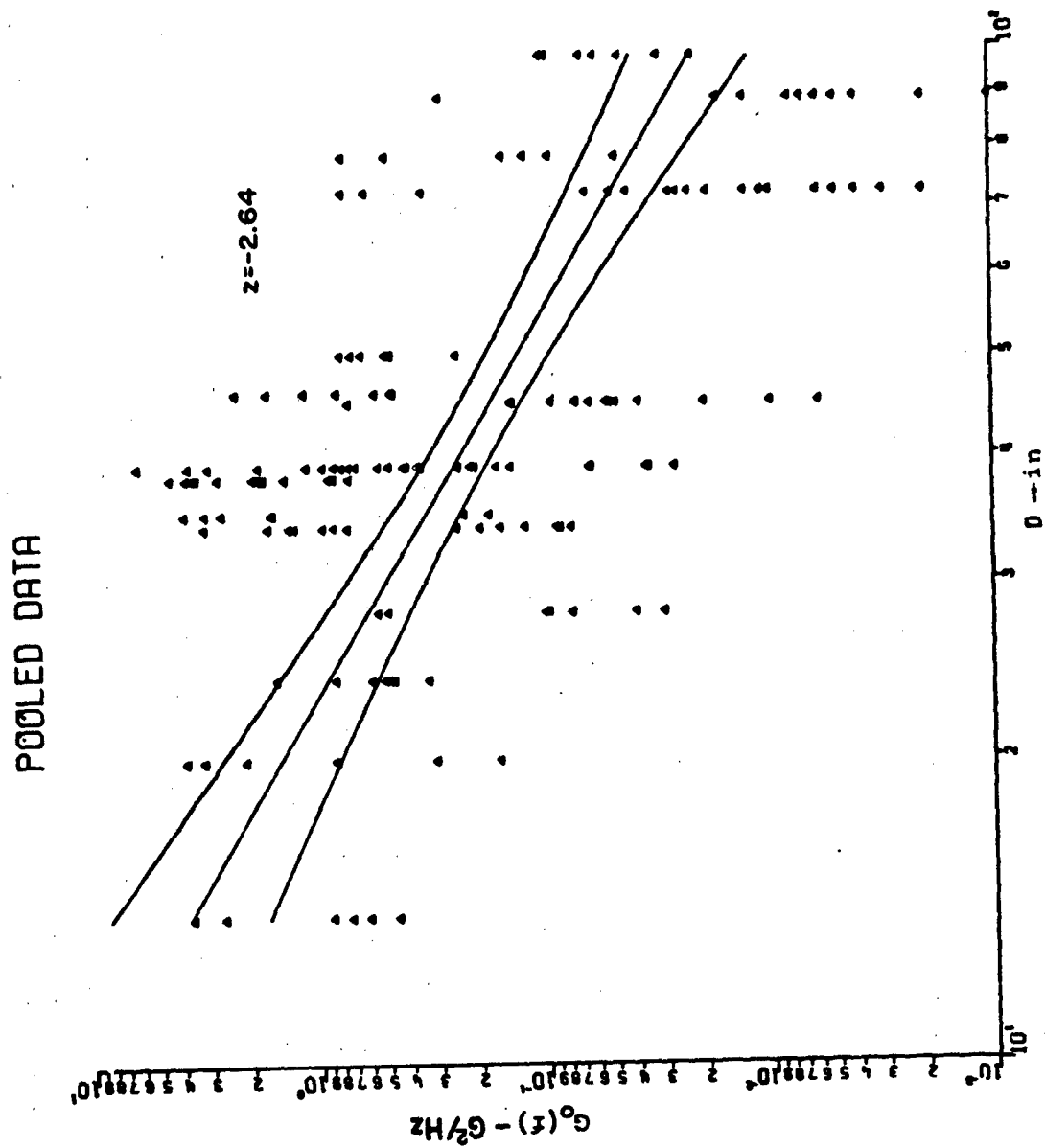
Figure 22. Regression Analysis for Four Gun Configurations
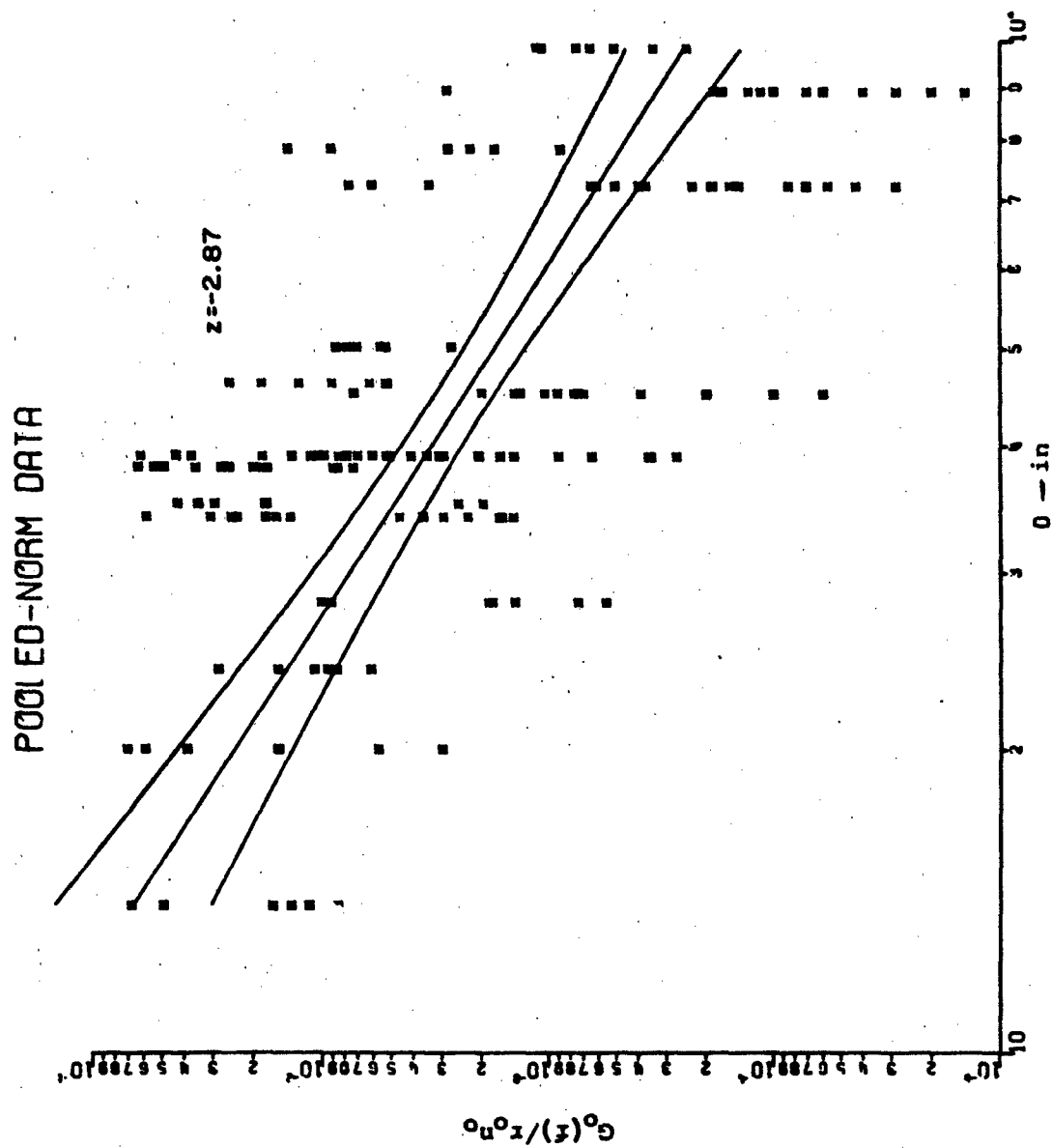
Figure 23. Regression Analysis for Four Gun Configurations

During the gunfire program of the F-5 (Reference 2), $\frac{1}{3}$ octave vibration data was recorded from an accelerometer with both guns firing and then with only one gun operating. Here, is a case for the power model in which n changes from 2 to n = 1. Under these conditions, the power form for the single gun requires that $G_n(f)$ be halved. Figure 24 shows a response plot for both cases. On the whole, the vibration level does decrease, and, on the average, a decrease of 3db would be a reasonable estimate. Unfortunately, a similar record was not available permitting a corresponding check of the firing rate, r.

In summary, the use of comparative analysis utilizing regression techniques supported by separate evidence, in which the test variable is n, lends support to the power model.

We proceed to the next step which involves further refinement of the data and the determination of the decay slope of the composite (pooled) data.
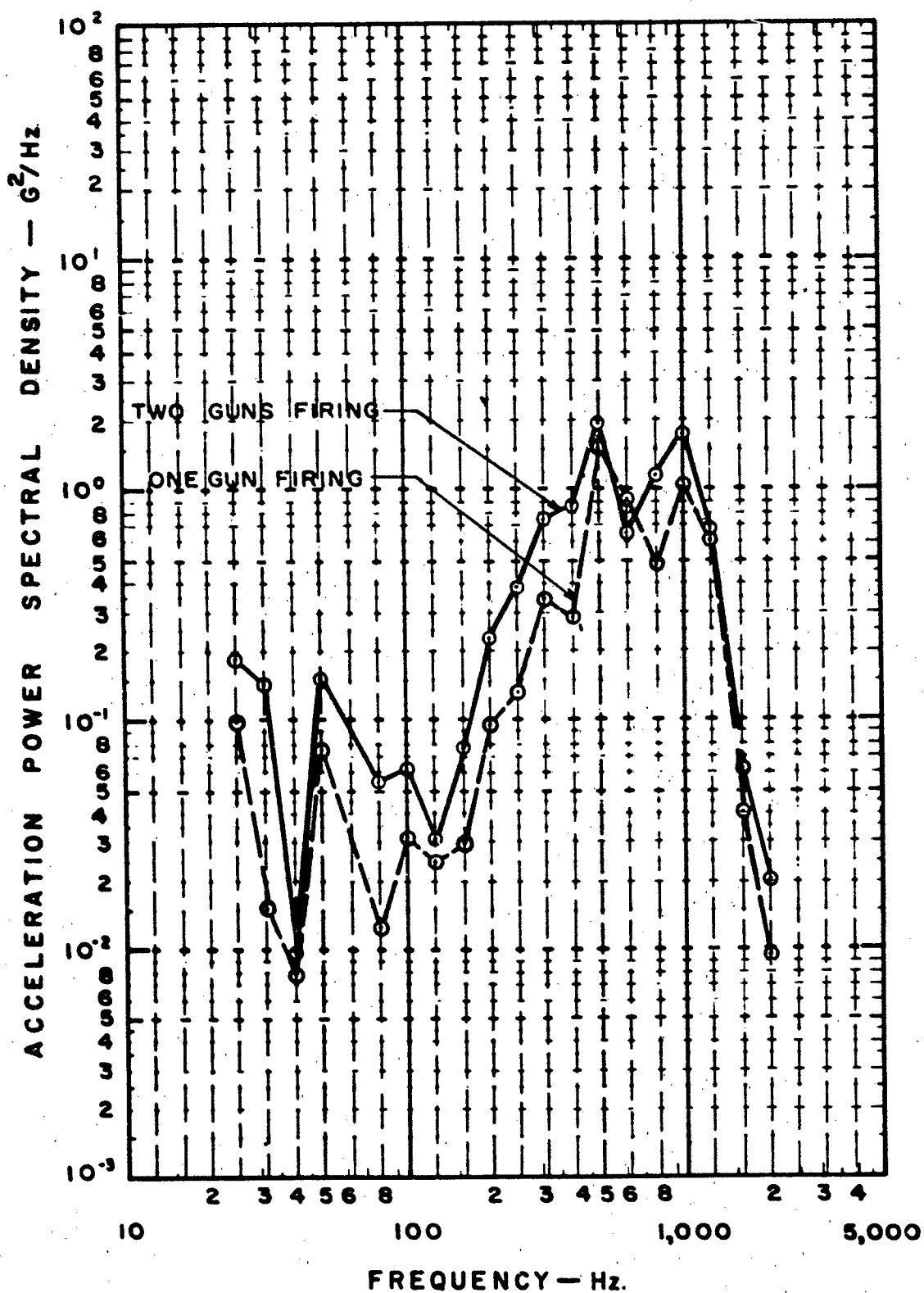
F–5
Figure 24. Structural Response for One and Two Guns

36

SECTION VI

SPECIFICATION SYNTHESIS AND APPLICATION

1. SYNTHESIS

Earlier, in Section III, it had been remarked that the F-5A employed special gun blast deflectors during normal gunfire operations. And now that we examine Figure 25 and observe that the slope of the F-5 data is in sharp contrast to the others, (a slope of approximately one) we wonder if there exists an association. An examination of several accelerometer gunfire records (there were only several available) recorded first with the deflectors retracted and then extended show that, on the average, the vibration levels were reduced when the deflectors were deployed. These accelerometer locations were near to and in front of the guns and correspond to most of the F-5 data points in the region covered by D less than 40 inches. Were these levels in Figure 25 to be increased, the end effect would be to increase the slope of the regression line.

Whether or not this explanation fully accounts for the slope difference cannot, with such limited data, be determined but it certainly appears to be a contributant. Another factor may involve the separation distance between the guns. At 24 inches, the guns are about 30 calibers apart and the near field loading area, relative to that assumed for one gun, is now being distributed over a more extensive region of the aircraft structure. With a broader distribution area, one would expect a somewhat more gradual decay of the response levels.

Initially, one is reluctant to remove the F-5 data; for one thing, we will have reduced the total sample size and keyed the remaining data to a single aircraft structure and to one data acquisition and reduction process. But then again, being reduced to one structural sample is not without some advantage. The coupling and response data may be amenable, in the future, to normalization techniques. That is, we may be able to apply surface (or volume) density weightings to other aircraft structural configurations to obtain an improved estimate of $G(f)$—especially for those structures that markedly deviate from what might now become the F-4 norm.

On balance, then, and primarily because of the use of deflectors which is in clear violation of model assumptions (with consequences that seem to be reflected in the data) we are persuaded to set aside the F-5 data sample.

If the F-5 data is removed, how will C_c and S_y' behave if we repeat the former comparative regression process? The results from this inquiry are shown in Table III, and a data display of each case is shown in Figures 26 and 27.

TABLE III

REGRESSION ANALYSIS WITHOUT F-5 DATA

	C_c	S_y	Slope(z)
Pooled, normalized without F-5 data	.7143	.6806	-4.58
Pooled, without F-5 data	.7190	.6675	-4.55

Similar to earlier results, there has been some improvement in the multiple correlation coefficient and in the sample standard error when the data model is viewed in the power (normalized) mode. From here on, we will utilize the pooled, normalized for (with the F-5 data removed) as the nucleus for developing a basic normalized reference level, $G_o(f)/r_o n_o$.

z=-1.17

$G_o(z) - G^2/Hz$

r - in

Figure 25. Regression Analysis of F-5

38

Figure 26. Regression Analysis of Pooled Configurations Without F-5

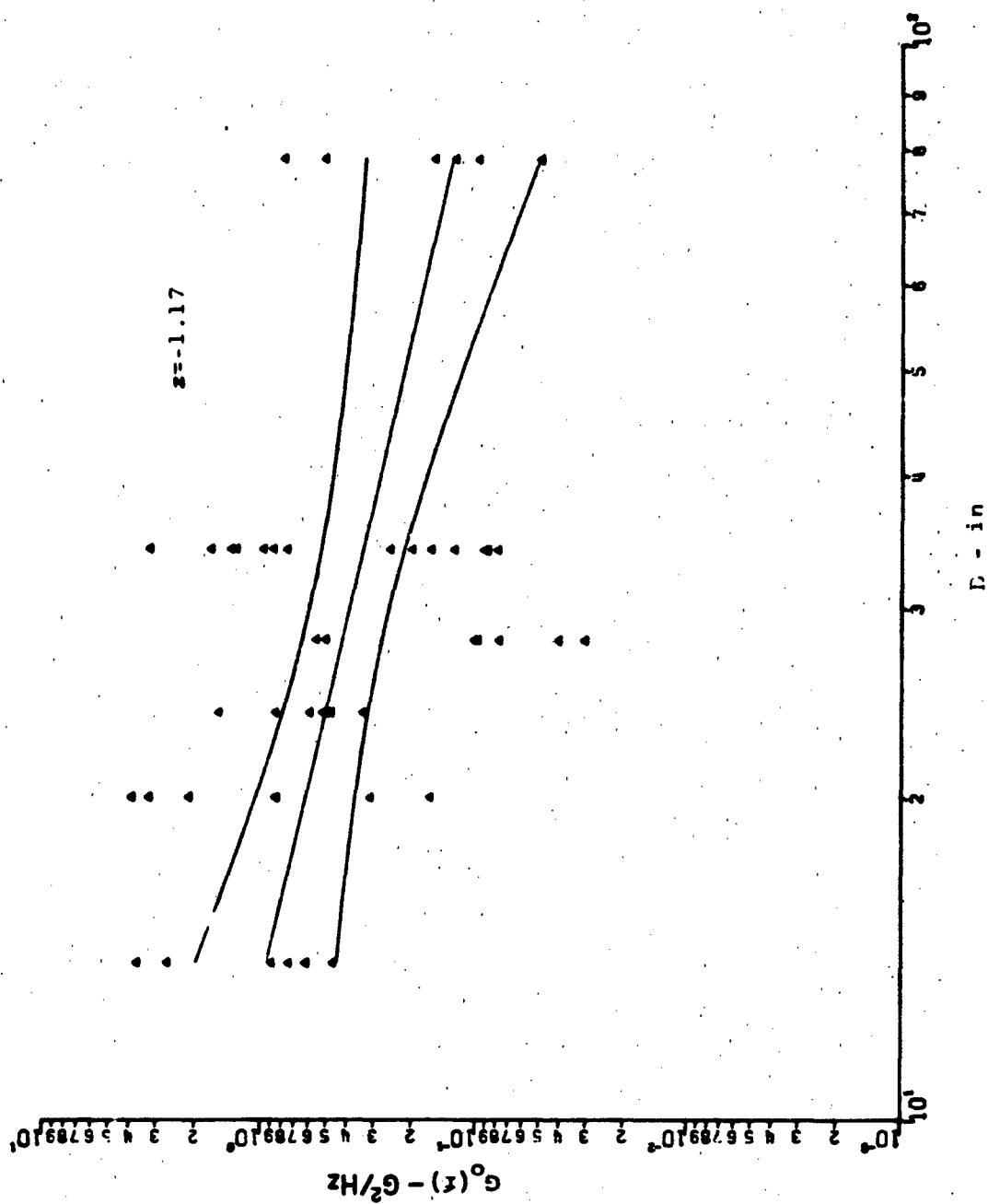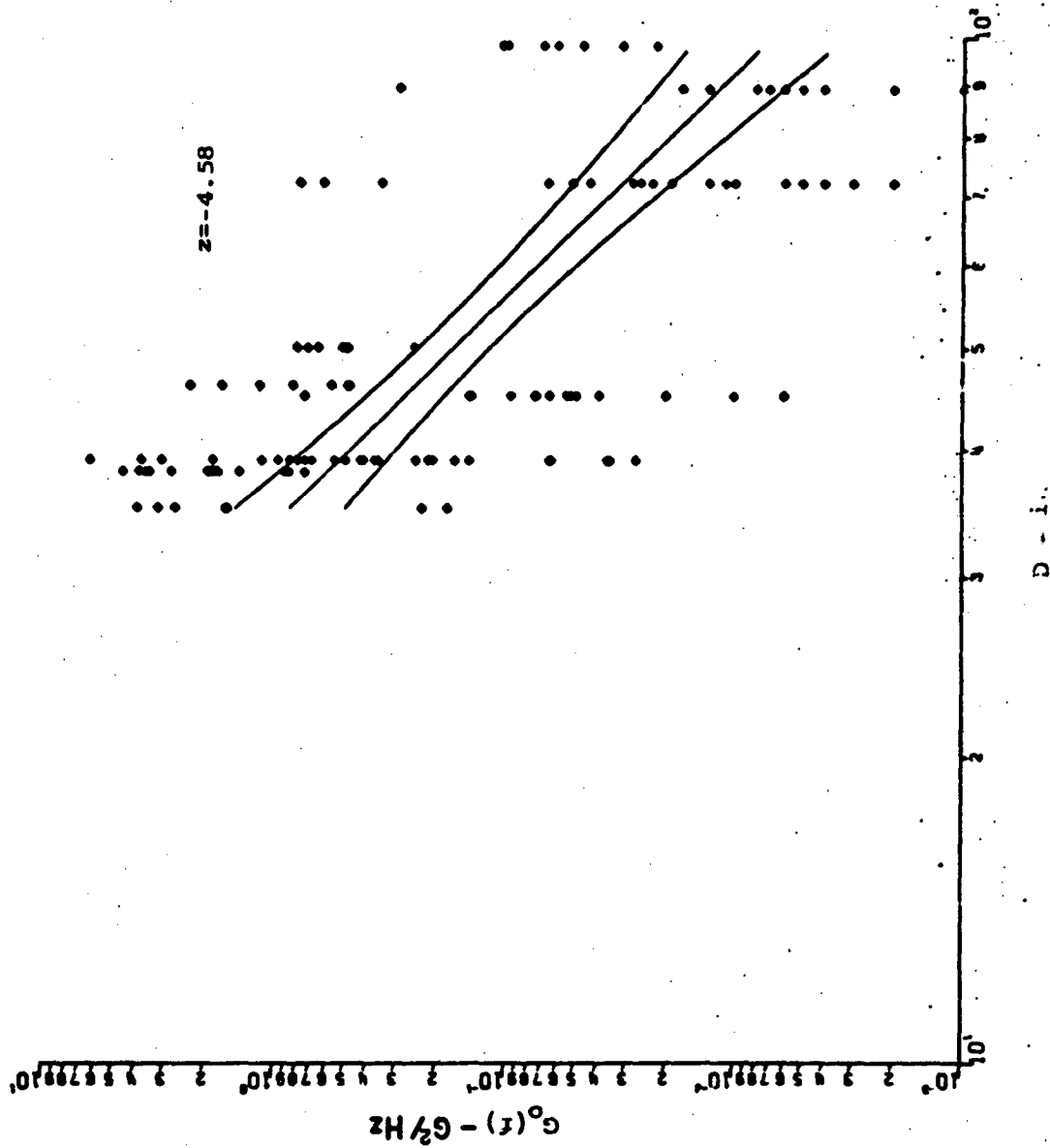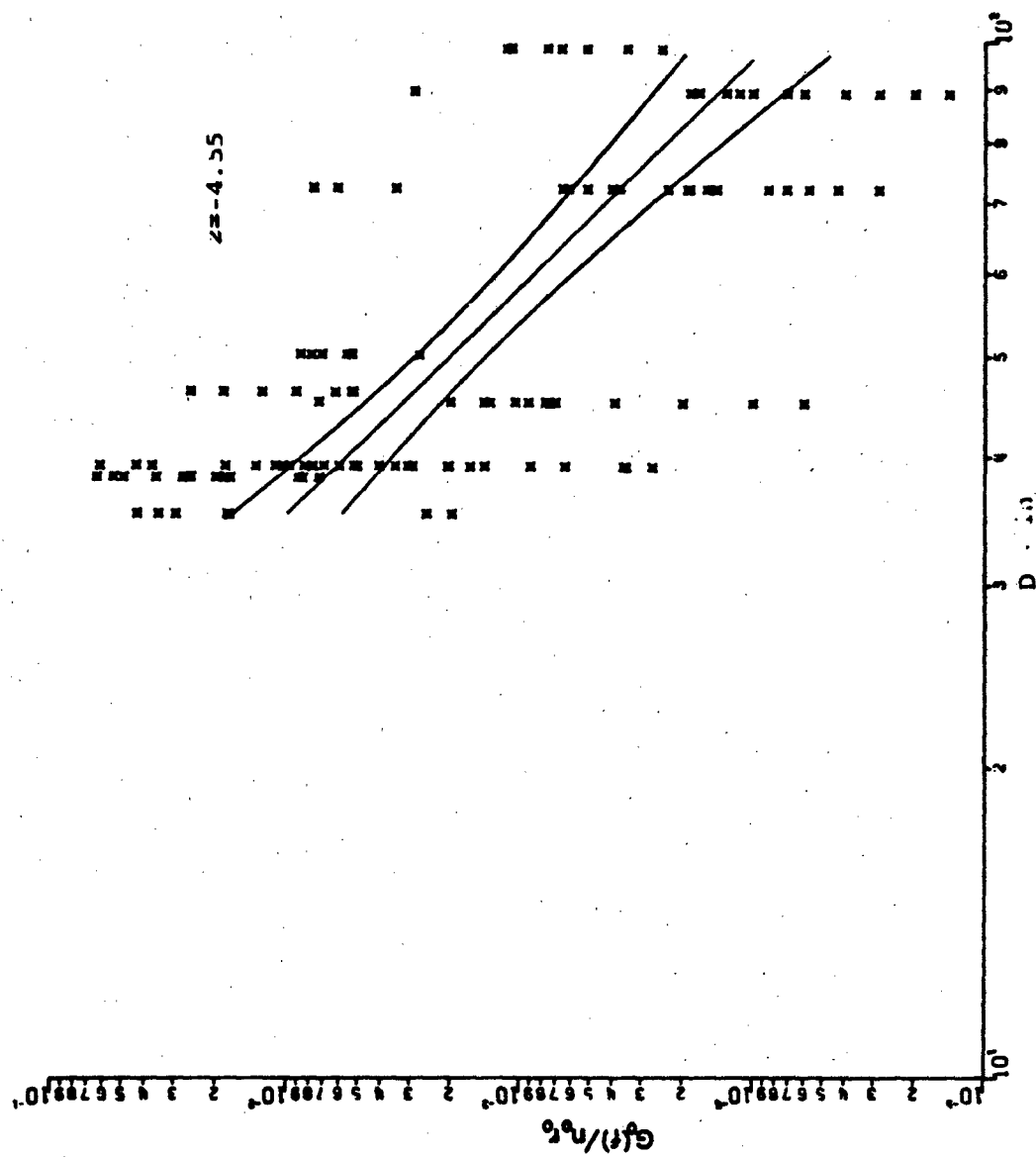Figure 27. Regression Analysis of Pooled Normalized Configurations Without F-5

The next step involves a vertical translation of the regression line by approximately 2 S,' to obtain 93% coverage of the data points. But before this, we wish to adjust the slope somewhat. Earlier, it had been observed that the slope of the MK-IV data sample exhibits a noticeably steeper value than that of the F-4 and SUU-16 samples (see Figure 21). Since we wish to be conservative and also since the vibration levels of the MK-IV accelerometer at D = 78 inches appear to be sufficiently low to allow a suspicion that this data channel might have been either faulty or unrepresentative, we rotate the regression line of Figure 27 counterclockwise to the full range allowed by the upper and lower confidence limits of the line as a whole (Figure 28).

The rotated regression line, with a slope of approximately −3, is then translated vertically to provide an approximate 2 S,' coverage of data points. Further conservatism is obtained during rotation by *not* rotating the line about D mean, as is customary, but by moving the center of rotation to a D of approximately 38 inches. This is done to insure that the line gives better coverage of those data points located close to the gun muzzle—the region where most gunfire failures are apt to occur.

The last step consists of fairing the curve into an asymptote to approximate the near field roll-off characteristic and, finally, a reverse curve is introduced at the far end of D to approximate the gradual blending of the gunfire levels with ambient vibration field, Figure 29.

$G_n(f)$ tends to be somewhat lower at D behind the gun muzzle when compared to $G_o(f)$ at an equivalent D in front of the muzzle (a regional differentiation indicated in Figure 29 by (−) and (+) signs, respectively). The difference, approximately 3 db, is derived from somewhat scanty data extracted from the F-5 and F-100 samples (References 9 and 13) and so the minus curve represents a rather coarse estimate. However, the existence of a minus curve does have a rational basis; the maximum blast pressure field is, of course, located directly in front of the muzzle.

The final curve (Figure 29) defines $G_o(f)/r_c n_c$ as a function of D and will be used henceforth as the normalized reference level by which an estimated level, $G(f)$, is established when E, r, n, and D are known or can be estimated.

2. APPLICATION

The following example is provided to demonstrate the application of the power model when it is desired to estimate the vibration levels of an aircraft equipment exposed to gunfire.

An equipment is located forward of two 20-mm cannons (n = 2). The distance parameter is determined to be 55 inches (D = 55 inches). The muzzle energy is known to be 43,500 ft/lbs ($E' = 43.5 \times 10^3$). The firing rate is 25 Hz (r = 25). The basic normalized curve of Figure 29, or Figure 519-1 of Appendix IV, is derived from guns with an $E'_o = 39.6 \times 10^3$ ft/lbs.

Steps:

1. Refer to Figure 29 or 519-1. Select from the positive curve, $G(f)/r_c n_c = 10^{-2}$, at D = 55 inches.

2. Substitute the appropriate values into Equation 23.

$$G(f) = E'/E'_o \cdot nr \cdot G(f)/r_c n_c$$

$$= \frac{(43.5) \ 10^3}{(39.6) \ 10^3} \cdot (2) (25) (10^{-2})$$

$$= (1.1) (50) (10^{-2})$$

$$G(f) = 0.55 \ g^2/Hz$$

3. Refer to Figure 519-4 of Appendix IV. Assign to G_{max} the value, 0.55 g^2/Hz.
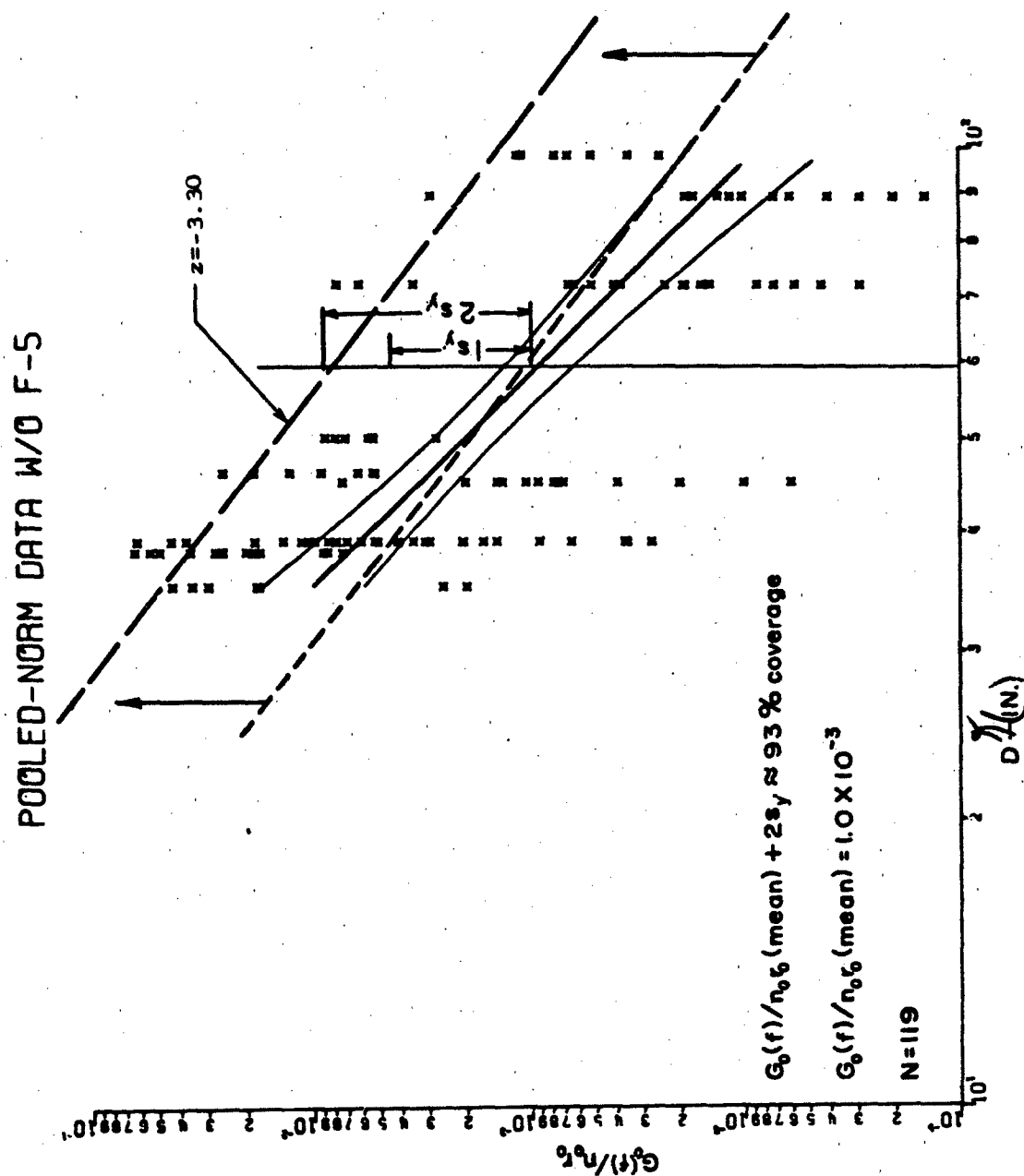
Figure 28. Rotation and Translation of Regression Line
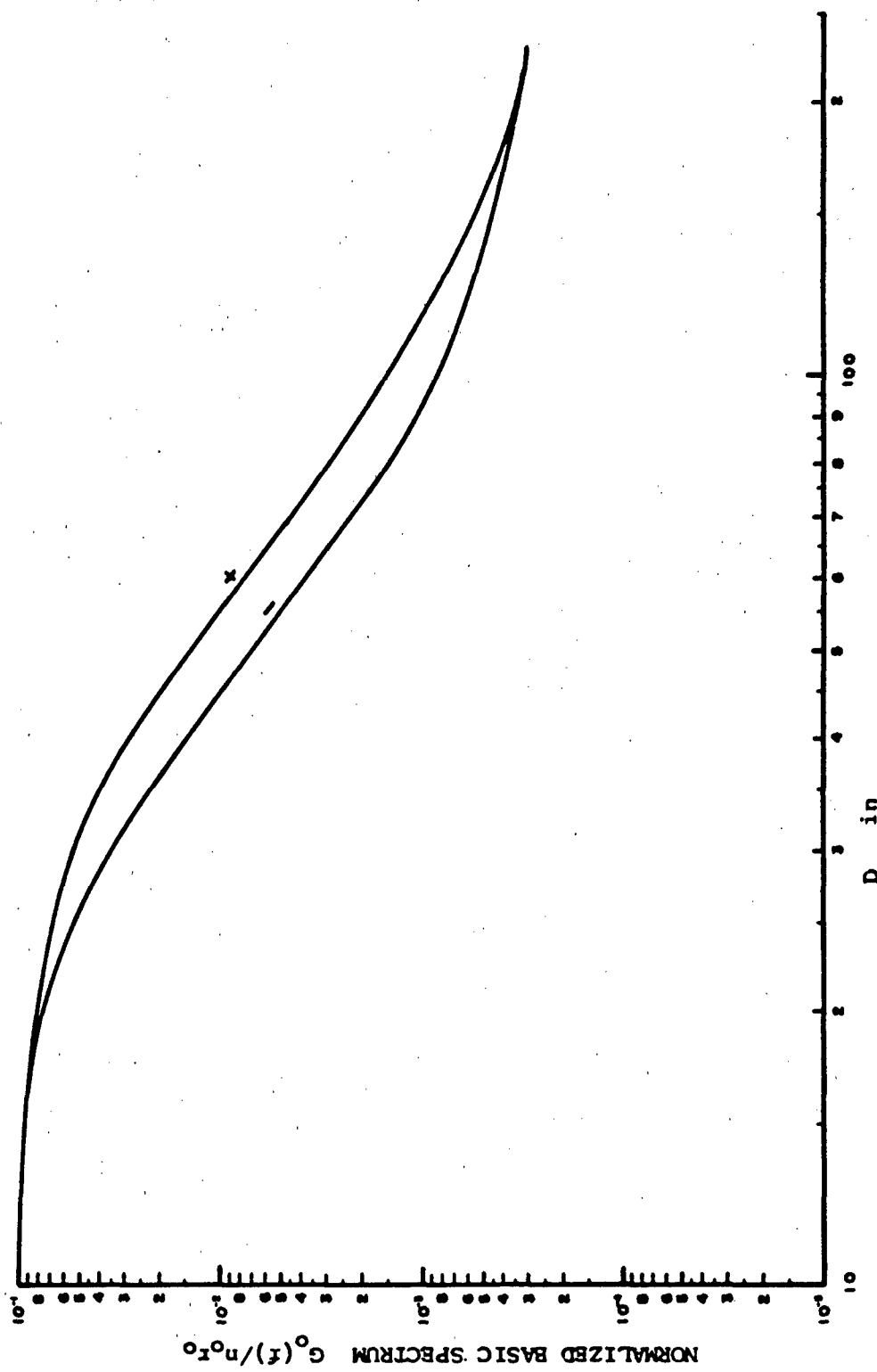
Figure 29. Final, Normalized Basic Spectrum of $G_o(f)$

NORMALIZED BASIC SPECTRUM $G_o(f)/n_o r_o$

D in

43

In Section I, we noted the desirability of utilizing real time as the choice for the gunfire test duration. During this study information was collected concerning the number of rounds fired, number of missions per total rounds expended, mission duration, gun firing rates, and so on. Reports and data were collected from SEA activities, gunnery range sources (Nellis AFB), and from private contractors. Although reports were frequently incomplete, an estimate of 30 minutes gunfire exposure time was determined, on the average, to be equivalent to at least 300 missions. Thus, a period of 30 minutes was chosen as the basic test time for T519 of MIL-STD-810B and appears in the time schedule of Procedure II of that method.

For additional examples and details, see Method T519, MIL-STD-810B, which is contained in Appendix IV.

SECTION VII

FURTHER CONSIDERATIONS CONCERNING GUNFIRE

The following resume is included to further elaborate on matters covered in the main body of the report, to discuss simulation methods which involve the low frequency portion of the gunfire spectrum; and to outline study areas the investigation of which should prove fruitful for the future.

1. MUZZLE DEFLECTORS: BAFFLES

In earlier assumptions, deflectors or special baffles were disallowed. In practice, most gun configurations feature some form of blast deflection. The SUU-16, MK-IV, and F-4E are no exceptions to the rule. A small lip or protuberance over the muzzle and a metallic webbing between muzzles are features of the SUU-16 and MK-IV, respectively. A perforated metal housing appears around the F-4E configuration. Such arrangements do not appear to be particularly effective, judging from the results of other investigators (Reference 1) in consequence, these nominal features are treated here as if the gun muzzles are clean—such is not the case with the F-5 configuration as noted in previous sections of this work.

2. MUZZLE ENERGY AND BLAST ENERGY

In the early sections of this work we set the energy of the blast proportional to the muzzle energy (Equation 20). This was done to establish the blast power which was then equated to the power spectrum of the structural response. The muzzle energy is also a convenient property consisting of the muzzle velocity and projectile mass—quantities readily obtained for a large variety of weapon classes.

Recent studies (Reference 10) suggest another energy definition of the gun blast energy that under certain circumstances may represent an improvement. This model equates the blast energy (E_p) to the difference between the energy of the explosive charge (E_c) and the muzzle energy $\left(\frac{mv^2}{2}\right)$. Stated in symbols:

$$E_p = E_c - \frac{mv^2}{2}$$

where

E_p = blast energy

E_c = explosive charge energy

m = projectile mass

v = projectile velocity

There are difficulties with this model centering chiefly around different energy values of various explosives (values depending upon whether pressure or temperature increases are used to determine the charge energy) and the relative scarcity of published information of blast data that is also related to the quantity or type of propellants used. Nonetheless, the model merits further investigation—revealing a particular advantage for the case when gun barrel lengths are varied substantially. For example, there are cases in which the cannon barrel is reduced to one-third of original length with a consequent reduction of muzzle velocity and an increase of blast pressure. Note that, for this case, the difference model predicts an increase in blast energy—the muzzle energy model, in contrast, requires a decrease. In future efforts we expect to study this model and, if appropriate values of E_c can be accumulated, consider seriously its adoption.

45

3. MUZZLE DISTANCE

The SUU-16 and MK-IV pods are mounted underneath the aircraft surface. The vertical distance (h) from the muzzle to the skin is approximately 12 inches, or 15 calibers. Both units are also attached to the aircraft by means of a centerline adapter. In this case, h is increased to 22 and 26 inches, respectively. In calibers (c) this now represents distances ranging from approximately 28 to 33, values somewhat larger than our earlier restriction of 25 calibers. The vibration data used in this program represents a mix of data taken with and without the adapter. Information on blast pressure field variations as a function of distance from a structural surface is not extensive, but Westine (Reference 10) conducted a series of measurements which may be of considerable value. A weapon is placed over a flat sheet containing six flush mounted microphones arranged in a line perpendicular to the trajectory (Figure 30). The weapon is translated parallel to the surface, thus allowing measurements to be made at different horizontal distances (L) from the gun muzzle to the microphone array. Also upon each positioning of L, the height (h) was varied; for example at an L/c of 20, pressures were recorded for h/c ratios of 16, 27, 38, and 50.

Reflected pressure, taken as a function of the perpendicular distance (h) between the muzzle to the plate surface, was extracted from the data of Westine. A spatial pressure average was obtained over a rectangular surface area (see dashed rectangle of Figure 30) located forward of the gun muzzle, beginning at L/c = 20, extending forward to L/c = 50; and bounded on each side of centerline, at ± 16 inches. This region represents an approximation to the near field blast region where blast coupling is presumed to generate the most severe vibration response. The average pressure of the surface was normalized to its maximum value and is presented as the dependent variable of h/c (Figure 31). The dashed line has been added to the figure in order to extrapolate the function into a greater and more useful region of h. Finally, the extended line is faired into an inverse square law curve beginning at, approximately, h/c > 70.

From this curve, two conclusions result: (1) The earlier height restriction imposed on the model (h/c < 25) seems justified. (2) The vibration data of this model should be adjusted to compensate for the mean blast pressure drop somewhere near the region of h/c > 40. Since the data from the SUU-16 and the MK-IV consists of a composite of h/c ≃ 22 and h/c ≃ 32, major adjustments of $G_n(f)$ are not anticipated. Nevertheless, it should be interesting to review this aspect and to determine if, as seems likely, correlation improves upon data adjustment. Of course, the end results arrived at here should be tempered with qualification that there exists a relative paucity of h/c data and that, granted these results, it remains true that aerodynamic flow and aircraft surface curvature and irregularities are, presumably, not reflected in the pressure vs h/c data used here. Additional studies involving in-flight data acquisition, in which h/c is made a variable, is to be much desired.

In the meantime, we propose to use the curve of Figure 32 as in interim guideline. Accordingly, the curve has been squared and transformed into a power model which allows for a reduction of the acceleration power spectral density of the structural response G_n (f), or G_{max} in the terminology of Method T519. This curve will be appended to the standard in the immediate future.

4. LOW FREQUENCY CONSIDERATIONS

In Section II, we noted that, for the case of a single cannon firing at an approximate fixed rate, the character of the vibration response seems most realistically simulated by incorporating a fundamental frequency component including harmonics that extend to cross-over region at approximately 400 Hz. For the case of multiple, unsynchronized guns

46

REGION OF SPATIAL AVERAGE

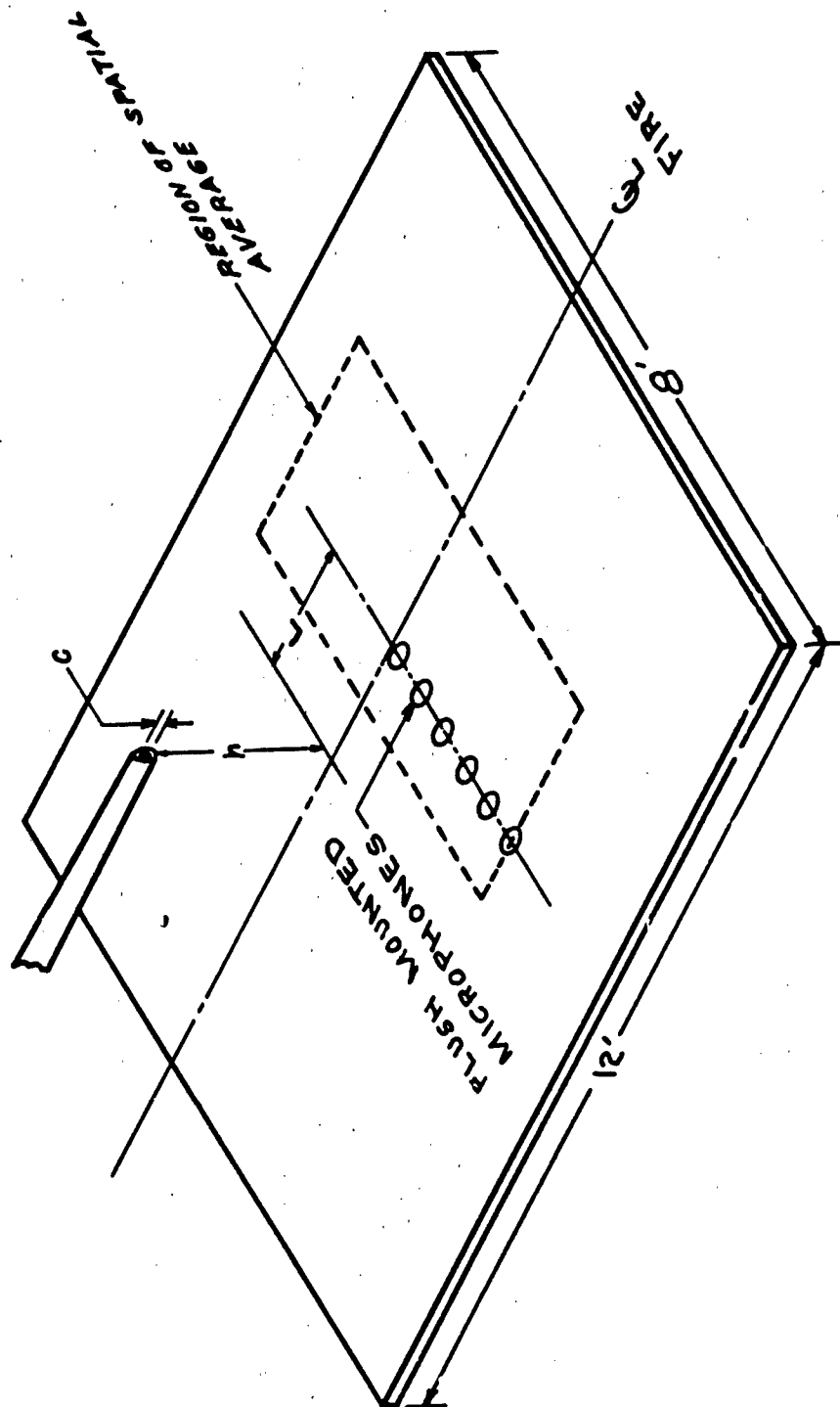FIRE

FLUSH MOUNTED MICROPHONES

8'

12'

c

h

Figure 30. Experimental Setup to Determine Gun Blast Pressure Field
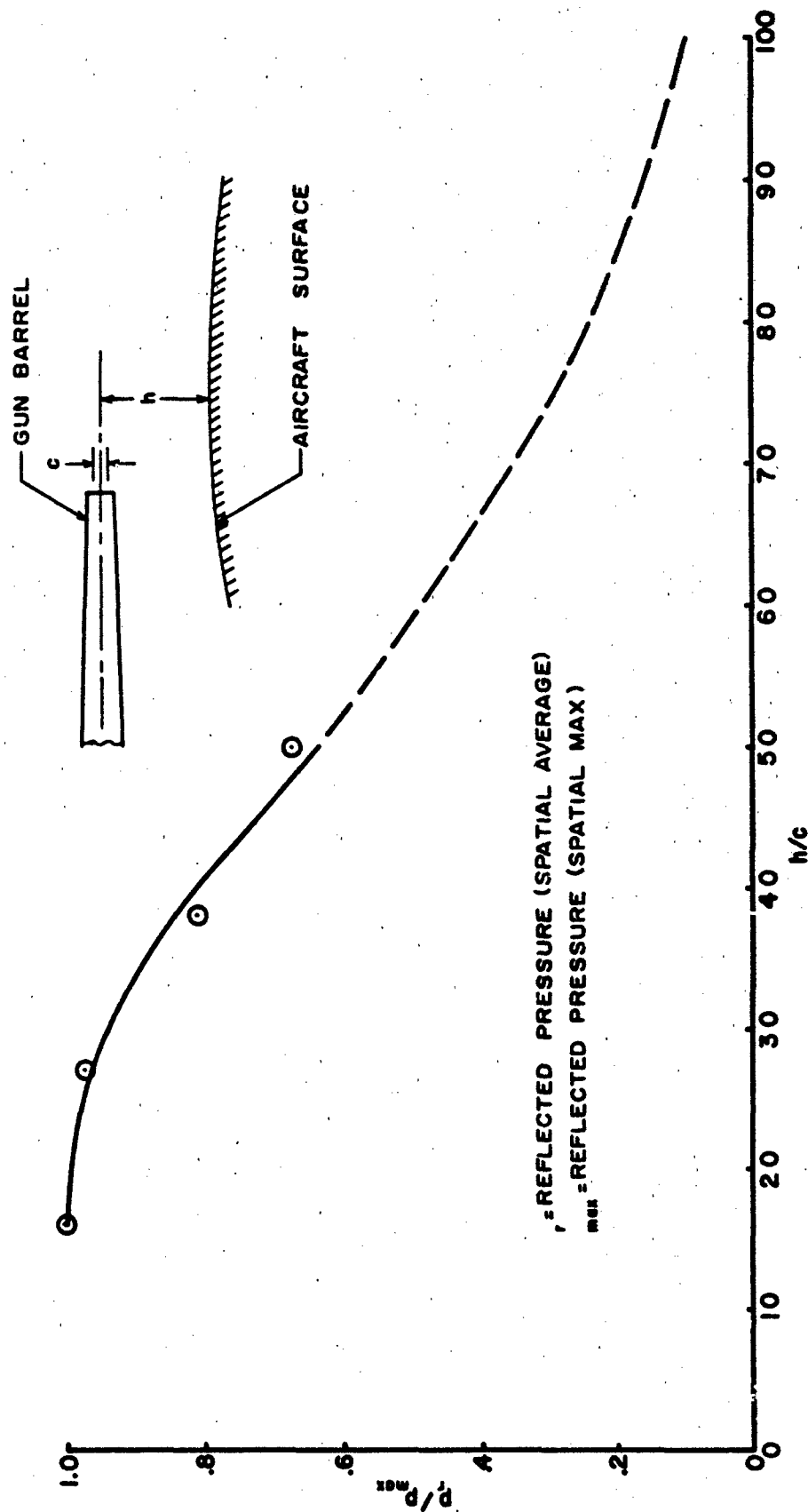
47

Figure 31. Normalized Average Reflected Pressure of
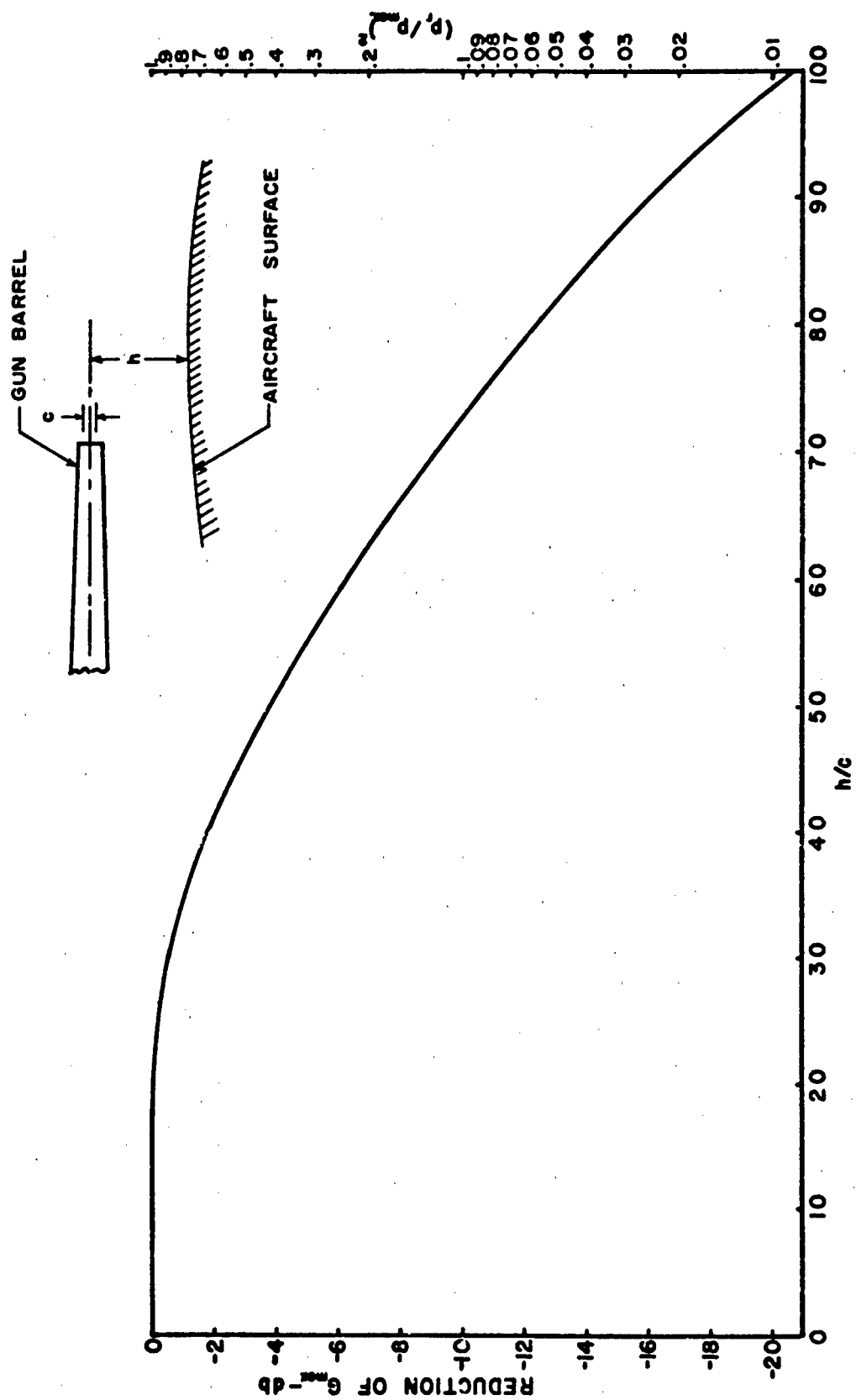Gun Blast vs Distance Parameter, h/c

Figure 32. Reduction of G_{max} vs Distance Parameter, h/c

49

low-frequency random characteristics appear predominate and this is reinforced as the number of guns increase, as in the case of the four gun configuration of the F-100 (Reference 9). In the first case, it is tempting to consider an array of pulsed decaying sinusoids appended to the low frequency segment of the random spectrum. For the second case, low frequency extension of the basic random spectrum down to the fundamental firing frequency appears acceptable. Clearly, the first case poses the greater difficulty and so will be discussed further.

It should be possible to disable the desired low frequency section of most random shaker systems (by-pass, roll-off, remove equalizer cards or preamplifiers, etc.) and to insert the required number of spectral components up to approximately 400 or 500 Hz. Deviations about the mean firing rate and, possibly, simulation of the gun runup-rundown variations might be achieved through frequency modulation of a ramp or pulse generator, as shown in Figure 33. Admittedly, unforseen difficulties may be encountered with such an approach; therefore, follow-up laboratory studies are planned to more thoroughly explore this and other possible techniques.

5. GUNFIRE MODEL EXTENSIONS

It is of interest to consider some extensional possibilities of the basic gunfire model. To briefly review, the present model results from an attempt to provide a tractable description of the vibration field of the outer structure including the contiguous primary structure of the aircraft. Thus, accelerometer data of the interior locations (usually proximate to or on black box or other equipments) was, with purpose, withheld. The D vector to be consistent with this model must then terminate at the structural surface, or more precisely, in the region of the surface bounded by a depth of approximately 10 inches. In practice and in the absence of extensional notions of the interior vibration field, we presently extrapolate the vector to the desired point. Perhaps this is sufficient—to put it plaintively, the best that can be done. But it has been observed by the authors that as the vibration propagates into the interior structure, the spectrum appears to undergo transformations that (if these changes can be shown to possess at least a statistical consistency) may be exploited to further useful purpose. That is, in a general way, the high frequencies are attenuated and, the low frequencies relatively speaking, undergo emphasis. In brief, there is a spectral downshift of the maximum responses; seemingly at the expense of the high frequency amplitudes. This seems to occur because the interior dynamics of equipment bays are characterized by concentrations of high density equipments with lower stiffness to mass ratios than are usually found near the aircraft surface. In transit damping losses and inertial loading, no doubt, add their contributions.

Given such a hopeful, viable view of vibration propagation (coupled with a dynamicists last resort, statistical acceptability) we may then allow the D vector to terminate at or near the structural surface and add an R vector normal to the surface, extending into the equipment bay to the desired location. Figure 34 illustrates the notion.

The earlier view of $G_o(f)$ is of the general functional form:

$$G_c(f) = f(nrE_p/D)$$

and, in the extensional view, might appear as

$$G_c(f) = f(nrE_p/DR)$$

The significant parameter changes (envelope) of the altered spectrum might be keyed functionally to R.
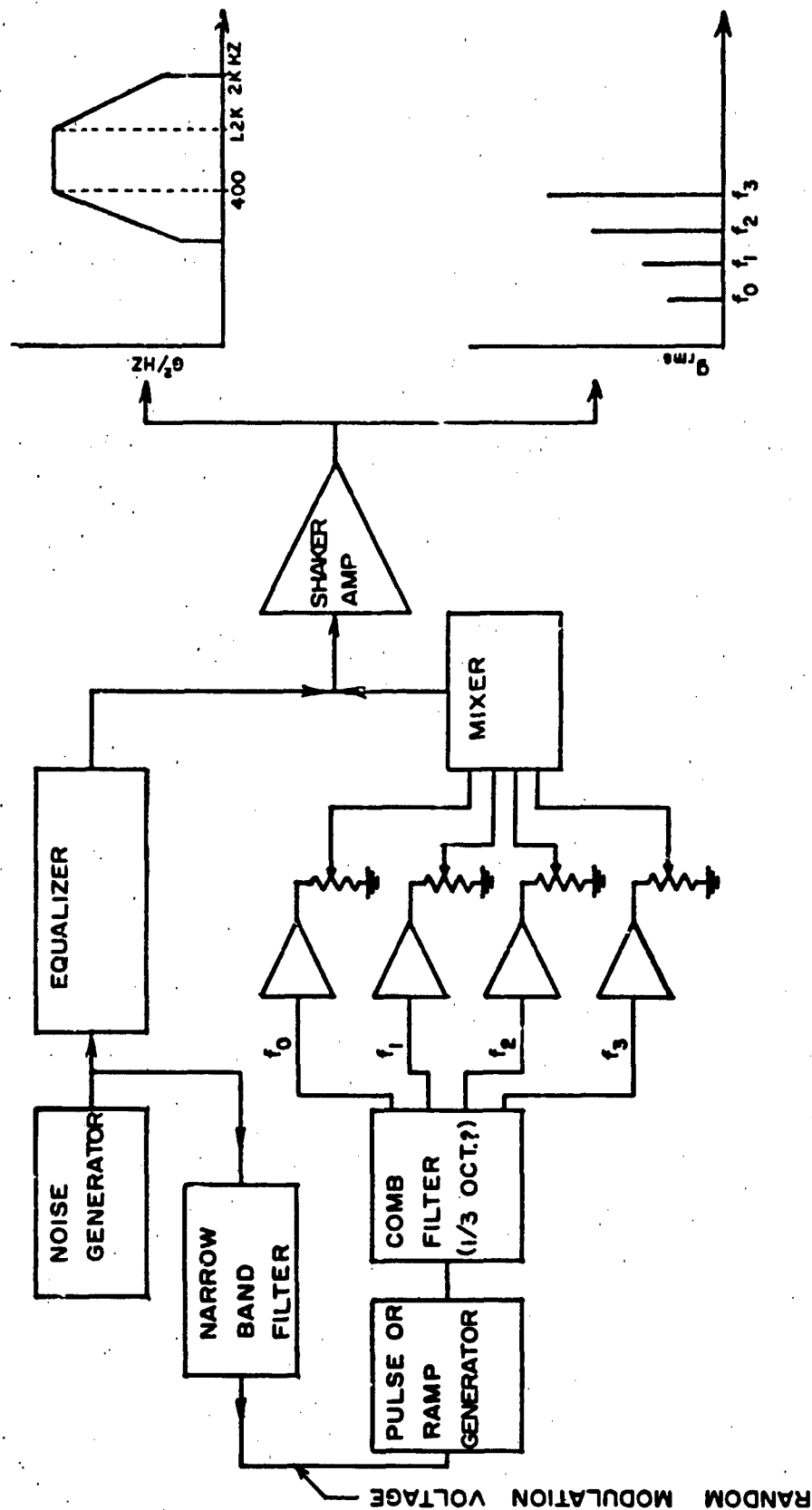
50

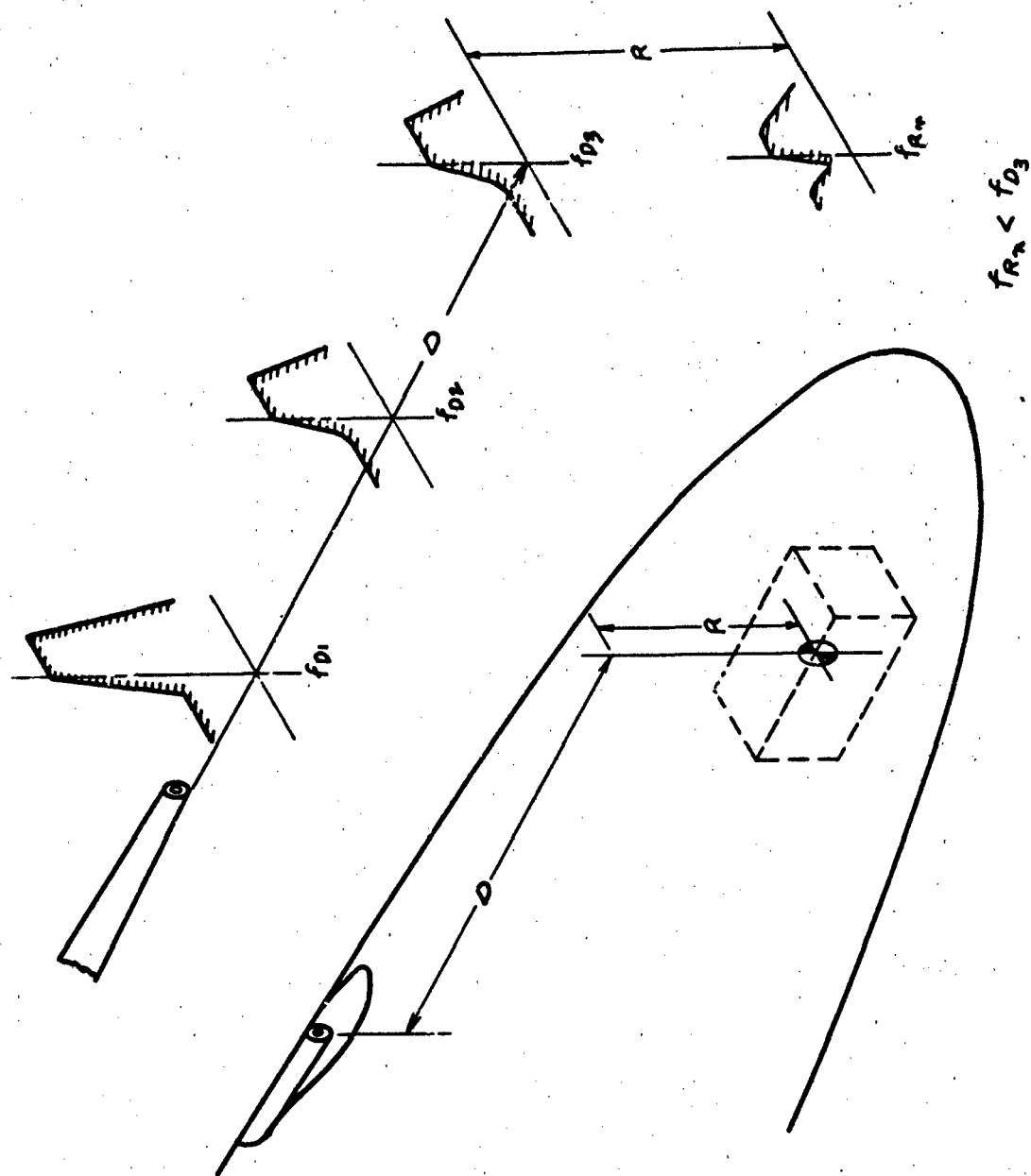Figure 33. Combined Sinusoidal and Random Simulation of Gunfire Spectrum

51

Figure 34. Gunfire Extensional Model

$$f_{R_n} < f_{D_3}$$

52

SECTION VIII

CONCLUSIONS

Structural vibration, induced by gunfire, is shown to be characterized by maximum levels concentrated in front of and near the gun muzzle. The levels exhibit a sharply decaying behavior as a function of the distance from the muzzle and can be approximated by an exponential function.

It is shown that a power model relating the gun parameters (firing rate, muzzle energy, number of guns) to the vibration levels provides a viable tool for the estimation of vibration levels and facilitates the derivation of gunfire test techniques.

A vibration test method has been synthesized that utilizes a basic random vibration spectrum. For the case of single gun configurations, it is desirable, in the future, to determine a suitable simulation method by which the low frequency region (below 300 Hz) may be augmented by vibration content consisting of a frequency modulated fundamental and its harmonic series.

APPENDIX I

HARMONIC ANALYSIS OF GUN BLAST
PULSES ON AIRCRAFT STRUCTURES

In the analysis of aircraft structural vibration excited by the aerodynamic loading associated with gunfire, it is necessary to obtain the relative magnitude of the various harmonic components of this forcing function. This is required when solving for the transfer function giving the relation between the aerodynamic power input and the resultant vibratory power in the aircraft structure. This aerodynamic loading is a result of the shock wave and the associated overpressure region impinging against the outer surface of the aircraft structure during its propagation from the gun muzzle. The variation in pressure as a function of time at any point on the aircraft structure subjected to this gun blast loading may be obtained from the following equation from (Reference 10):

$$p(t) = p_m \left(1 - \frac{t}{t_o}\right) \cdot e - \frac{t}{t_o}$$

1. CONSTANT FIRING RATE MODEL

A representative pattern of this gun blast loading at a constant firing rate is shown in Figure 35. This is the basic configuration, or mathematical model, of the gunfire pattern. This constant firing rate may be expressed by a periodic function, $p(t)$, which can be represented by the following Fourier series in the complex form.

The Fourier series in complex form for the periodic function, $p(t)$, shown in Figure 36 is

$$p(t) = \sum_{k=-\infty}^{+\infty} a_k e^{j2\pi \frac{k}{T}t}$$

$$\text{where } a_k = \frac{1}{T} \int_{t_a}^{t_a + T} f(t) e^{-j2\pi \frac{k}{T}t} \, dt$$

The a_k is the complex Fourier coefficient, T is the period of $f(t)$, and t_a is arbitrary. It is convenient to choose $t_a = 0$ so that the limits of integration are 0 and T.

$p(t)$ is defined over the interval $0 < t < T$ as follows:

$$p(t) = p_m \cdot \left(1 - \frac{t}{t_o}\right) \cdot e^{-\frac{t}{t_o}} \qquad o < t < t_o$$
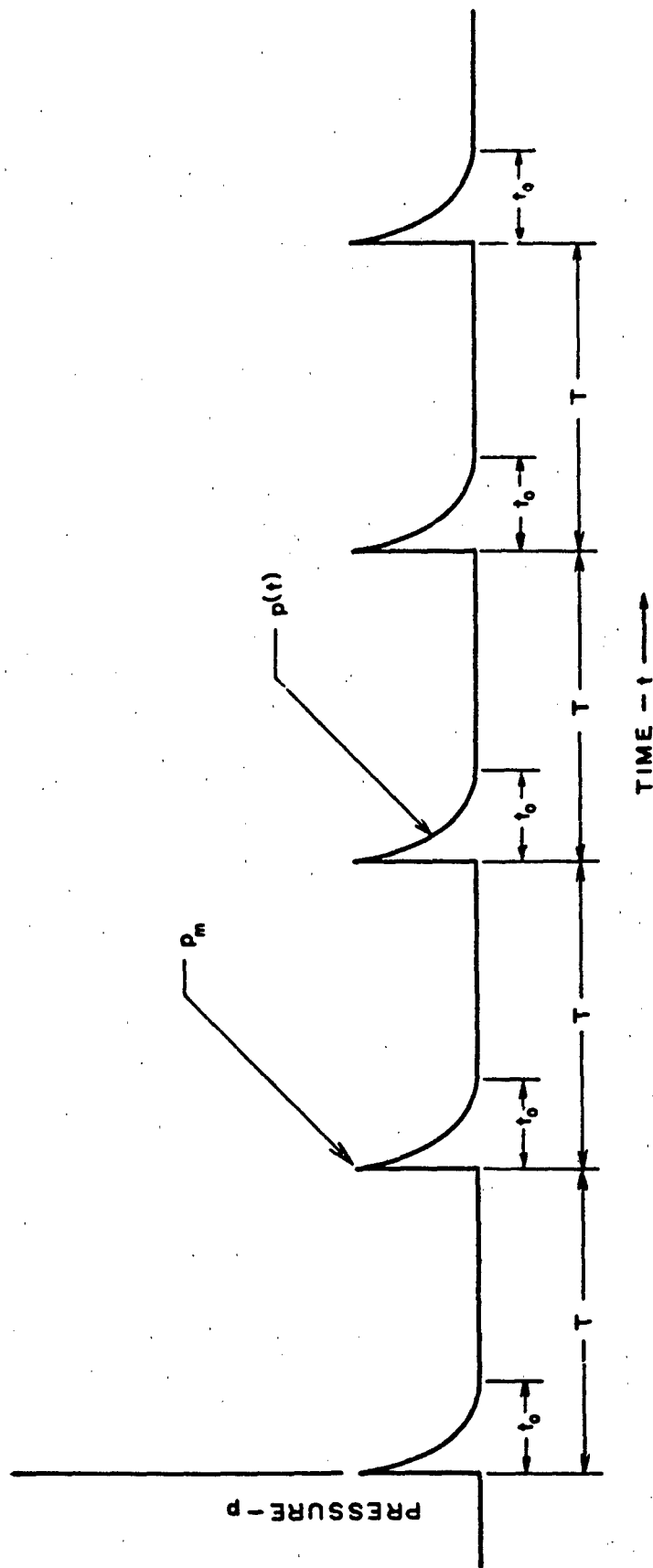
$$p(t) = 0 \qquad t_o < t < T$$

54

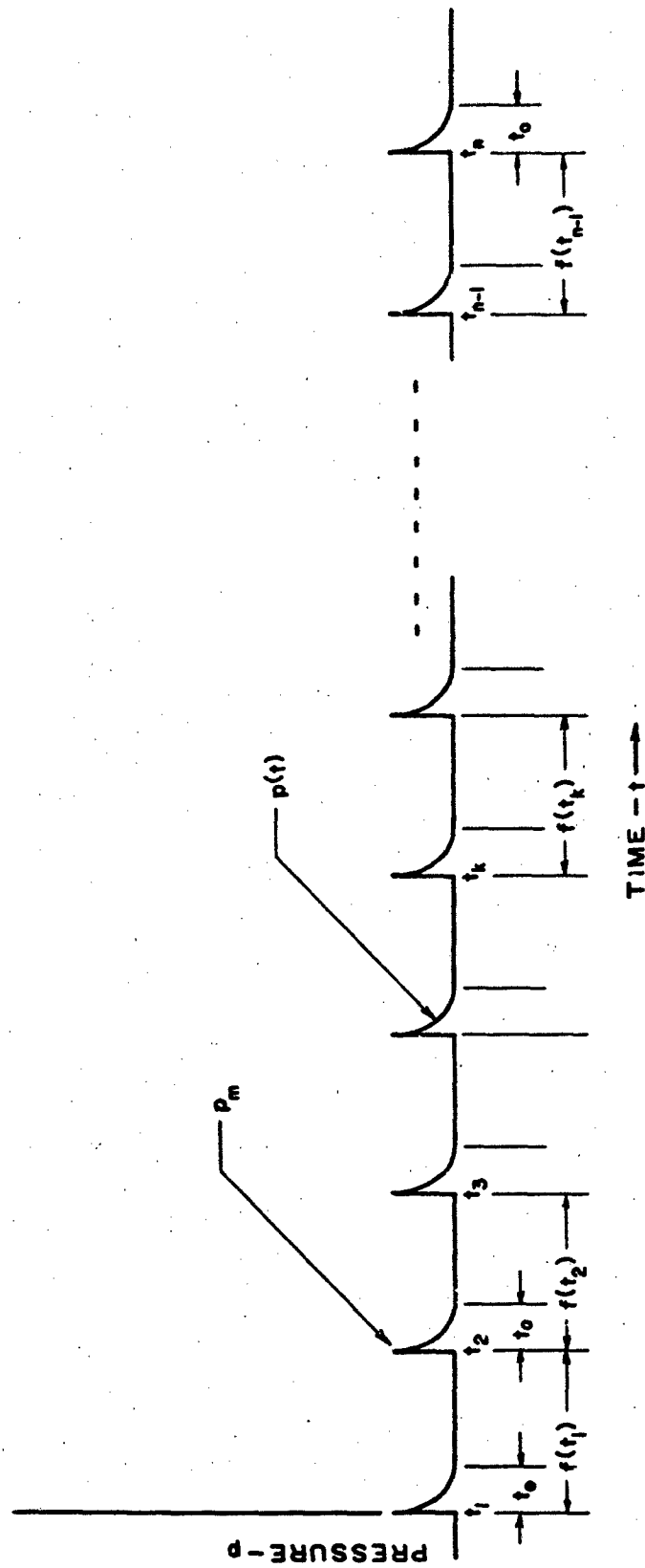Figure 35. Pulse-Time History for Constant Firing Rate

55

Figure 36. Pulse-Time History for Variable Firing Rate

The expression for a_k which must be evaluated accordingly is:

$$a_k = \frac{1}{T} \int_0^{t_o} p_m \left(1 - \frac{t}{t_o}\right) e^{\frac{t}{t_o}} \cdot e^{-j2\pi \frac{k}{T} t} \, dt$$

This integral can be evaluated analytically and the final expression for a_k will be put in the polar form of a complex number.

$$\text{Let } \omega_k = 2\pi \frac{k}{T}$$

$$a_k = \frac{p_m}{T} \int_o^{t_o} e^{-\left(\frac{1}{t_o} + j\omega_k\right)t} \, dt - \frac{p_m}{T t_o} \int_o^{t_o} t \, e^{-\left(\frac{1}{t_o} + j\omega_k\right)t} \, dt$$

$$\text{Let } p_k = \frac{1}{t_o} + j\omega_k$$

$$\text{Since } \int e^{ax} dx = \frac{1}{a} e^{ax} \text{ and } \int x e^{ax} dx = \frac{e^{ax}}{a^2}(ax - 1)$$

$$a_k = \left(\frac{p_m}{T t_o} \frac{e^{-p_k t}}{-p_k} - \frac{p_m}{T t_o} \frac{e^{-p_k t}}{p_k^2}(-p_k t - 1)\right)\Big|_o^{t_o}$$

$$a_k = \frac{p_m}{T t_o p_k^2} \left((1 + p_k t) e^{-p_k t} - p_k t_o e^{-p_k t}\right)\Big|_o^{t_o}$$

$$a_k = \frac{p_m}{T t_o p_k^2} \left(e^{-p_k t_o} - 1 + p_k t_o\right)$$

$$\text{Since } p_k = \frac{1}{t_o} + j\omega_k$$

$$a_k = \frac{p_m}{\frac{T}{t_o} \left[t_o \left(\frac{1}{t_o} + j\omega_k\right)\right]^2} \left(e^{-(1 + 1 + j\omega_k t_o)} - (1 + j\omega_k t_o)\right)$$

$$a_k = p_m \frac{T}{t_o} \left(\frac{1}{1 + j\omega_k t_o}\right)^2 \cdot \left(j\omega_k t_o + e^{-1} \cdot e^{-j\omega_k t_o}\right)$$

$$a_k = p_m \frac{t_o}{eT} \left(\frac{1}{1 + j\omega_k t_o}\right)^2 \cdot \left(j\omega_k t_o + \cos(\omega_k t_o) - j\sin(\omega_k t_o)\right)$$

57

Let $(1 + j\omega_k t_o) = \sqrt{1 + (\omega_k t_o)^2}\, e^{j\alpha_k}$, where $\alpha_k = \arctan(\omega_k t_o)$

$$a_k = p_m \cdot \frac{t_o}{eT} \cdot \frac{e^{j2\alpha_k}}{[1 + (\omega_k t_o)^2]j}\left(\cos(\omega_k t_o) + j(e\omega_k t_o - \sin(\omega_k t_o))\right)$$

The complex number enclosed in brackets will be put in polar form. Denote this number by h_k

$$h_k = \cos(\omega_k t_o) + j(e\omega_k t_o - \sin(\omega_k t_o))$$

$$h_k = \sqrt{\cos^2(\omega_k t_o) + [e\omega_k t_o - \sin(\omega_k t_o)]^2}\, e^{j\beta_k}$$

$$h_k = \sqrt{1 + (e\omega_k t_o)^2 - 2(e\omega_k t_o)\sin(\omega_k t_o)}\, e^{j\beta_k}$$

where $\beta_k = \arctan\left(\dfrac{e\omega_k t_o - \sin(\omega_k t_o)}{\cos(\omega_k t_o)}\right)$

Substituting this expression for h_k in the last expression for a_k gives

$$a_k = p_m \frac{t_o}{eT} \frac{\sqrt{1 + (e\omega_k t_o)^2 - 2(e\omega_k t_o)\sin(\omega_k t_o)}}{[1 + (\omega_k t_o)^2]} \cdot e^{j(\beta_k - 2\alpha_k)}$$

Let $A_k = p_m \dfrac{t_o}{ET} \dfrac{\sqrt{1 + (e\omega_k t_o)^2 - 2(e\omega_k t_o)\sin(\omega_k t_o)}}{[1 + (\omega_k t_o)^2]}$

Let $\Phi_k = \beta_k - 2\alpha_k$

Then the final polar form for the complex Fourier coefficient is

$$a_k = A_k e^{j\Phi_k}$$

Substituting this expression for a_k in the series gives

$$p(t) = \sum_{k=-\infty}^{+\infty} A_k e^{j\Phi_k} e^{j\omega_k t}$$

The A_k is the amplitude of the harmonics at negative as well as positive frequencies. The amplitudes for positive frequencies only can be obtained by changing from this complex form

to the corresponding cosine form of the series which is:

$$p(t) = A_o + \sum_{k=1}^{\infty} 2A_k \cos(\omega_k t + \phi_k)$$

This change in form can be accomplished as follows:

$$p(t) = \sum_{k=-\infty}^{+\infty} A_k e^{j(\omega_k t + \phi_k)} = A_o + \sum_{k=1}^{\infty} (A_k e^{j(\omega_k t + \phi_k)} + A_{-k} e^{j(\omega_k t + \phi_k)})$$

Since $A_{-k} = A_k$, $\phi_{-k} = -\phi_k$ and $\omega_{-k} = -\omega_k$

$$p(t) = A_o + \sum_{k=1}^{\infty} A_k (e^{j(\omega_k t + \phi_k)} + e^{-j(\omega_k t + \phi_k)})$$

$$p(t) = A_o + \sum_{k=1}^{\infty} 2 A_k \cos(\omega_k t + \phi_k)$$

A_o, the DC term, is the average value of $p(t)$.

The amplitude of the harmonic at the frequency $\omega_k = 2\pi \dfrac{k}{T}$ radians per unit of time is $2A_k$.

The complex Fourier coefficient, a_k, from the preceding equations, has been computed by the use of a computer program, for constant firing-rates of 25, 50, and 100 rounds/sec. The magnitude is plotted in Figure 2 as a function of the harmonic frequencies.

2. VARIABLE FIRING RATE MODEL

A schematic figure of the pressure pulses for a variable firing rate mathematical model is shown in Figure 4. The period T, of the firing rate is plotted versus the occurence time, t, as shown in Figure 3. The variation of the instantaneous blast pressure, p, as a function of time is determined from the following mathematical analysis:

Let the sequence of N pressure pulses shown in Figure 36 be represented by the non-periodic function $p(t)$ which is defined as follows:

$$p(t) = 0, \qquad t < t_o$$

$$p(t) = p_m \left(1 - \frac{(t-t_k)}{t_o}\right) e^{\frac{-(t-t_k)}{t_o}}, \qquad t_k < t < (t_k + t_o)$$

$$\text{for } k = 1, 2, 3, \cdots, N$$

$$p(t) = 0, \qquad (t_k + t_o) < t < t_{k+1}, \, k = 1, 2, 3, \cdots, (N-1)$$

$$p(t) = 0, \qquad t > (t_N + t_o)$$

59

The duration of each pulse is t_o and t_k is the occurence times of the leading edge of the pulses.

The Fourier transform of p(t) is

$$g(\omega) = \int_{-\infty}^{+\infty} p(t) e^{-j\omega t} dt$$

where $\omega = 2\pi f$, f being frequency in cycles per second.

The transform, $g(\omega)$, will be complex and can be put in the polar form:

$$g(\omega) = A(\omega) e^{\psi(\omega)}$$

$A(\omega)$ and $\psi(\omega)$ are the amplitude and phase spectrums of p(t), respectively.

Since p(t) = 0, for $t < t_1$ and $t > t_N + t_o$

$$g(\omega) = \int_{t_1}^{t_N + t_o} p(t) e^{-j\omega t} dt$$

This integral can be expressed as the sum of N integrals since p(t) = 0 between adjacent pulses.

$$g(\omega) = \sum_{k=1}^{N} \left(\int_{t_k}^{t_k + t_o} p_m (1 - \frac{(t - t_k)}{t_o}) e^{\frac{-(t - t_k)}{t_o}} e^{-j\omega t} dt \right)$$

Changing the variable of integration in each integral by the substitution $z = t - t_k$ in the kth terms, $g(\omega)$ becomes:

$$g(\omega) = \sum_{k=1}^{N} \left(\int_{0}^{t_o} p_m (1 - \frac{z}{t_o}) e^{-\frac{z}{t_o}} e^{-j\omega(z + t_k)} dz \right)$$

$$g(\omega) = \sum_{k=1}^{N} \left(e^{-j\omega t_k} \int_{0}^{t_o} p_m (1 - \frac{z}{t_o}) e^{-\frac{z}{t_o}} e^{-j\omega z} dz \right)$$

$$g(\omega) = \int_{0}^{t_o} p_m (1 - \frac{z}{t_o}) e^{-\frac{z}{t_o}} e^{-j\omega z} dz \cdot \left(\sum_{1}^{N} e^{-j\omega t_k} \right)$$

60

This result shows that the transform of p(t) is the product of the transform of a single pulse occurring at zero time and a factor which consists of a sum of N complex numbers each of unit magnitude and with a phase angle which is determined by one of the occurrence times, t_k.

Since $e^{-j\omega t_k} = \cos(\omega t_k) - j\sin(\omega t_k)$

$$g(\omega) = \int_0^{t_o} p_m \left(1 - \frac{z}{t_o}\right) e^{-\frac{z}{t_o}} e^{-j\omega z} dz \cdot \left[\sum_1^N \cos(\omega t_k) - j\sum_1^N \sin \omega t_k \right]$$

Let $C(\omega) e^{j\theta(\omega)} = \left[\sum_1^N \cos(\omega t_k) - j\sum_1^N \sin(\omega t_k) \right]$

where $|C(\omega)| = \sqrt{\left(\sum_1^N \cos(\omega t_k)\right)^2 + \left(\sum_1^N \sin(\omega t_k)\right)^2}$

$$\theta(\omega) = \arctan\left(-\frac{\sum_1^N \sin(\omega t_k)}{\sum_1^N \cos(\omega t_k)}\right)$$

The integral can be evaluated analytically and it can be shown that

$$\int_0^{t_o} p_m \left(1 - \frac{z}{t_o}\right) e^{-\frac{z}{t_o}} e^{-j\omega z} dz = B(\omega) e^{j\Phi(\omega)}$$

where $B(\omega) = p_m \dfrac{t_o}{e} \dfrac{\sqrt{1 + (\omega t_o)^2 - 2(\omega t_o)\sin(\omega t_o)}}{(1 + (\omega t_o)^2)}$

$$\Phi(\omega) = \arctan\left(\frac{\omega t_o - \sin(\omega t_o)}{\cos(\omega t_o)}\right) - 2\arctan(\omega t_o)$$

Thus $g(\omega) = B(\omega) C(\omega) e^{j[\theta(\omega) + \Phi(\omega)]} = |A(\omega)| e^{j\psi(\omega)}$

The inverse Fourier transform of p(t) by which p(t) is synthesized from sinusoids with negative and positive frequencies is

$$p(t) = \frac{1}{2\pi} \int_{-\infty}^{+\infty} g(\omega) e^{j\omega t} d\omega = \frac{1}{2\pi} \int_{-\infty}^{+\infty} A(\omega) e^{j(\omega t + \psi(\omega))} d\omega$$

61

The form of the inverse transform which involves positive frequencies only is

$$p(t) = \frac{1}{2\pi} \int_0^\infty 2 A(\omega) \cos(\omega t + \psi(\omega)) d\omega$$

This expression can be obtained from the first form as follows:

$$p(t) = \frac{1}{2\pi} \int_0^\infty g(\omega) e^{j\omega t} d\omega - \frac{1}{2\pi} \int_0^{-\infty} g(\omega) e^{j\omega t} d\omega$$

$$p(t) = \frac{1}{2\pi} \int_0^\infty g(\omega) e^{j\omega t} d\omega - \frac{1}{2\pi} \int_0^\infty g(-\omega) e^{j(-\omega)t} d(-\omega)$$

$$p(t) = \frac{1}{2\pi} \int_0^\infty [g(\omega) e^{j\omega t} + g(-\omega) e^{-j\omega t}] d\omega$$

$$g(-\omega) = g(\omega)^* = |A(\omega)| e^{-j\psi(\omega)}$$

Where the asterisk denotes the complex conjugate. Substituting for $g(\omega)$ and $g(-\omega)$ in the last expression for $p(t)$

$$p(t) = \frac{1}{2\pi} \int_0^\infty |A(\omega)| \left[e^{j[\omega t + \psi(\omega)]} + e^{-j[\omega t + \psi(\omega)]} \right] d\omega$$

$$p(t) = \frac{1}{2\pi} \int_0^\infty 2|A(\omega)| \cos[\omega t + \psi(\omega)] d\omega$$

$$p(t) = \frac{1}{2\pi} \int_0^\infty 2|B(\omega)| |C(\omega)| \cos[\omega t + \theta(\omega) + \phi(\omega)] d\omega$$

The amplitude spectrum of $p(t)$ is the continuous function of frequency $\frac{1}{\pi} B(\omega) C(\omega)$, $\omega > 0$.

$B(\omega)$ and $\phi(\omega)$ can be evaluated from the expression given above for any specified value of t_0.

$C(\omega)$ and $\theta(\omega)$ can be evaluated if the N values, t_n, are known. They will be determined for the profile shown in Figure 3.

62

The t_kth respective times at which the leading edge of the pulses occurs, are determined from the recursion equation

$$t_k = t_{k-1} + f(t_{k-1}), k = 2, 3, \ldots\ldots, N$$

t_1 being known. The value of t_1 affects the phase spectrum but not the amplitude spectrum of $p(t)$. The amplitude spectrum is primarily of interest so, for convenience, it henceforth will be assumed that $t_1 = 0$.

$f(t_{k-1})$ is a single valued function of time whose value is the period of the $(k-1)$th pulse. The recursion equation thus states that the time at which the leading edge of a pulse occurs equals the occurrence time of the leading edge of the previous pulse plus the period of the previous pulse.

Figure 3 shows an idealized profile of the period of a pressure pulse as a function of the time of occurrence of its leading edge. It also can be considered to be the profile of the firing rate as a function of the time that has elapsed since the start of firing.

This profile consists of three parts corresponding to the time intervals during which the period is decreasing (Part 1), constant (Part 2), and increasing (Part 3).

In Figure 4, it is assumed that K, L, and M pulses occur during Parts 1, 2, and 3, respectively, where K, L, and M are integers and $N = K + L + M$.

The recursive equation applicable to each part of the profile is shown as follows:

Part 1: $t_1 = o$

$t_q = t_{q-1} + (2 - t_{q-1})\,T, q = 2, 3, \ldots, K$

$t_{k-1} = t_k = t_k + (2 - t_k)T$

Part 2: $t_q = t_{q-1} + (2 - t_q)T, q = K + 2, K + 3, \ldots, K + L$

$t_{K-L-1} = t_q = t_{K-L} + (2 - t_q)T$

Part 3: $t_q = t_{q-1} + (2 - t_q)T + (t_{q-1} - t_q)T$

$$q = K + L + 2, K + L + 3, \ldots, K + L + M = N$$

From these equations it can be seen that the period of the first pulse in Part 1, $t_2 - t_1$, is 2T and that the period of all pulses in Part 2 is $(2 - t_q)\,T$ which would equal T for $t_q = 1$. The period of the first pulse in Part 3 is $(2 - t_q)$ T and the period of the last pulse is approximately 2T.

If the sequence of N pulses is assumed to be periodic with a period of T ~ 3 sec instead of being non-periodic (as was conveniently assumed in the preceding analysis and derivation of the Fourier transform, $|g(\omega)|$) then the coefficient $|a_n|$, of the corresponding Fourier series may be expressed in terms of the transform as follows:

$$|a_k| = \frac{|g\left(\frac{k}{T}\right)|}{T}$$

And the magnitude of the spectra is:

$$2|a_k|$$

The magnitude, $2|a_k|$, from the foregoing equations has been determined with a computer program for an average firing-rate of 75 rounds/sec over 1.0 sec, a steady firing-rate of 100 rounds/sec for 1.0 sec, and a final average firing-rate of 75 rounds/sec over 1.0 sec. The line spectrum magnitude of these coefficients as a function of the harmonics of the variable firing rate, is shown in Figure 5. A check of the magnitude of this coefficient at frequencies other than the harmonics indicated the maximum value occurred at each harmonic as shown in Figure 6. Thus, it is seen that, for this model of the excitation from a variable firing-rate gun, the Fourier coefficient has a maximum value at the harmonics of the constant firing-rate portion of the model.

APPENDIX II

REGRESSION ANALYSIS

REGRESSION ANALYSIS

Regression analysis is the determination of the position of a line which yields a minimum value for the sum of squares of the deviations of the data values from the line in the y (dependent variable) direction. This line represents the locus of the average values of the dependent variable. The position of the line is determined in terms of its slope and intercept utilizing the method of least squares.

A typical set of data plotted in the Cartesian plane is shown in Figure 19. An examination of this plot indicates that the data could be fitted by a curve with the functional form

$$G_n(f) = \beta D^{-z} \tag{28}$$

Since the solution of the equations used in the method of linear least squares requires that they be linear in the unknown parameters, it is necessary to transform equation 28 to a linear form by taking the logarithmic function of each side of the equation as follows

$$\log G_o(f) = \log \beta - z \log D \tag{29}$$

To simplify, let

$$x = \log D$$
$$y = \log G_n (f)$$
$$a = \log \beta$$
$$y = a - zx \tag{30}$$

Equation 30 represents the curve in the log-log plane and is of a form amenable to a regression analysis by the method of linear least squares. The sample of test data shown in the Cartesian plane in Figure 19 is spread out and more easily analyzed when plotted in the log G_n-log D plane as shown in Figure 20. The true values a and z of Equation 30 are replaced by the estimate a and b, respectively, in the regression equation of a line through the data points:

$$y' = a + bx \tag{31}$$

The properties b and a are defined as follows: $\tag{32}$

$$b = \frac{\sum\limits_{k=1}^{N} (x_k - \bar{x})(y_k - \bar{y})}{\sum\limits_{k=1}^{N} (x_k - x)^2} \tag{33}$$

65

where:

$$a = \bar{y} - b\bar{x}$$

$a =$ intercept of the regression line

$b =$ slope of the regression line

$\bar{x} =$ arithmetic average of the log D data values

$\bar{y} =$ arithemetic average of the log $G_o(f)$ data values

The computer program used in this regression analysis was obtained from Reference 11.

In this analysis, a confidence level $(1-\alpha)$ of 0.95 was selected, corresponding to a significance level of 0.05.

After the desired confidence level $(1-\alpha)$ has been selected, it is then possible to determine the confidence interval y_{cb} within which the estimated line as a whole may fall. The upper and lower limits are determined for selected values of x from the following equation given in Reference 12.

$$y_{cb} = \bar{y} + b(x - \bar{x}) \pm \sqrt{2F_{1-\alpha}} \; S_y' \sqrt{\frac{1}{n} + \frac{(x - \bar{x})^2}{\sum_{k=1}^{N}(x_k - \bar{x})^2}} \tag{34}$$

where

$F_{1-\alpha}$ for $(2, n-2)$ degrees of freedom is found from Table A-5 (T-7) of Reference 2.

$F =$ distribution of variance, joint statistic

$S_y' =$ standard error of the estimate

$$S_y' = \sqrt{\frac{\sum_{k=1}^{N}(y_k - a - bx_k)^2}{n - 2}} \tag{35}$$

The index of the goodness of fit or multiple correlation coefficient is obtained from the following equation:

$$C_o = \sqrt{\frac{\sum_{k=1}^{N}(y_k' - \bar{y})^2}{\sum_{k=1}^{N}(y_k - \bar{y})^2}} \tag{36}$$

A regression analysis was conducted on the vibration test data from the gun configurations SUU-16, F-4, MK-4, and F-5. The results of this analysis are listed in Table IV and plotted in Figure 22, 23, 25, 26, 27, 37, 38, 39, and 40. The slope and intercept of the regression line represented by Equation 31 were obtained from Equations 32 and 33. The upper and lower limits of the confidence band about the regression line are computed from Equations 34 and 35 and are plotted as slight curves in Figures 22, 23, 25, 26, 27, 37, 38, 39, and 40. The standard error of the estimate and the correlation coefficient of each regression analysis were obtained from Equations 35 and 36 and are listed in Table IV.

66

TABLE IV

DATA FROM REGRESSION ANALYSIS

Configuration	Regression Line		
	Slope z	Standard Error of Estimate S_y'	Correlation Coefficient C_r
UNNORMALIZED			
SUU-16	-3.70151690	.7782	.57883
F-4	-3.16325936	.8398	.84629
MK-4 (N = 42)	-5.89516664	.4648	.88419
MK-4 (N = 49)	-6.39002055	.4749	.89391
F-5	-1.17115337	.5058	.45514
POOLED DATA, UNNORMALIZED			
SUU-16, F-4 MK-4, F-5	-2.64185137	.7062	.61622
SUU-16, F-4, MK-4	-4.57850122	.6806	.71425
POOLED DATA, NORMALIZED			
SUU-16, F-4, MK-4, F-5	-2.86865619	.6881	.65719
SUU-16, F-4, MK-4	-4.55262142	.6676	.71900
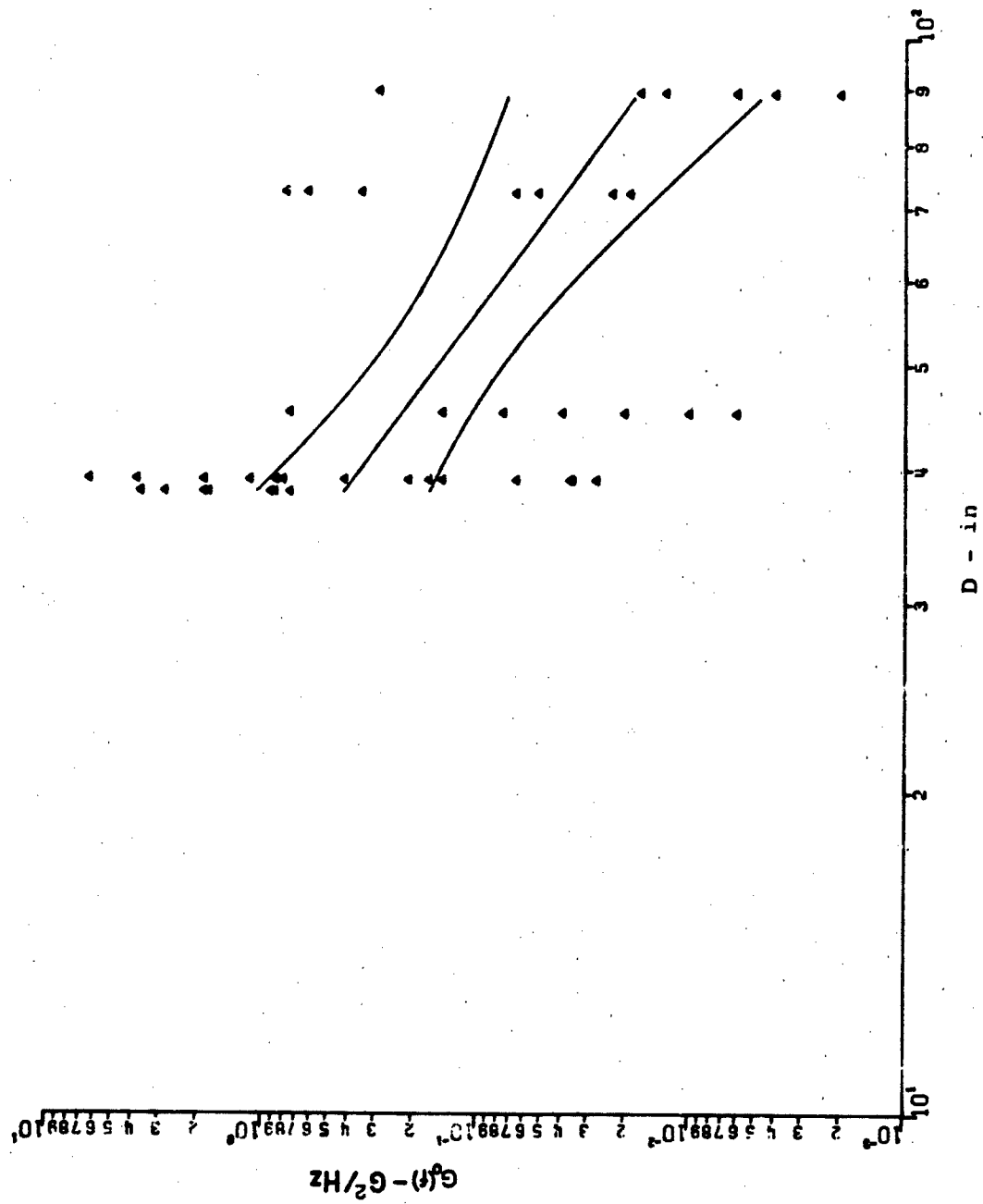
Figure 37. Regression Line and Limits of Confidence Intervals for SUU-16

$G_0(f) - G^2/Hz$

$D - i.\gamma$
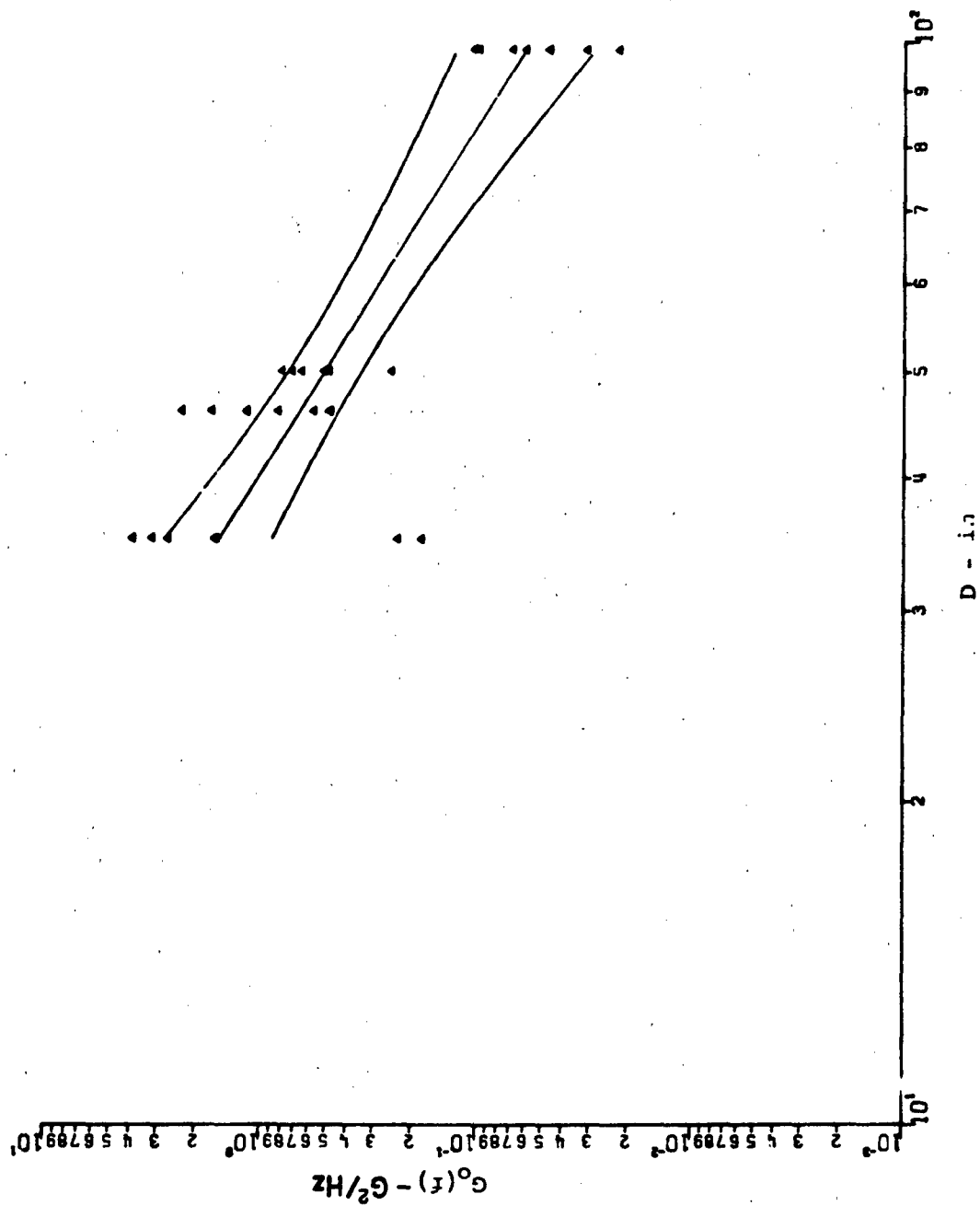
Figure 38. Regression Line and Limits of Confidence Interval for F-4
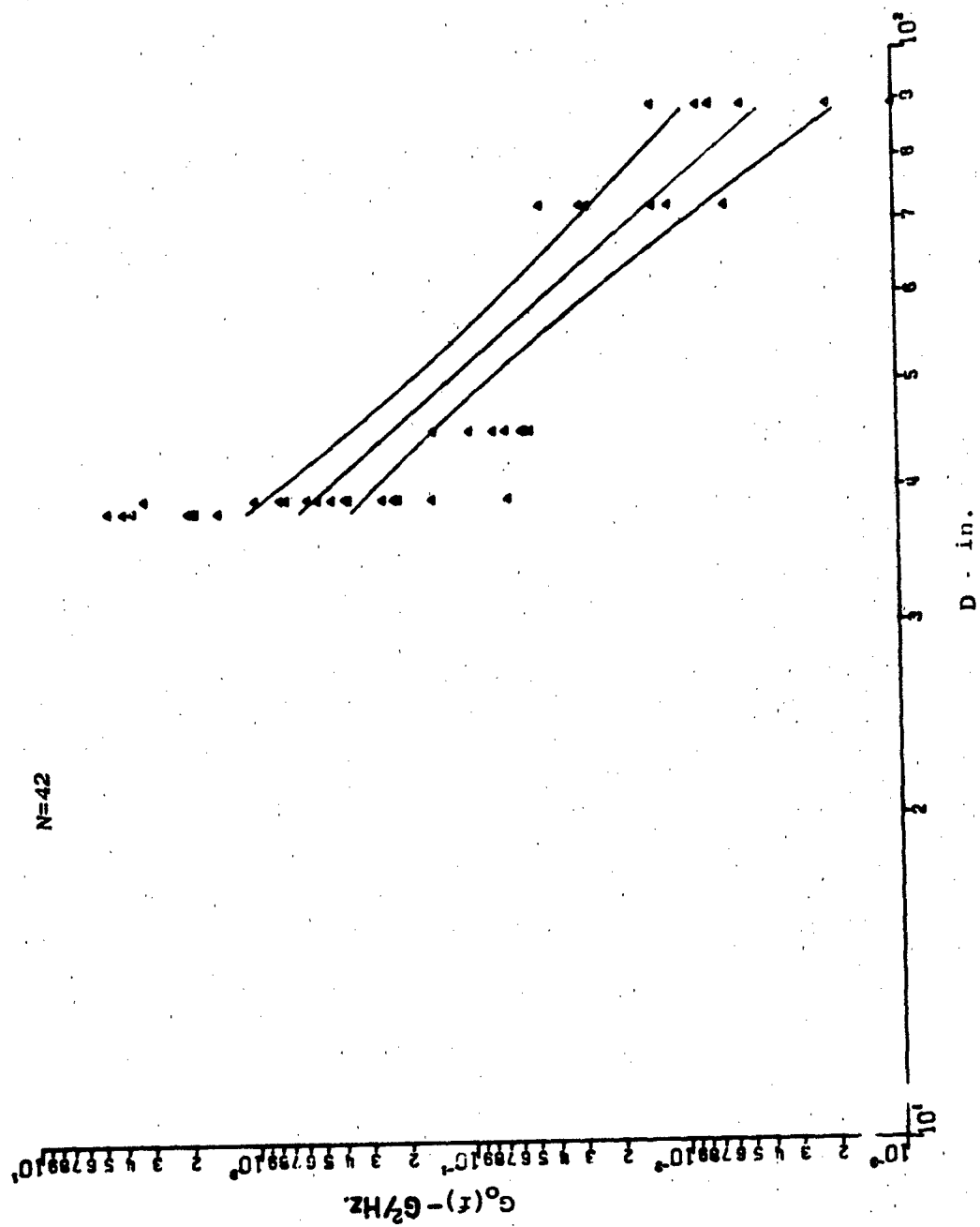
Figure 39. Regression Line and Limits of Confidence Interval for Mark IV, n = 42
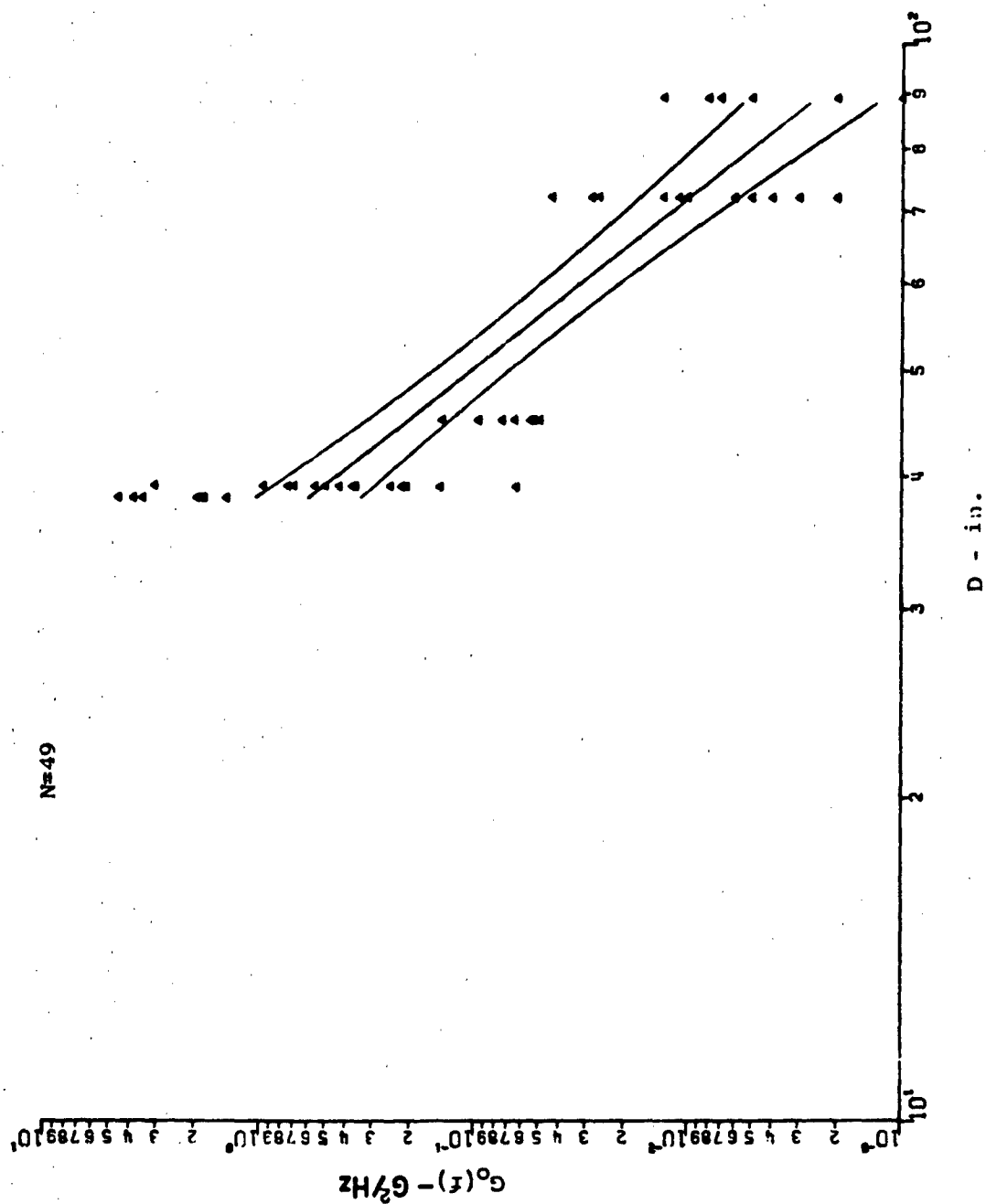
Figure 40. Regression Line and Limits of Confidence Interval for Mark IV, n = 49

APPENDIX III

GUNFIRE VIBRATION DATA

The data samples (Figures 41 through 44) show the truncated response function (described in Section IV) superposed over the samples. Note that best agreement results when $D < 76$ inches for the F-4, SUU-16, and MK-14 samples. This seems to be so because the gunfire levels rapidly converge to the ambient vibration levels as D increases. As this happens, it appears that the low-frequency gunfire contribution does not decay as rapidly as the high frequency content, thus resulting in a gradually modified spectral shape.

The F-5 data seems to reflect the influence of the deflectors, resulting in a marked alteration of the spectrum from that normally expected. The consequences of the deflector influence are discussed in Section VI.
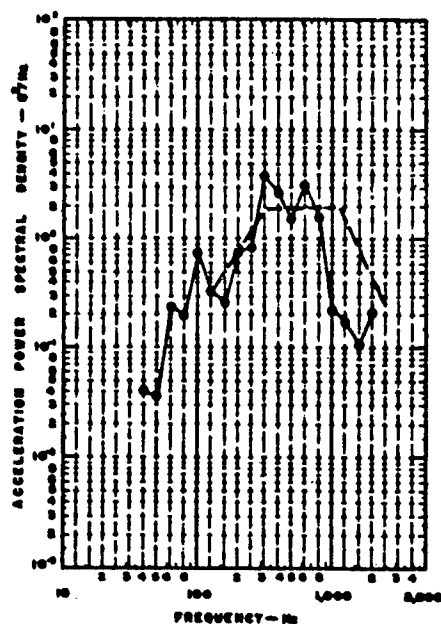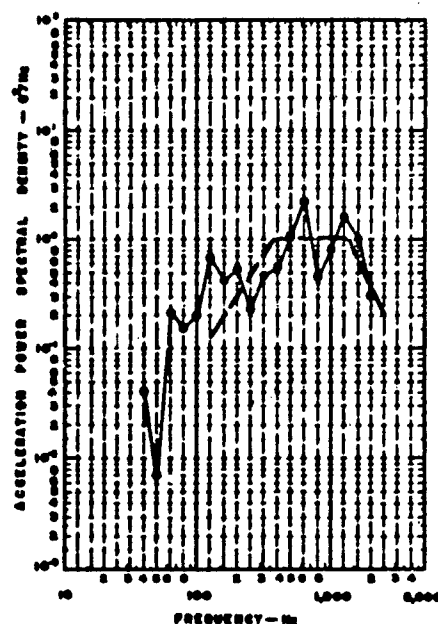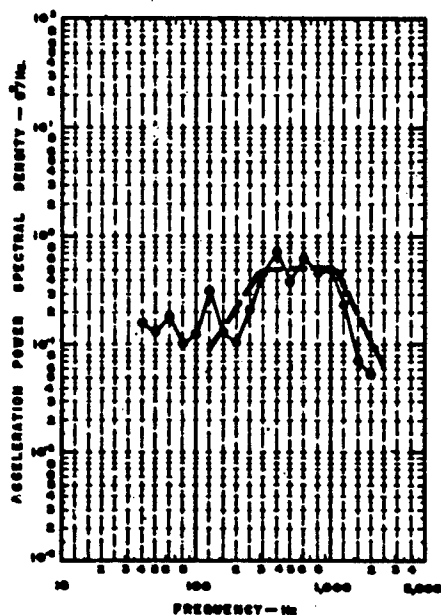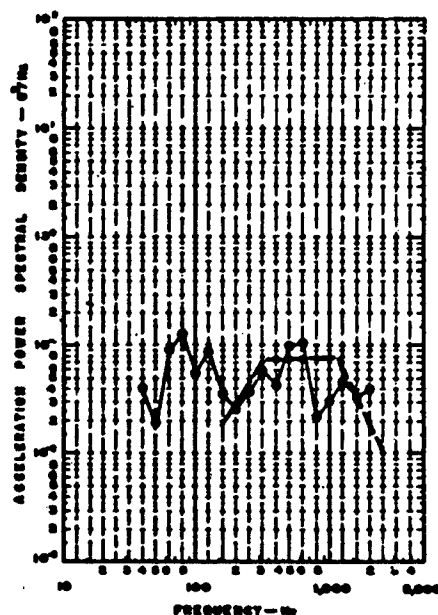
Figure 41. F-4 Gunfire Vibration Level

73

Figure 42. SUU-16 Gunfire Vibration Level

74

Figure 42. SUU-16 Gunfire Vibration Level (Continued)

75

Figure 43. Mark IV Gunfire Vibration Level

Figure 43. Mark IV Gunfire Vibration Level (Continued)

77

Figure 44. F-5 Gunfire Vibration Level

78

Figure 44. F-5 Gunfire Vibration Level (Continued)

APPENDIX IV

MILITARY STANDARD ENVIRONMENTAL TEST METHODS

TO ALL HOLDERS OF MIL-STD-810B:

1. The following new method is to be added:

NEW METHOD		DATE
T519	Gunfire Vibration, Aircraft	29 September 1969

2. This U.S. Air Force Notice forms a part of MIL-STD-810B dated 15 June 1967. The general requirements of MIL-STD-810B shall apply to any application of this notice.

3. THIS NOTICE IS NONCUMULATIVE, RETAIN AND INSERT BEFORE THE TABLE OF CONTENTS.

4. Holders of MIL-STD-810B will verify above addition has been entered. This issuance, together with appended pages is a separate publication. Each notice is to be retained by stocking points until the Military Standard is completely revised or cancelled.

Custodian:
  Air Force—11

Preparing activity:
  Air Force—11

(Project No. MISC-F650)

FSC MISC

This tentative test method has been approved by the Department of the Air Force. It is optional for use by all activities.

METHOD T519

GUNFIRE VIBRATION, AIRCRAFT

1. *Purpose.* The gunfire vibration test is conducted to simulate the relatively brief but very intense vibration fields resulting from blast pressure fields generated by repetitive firing guns mounted in, on, or near the aircraft structure.

2. *Apparatus.* Vibration equipment with required instrumentation.

3. *Criteria for application.* The most severe vibration field results from blast pressure pulses coupling to the aircraft structure and inducing vibration fields that are of maximum intensity near the gun muzzle region. This field, designated by a curve A on figure 519-1, decreases in an inverse relationship to the distance as viewed in a forward direction from the gun muzzle. The vibration field, designated by curve B on figure 519-1, decays similar to the primary field beginning at the gun muzzle and extending in the aft direction. This field, beyond the near field region of the muzzle, is of lower intensity. In no case should this test method be substituted for conventional vibration tests. Guns, physical locations, and ballistic parameters should be carefully and accurately identified prior to application of this test method. If the maximum test spectrum level of the gunfire configuration is equal to or less than .04 g^2/Hz, the gunfire method need not be conducted.

3.1 *Sensitive equipment.* Equipment found most susceptible to gunfire are those equipments that are usually located within a 3-foot radius of the gun muzzle and are mounted on the structural surface exposed to the gun blast. Prime examples are UHF antennas of the blade, V, and the flush-mounted configurations, including their bracketry, coaxial connectors, and lines. Next in order of failure susceptibility is equipment mounted on drop-down doors and access panels, equipment mounted in cavities adjacent to the aircraft surface, and finally, equipment located in the interior of the vehicle structure. Typical vulnerable equipment in these latter categories are auxiliary hydraulic and power units (including mounting bracketry), switches, relays, IR, photographic, communication and navigation equipment and radar systems, including items either shock or hard mounted.

3.2 *Determination of test levels*

3.2.1 *Selection of the maximum test level.* The maximum gunfire vibration level is defined by the following equation:

$$G_{max} = E_1/E_n (G_n/r_n n_n) (80/W_E)^2 (r_1 n_1); \text{ in PSD units (}g^2\text{/Hz)}$$

where: $80/W_E = 1$, for equipment weight $W_E < 80$ pounds

and: $80/W_E = \frac{1}{4}$ for equipment weight $W_E > 160$ pounds

The test level (G_{max}) is obtained from the basic normalized level ($G_n/r_n n_n$) which is adjusted to the muzzle energy (E_1), the firing rate (r_1), and the number of guns (n_1) of the particular gun(s) under consideration. The normalizing energy (E_n) is equal to 39,600 foot-pounds. The last term ($80/W_E$) represents a mass adjustment factor and permits the reduction of G_{max} when the equipment weight is greater than 80 pounds. Table 519-1 designates

the muzzle energies, the energy adjustment factors, and the nominal firing rates of commonly used gun configurations. Figure 519-1 provides $G_o/r_o n_o$ as a function of the distance parameter (D). The mass adjustment factor is determined from figure 519-2.

3.2.2 *Determination of the distance parameter* (D). The distance parameter represents the vector distance, measured (or estimated) from the gun muzzle to the mean distance between equipment support points. Where equipment support points are indeterminate, the equipment center of gravity shall represent the terminal point of D. The vector D is usually generated from the orthogonal distances referenced to the fuselage station, the water, and the butt line data. The D vector and the computation is shown on figure 519-3.

3.2.3 *Multiple guns*. For configurations involving multiple guns, the origin of D is determined from the centroidal point of the gun muzzles. Figure 519-4 shows the origin location for a typical four-gun staggered array.

Example No. 1—A 2-pound UHF antenna, is to be flush mounted to the under-surface of the aircraft and located forward of the muzzle of four M-61 type cannons. The expected firing rate is 25 Hz ($r_1 = 25$). (If the firing rate is unknown, the maximum specified rate shall be used). Since, in this configuration, each barrel fires independently and the number of guns is equal to four, then $n_1 = 4$ (see 1/).

Steps

   a. The antenna location determined from the aircraft spatial coordinates (see figure 519-3) is found to be 39 inches or D = 39 inches.

   b. Refer to Figure 519-1. Select curve A and obtain the ordinate value of $G_o/r_o n_o$ for D = 39 inches. In this case $G_o/r_o n_o = 3.0 \times 10^{-2}$

   c. From table 519-I(select E_1/E_o for the M-61 gun (see 2/).
      Here, $E_1/E_o = 1$

   d. Since the antenna weight is less than 80 pounds, the mass adjustment factor becomes unity and a reduction of G_{max} is not allowed (see figure 519-2)

   e. Determine the normalized level, $G_1/r_1 n_1$, by adjusting $G_o/r_o n_o$ by E_1/E_o as follows:
      $G_1/r_1 n_1 = E_1/E_o (G_o/r_o n_o)$ or $G_1/r_1 n_1 = (1) 3.0 \times 10^{-2}$

   f. Multiply $G_1/r_1 n_1$ by $n_1 r_1$ to obtain the maximum test level, G_{max}:

   $$G_{max} = G_1/r_1 n_1 (r_1 n_1)$$

   $$G_{max} = 3.0 \times 10^{-2} (10^2)$$

   $$G_{max} = 3.0 \ g^2/Hz$$

   g. Apply G_{max} to figure 519-5 to obtain the test spectrum.

Example No. 2—An electronic equipment weighing 102 pounds is located in the aircraft nose section forward of the gun muzzle. The distance (D) is 45 inches. The firing rate of the revolving barrels of the cannon totals 100 Hz with $n_1 = 1$.

The muzzle energy (E_1) is 83,000 foot-pounds.

Steps:

   a. Repeating steps (a) and (b) as before:
      $G_o/r_o n_o = 1.9 \times 10^{-2}$

   b. From note 2, divide E_1/E_o:
      $83 \times 10^3/39.6 \times 10^3 = 2.1$

82

c. Adjusting for E_i/E_o:

$G_i/r_i n_i = (2.1) (1.9 \times 10^{-2})$

or $G_i/r_i n_i = 4.0 \times 10^{-2}$

d. Obtain G_{max} as before:

$G_{max} = 4.0 \times 10^{-2} (10^2) (1) = 4.0 \ g^2/Hz$

e. Noting from 3.2.1 that $W_k > 80$ pounds and referring to figure 519–2, where the derated value (G'_{max}) is found to be 2 dB down (–2 dB) from 4.0 g^2/Hz

From dB power tables:

$-2 \ dB = LOG_{10} \ G'_{max}/4.0$

or $G'_{max} = 2.5 \ g^2/Hz$

f. Apply G'_{max} to figure 519–5 to obtain the test spectrum.

1/ Some M-61 gun configurations (see MK-IV, gun pod, table 519–I) feature two barrels per pod; firing simultaeously. In such a case, $n_i = 2$ per pod.

2/ If E_i is unknown, determine E_i from ballistic data using $E_i = m_i v_i^2/2$ where:

$m_i =$ the projectile mass and $v_i =$ muzzle velocity. Divide by E_o (see table 519–?) and proceed as in step (e).

4. Test procedures. Test procedures used shall be as specified in the equipment specification or test plan.

4.1 Test item operation. Unless otherwise specified, the test item shall be operated during application of vibration so that functional effects caused by these tests may be evaluated. When a test item performance test is required during vibration and the time required for the performance is greater than the duration of the vibration test, the performance test shall be abbreviated accordingly. At the conclusion of the test, the test item shall be operated and the results compared with the data obtained in accordance with section 3, General Requirements, paragraph 3.2.1. The test item then shall be inspected in accordance with section 3, General Requirements, paragraph 3.2.4.

4.2 Mounting techniques. In accordance with section 3, General Requirements, paragraphs 3.2.2, the test item shall be attached to the vibration exciter table by its normal mounting means or by means of a rigid fixture capable of transmitting the vibration conditions specified herein. Precautions shall be taken in the establishment of mechanical interfaces to minimize the introduction of undesirable responses in the test setup. Whenever possible, the test load shall be distributed uniformly on the vibration exciter table in order to minimize effects of unbalanced loads. Vibration amplitudes and frequencies shall be measured by techniques that will not significantly affect the test item input control or response. The input control accelerometer(s) shall be rigidly attached to the vibration table or to the intermediate structure, if used, at or as near as possible to the attachment point(s) of the test item.

5. Test procedures

5.1 Procedure I, Random vibration test. The test item shall be subjected to random vibration along each mutually perpendicular axis. Test times shall be in accordance with time schedule I from table 519–II. The instantaneous peaks of the random vibration acceleration may be limited to 2.5 times the rms acceleration level. The power spectral density of the test level control signal shall not deviate from the specified requirements by more than +40 −30 percent (±1.5 dB) below 500 Hz and +100 −50 percent (±3.0 dB) between 500 and 2,000 Hz, except that deviations as large as +300 −75 percent (±6 dB) shall be allowed over a cumulative bandwidth of 100 Hz between 1,000 and 2,000 Hz for equipment items whose weight is equal to or less than 50 pounds. For items weighing more than 60 pounds,

83

the same deviation shall be allowed over the extended range from 500 to 2,000 Hz provided the cumulative bandwidth deviation does not apply to the swept bandwidth of noise as detailed in 5.3.1.2.

5.2 *Procedure II, Single direction test.* If the equipment item is mounted with the base peripherally attached to and in the plane of the aircraft skin, then the test direction may be restricted to the direction normal to the aircraft skin (see figure 519-6). The total test time in this case shall be as stated in time schedule II of table 519–II.

5.3 *Procedure III, Composite or alternate test.* For locations near the gun muzzle and for equipment weighing in the region of 60 pounds, the test levels may exceed the force capabilities of all but the largest shaker systems. For such cases, the following test method may be substituted provided the following criteria are met:

when: $G_{max} > 3.0$ g^2/Hz $> 8.6 \times 10^{-4}$ $(F_r/W_T)^2$

where: $W_E > 55$ pounds and: $W_J < 1.2$ W_E

F_r = Maximum RMS shaker force output—pounds

$W_T = W_E + W_A + W_J$

W_E = Equipment weight—pounds

W_A = Armature weight—pounds

W_J = Test jig weight—pounds

5.3.1 *Selection of composite elements.* A broad band, random vibration test level G_B shall be selected equal to $G_{max}/4$ (6 dB down). A random noise signal of 100 Hz bandwidth (3 dB down points) shall be superimposed on G_B having a G_{max} equal to the original determined value. The composite spectrum is shown on figure 519–7.

5.3.1.2 *Test procedure.* The test shall be conducted in accordance with 5.1, except the narrow band noise shall be swept from 300 to 1,000 Hz, referenced to the narrow band center frequency. The sweep time shall be in accordance with time schedule III in table 519–II.

6. *Test level overall rms.* The overall rms test level shall be no less than the area enclosed by the solid curve of figure 519–5, –21 percent (–2 dB). The overall rms is defined by the following equation.

$$OAR = (1163 \, G_{max})^{\frac{1}{2}}$$

7. *Summary.* The following details shall be specified in the equipment specification or test plan:

a. Procedure number (see 5)

b. Pretest data required (section 3, General Requirements, paragraph 3.2.1)

c. Nonoperation of equipment during test, if desired (see 4.1)

d. Unique or special test considerations.

84

REFERENCES

1. *F-4E Final Results of the Structural Dynamics Production Prototype Gunfire Development Program*. Memo 236-4100. McDonnell Aircraft Corporation. 1 May 1968.

2. *Vibracoustic Evaluation of the F-5A Gun Nose Installation (Change A.)* Norair Division Report NOR-63-100. Northrop Corporation. 4 October 1966.

3. C. R. Wylie, Jr., *Advanced Engineering Mathematics*. McGraw-Hill Book Company, Inc., New York. 1960.

4. *LaPlace & Fourier Transforms for Electrical Engineers*. Craig, Holt, Rhinehart, & Winston. 1964.

5. David K. Cunningham. *Engineering Evaluation of the 20-mm Gas Driven SUU 23/A Gun Pod*. APGC-TR-68-48. AD 487 396. Air Proving Ground Center, Eglin AFB, Fla. July 1966.

6. *Vibracoustic Evaluation of the F-5A Gun Nose Installation*. Norair Division Report NOR-63-100. Northrop Corporation. 1 May 1965.

7. *Summary of Structural Dynamic Effect on Production SUU-16A Gun Pod Program*. Memo 236-2413. McDonnell Aircraft Corporation. 16 October 1965.

8. *Summary of Dept. 236 Effort on the Center-Line MK-IV Gun Pod Program*. Memo 236-2427. McDonnell Aircraft Corporation. 4 November 1965.

9. A. G. Tipton. *Vibration and Acoustic Survey on F-100D Aircraft Nose Section During Gunfire*. NA-66 1386. North American Aviation, Los Angeles Division. December 1966.

10. Peter S. Westine. *Structural Responses of Helicopters to Muzzle and Breech Blast* (Vol. 1 of Final Technical Report, Blast Field about Weapons). Final Technical Report 02-2029. Southwest Research Institute. November 1968.

11. *BMD-Biomedical Computer Program*. Editor, W. J. Dixon. Health Science Computing Facility, School of Medicine, University of California, Los Angeles. 1 January 1964, Revised 1 September 1965.

12. M. G. Natrella. *Experimental Statistics NBS Handbook 91*. National Bureau of Standards. 1964.

13. Jones, Nashif, Bruns, Sevy, Owen, Henderson, and Conner. *Development of a Tuned Damper to Reduce Vibration Damage in an Aircraft Radar Antenna*. AFML-TR-67-307. AF Materials Laboratory. 1967.

BIBLIOGRAPHY

Bennett, Carl A., and Norman L. Franklin. *Statistical Analysis in Chemistry and the Chemical Industry.* John Wiley and Sons, Inc., New York. 1963.

Blum, Joseph E., Major, USAF. *Fourier Analysis of an Exponential Approximation for a Nuclear Blast Pressure Pulse.* AFSWC-TR-68-16. AF Special Weapons Center. August 1968.

Crandall. *Random Vibration, Vol. 1.* MIT Press.

Dixon, Wilfrid J., and Frank J. Massey, Jr. *Introduction to Statistical Analysis.* McGraw-Hill Book Company, Inc. 1957.

Hinote, G. E. *TA-4 Generator and Canopy Access Door's Gunfire Interrupter Switch Vibration Test.* Report DAC-66726. Douglas Aircraft Co. November 1967.

Ostle, Bernard. *Statistics in Research.* Iowa State College Press. 1954.

A-4E/MK-4 Mod. 0 Gun Firing Demonstration. Report DEV-4699. Douglas Aircraft Company, Aircraft Division, Flight Development. 18 January 1966.

DOCUMENT CONTROL DATA - R & D

(Security classification of title, body of abstract and indexing annotation must be entered when the overall report is classified)

1. ORIGINATING ACTIVITY (Corporate author)	2a. REPORT SECURITY CLASSIFICATION
Air Force Flight Dynamics Laboratory Wright-Patterson Air Force Base, Ohio 45433	Unclassified
	2b. GROUP

3. REPORT TITLE

AIRCRAFT GUNFIRE VIBRATION
The Development and Prediction Methods and The Synthesis of Equipment Vibration
Techniques

4. DESCRIPTIVE NOTES (Type of report and inclusive dates)
Covers period from 1 November 1968 to April 1970

5. AUTHOR(S) (First name, middle initial, last name)

Robert W. Sevy
James Clark

6. REPORT DATE	7a. TOTAL NO. OF PAGES	7b. NO. OF REFS
November 1970	158	13

8a. CONTRACT OR GRANT NO.	9a. ORIGINATOR'S REPORT NUMBER(S)
b. PROJECT NO. 1309	AFFDL-TR-70-131
c. Task No.130904	9b. OTHER REPORT NO(S) (Any other numbers that may be assigned this report)
d.	

10. DISTRIBUTION STATEMENT   This document is subject to special export controls and each
transmittal to foreign governments or foreign nationals may be made only with prior
approval of the Vehicle Equipment Division, Air Force Flight Dynamics Laboratory
(FEE), Wright-Patterson Air Force Base, Ohio   45433.

11. SUPPLEMENTARY NOTES	12. SPONSORING MILITARY ACTIVITY
	Air Force Flight Dynamics Laboratory Wright-Patterson Air Force Base, Ohio 45433

13. ABSTRACT

This study describes in-house efforts that comprise two primary objectives. (1)
the development of a prediction rationale for estimating the magnitude and
character of gunfire induced, structurally-borne vibration which, in turn, re-
presents a definition of equipment vibration inputs, and (2) the synthesis of
a laboratory vibration test procedure which may be used to qualify future
equipment.

Power analogies, relating gunfire blast to structural response, are meshed with
a spatial parameter to describe vibration levels that are functionally related
to the gunfire blast pulse in terms of gun configuration, muzzle energy, gun-
fire rate, and the vector distance separating the equipment from the gun muzzle.

A basic, normalized, test level function has been synthesized and integrated in-
to a laboratory vibration test procedure. The test technique developed from
this work has been published as Method T519 of MIL-STD-810B

DD FORM 1473
1 NOV 65

14. KEY WORDS	LINK A		LINK B		LINK C	
	ROLE	WT	ROLE	WT	ROLE	WT
Gunfire						
Vibration						
Prediction						
Equipment						
Simulation						